Diss. ETH No. 16550

ANDRÉ S.P. NIEDERBERGER

INVESTIGATIONS OF

THERMOACOUSTIC OSCILLATIONS

MODELING, IDENTIFICATION AND CONTROL

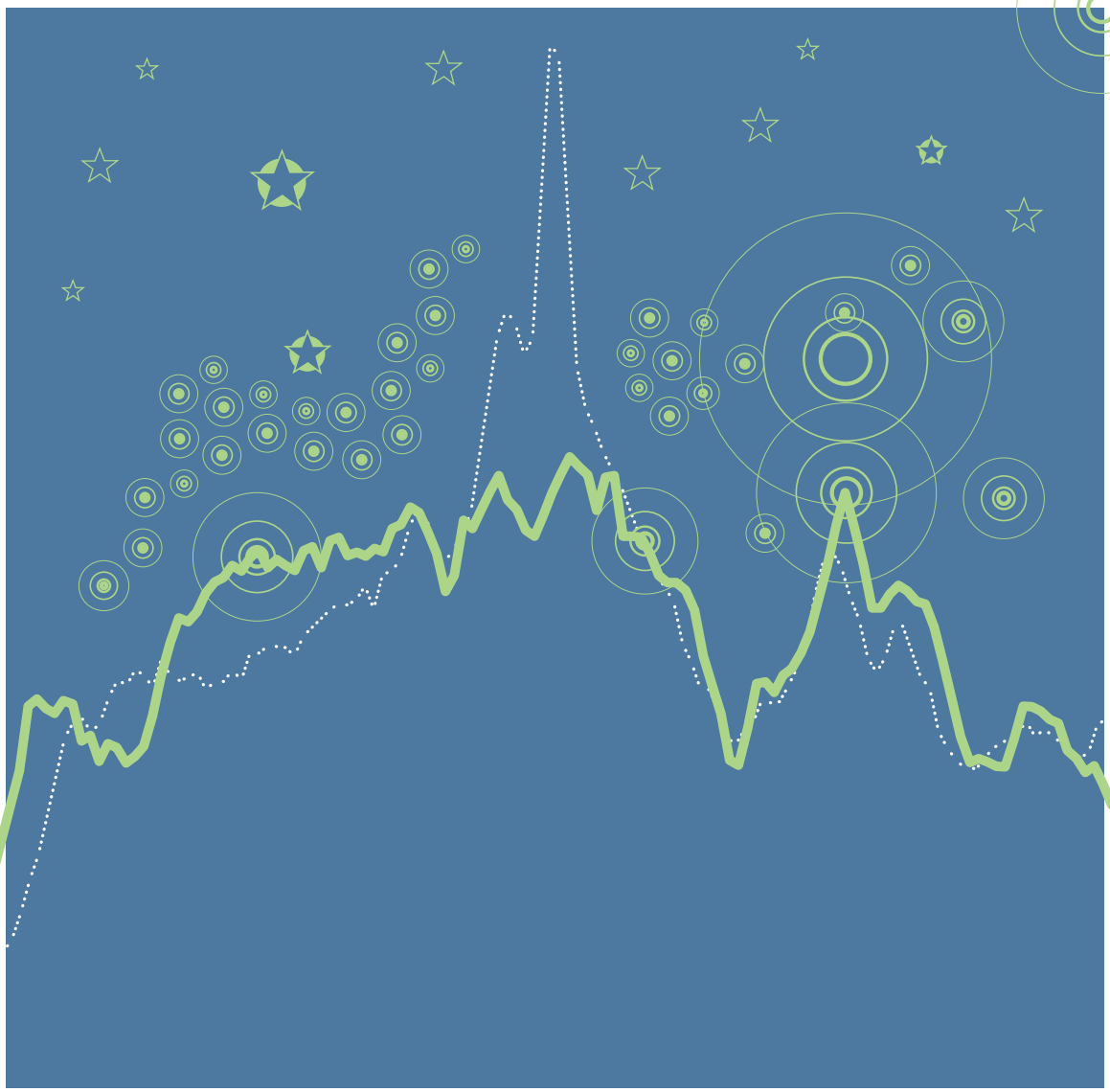

Diss. ETH No. 16550

Investigations of Thermoacoustic Oscillations: Modeling, Identification and Control

A dissertation submitted to the

SWISS FEDERAL INSTITUTE OF TECHNOLOGY
ETH ZÜRICH

for the degree of
DOCTOR OF TECHNICAL SCIENCES

presented by

ANDRE SVEN PAUL NIEDERBERGER
Ing. méc. dipl. EPF Lausanne
born February 6th, 1978
citizen of Wolfenschiessen, NW

accepted on the recommendation of

Prof. Dr. L. Guzzella, examiner
Prof. Dr. C.O. Paschereit, co-examiner
Dr. B.B.H. Schuermans, co-examiner

2006

Bibliografische Information Der Deutschen Bibliothek
Die Deutsche Bibliothek verzeichnet diese Publikation in der Deutschen Nationalbibliografie; detaillierte bibliografische Daten sind im Internet über http://dnb.ddb.de abrufbar.
1. Aufl. - Göttingen : Cuvillier, 2006
Zugl.: Zürich, Univ., Diss., 2006
ISBN 3-86537-905-2

Nonnenstieg 8, 37075 Göttingen
Telefon: 0551-54724-0
Telefax: 0551-54724-21
www.cuvillier.de

1. Auflage, 2006
Gedruckt auf säurefreiem Papier

ISBN 3-86537-905-2

"If I have seen further, it is by standing
on the shoulders of giants."

Sir Isaac Newton, 1643–1727

Fir au Diä wo Fräid hend

Contents

Main Achievements **ix**

Thanks, y'all! **xi**

Outline of this Dissertation **xiii**

Zusammenfassung **xv**

Notation **xvii**

1 Thermoacoustic Oscillations **1**
1.1 Abatement of Emissions: Solutions and Problems 1
1.2 Instability Mechanisms 3
1.2.1 Premixed Swirl-Stabilized Burners 4
1.3 Approaches to the Problem 5
1.3.1 Passive Control 5
1.3.2 Active Control 6

2 Literature Review **7**
2.1 Reported Control Concepts 7
2.2 Work of Various Research Groups 9

3 Experimental Setup and Characterization of the Test Rig **13**
3.1 Experimental Setup 13
3.2 Acoustics: Techniques and Definitions 16
3.2.1 Multi-Microphone Method 16
3.2.2 Reflection Coefficients and Impedances 17
3.2.3 Averaged Sound-Pressure Level and Spectral Density of Pressure 18
3.3 Operating Conditions, Coding Conventions 19

4 Network Modeling and Identification **23**
4.1 Physics-Based Network Modeling 23
4.1.1 The Network Model Setup 23
4.1.2 The Up- and Downstream Ducts and End Conditions 25
4.1.3 The Burner and the $L-\zeta$ Model 29
4.1.4 The Flame and the $n-\tau$ Model 32
4.1.5 The Noise Source Term 35
4.1.6 The Loudspeaker 36
4.1.7 The Fuel Injector 38
4.2 Assembling the Model 39
4.3 Identification for Control 49
4.3.1 Loudspeaker as Actuator 49
4.3.2 Fuel Injector as Actuator 50

5 Passive and Active Control **53**
5.1 Passive Control and Helmholtz Resonators 53
5.1.1 Effect of Helmholtz Resonators 54
5.1.2 Effect of Electrically Shorted Loudspeaker 58
5.2 Active Feedback Control 59
5.2.1 Fundamental Limits of Active Control 59
5.2.2 Control Setup 60
5.2.3 Actuators 61
5.2.4 Controllers 62
5.2.5 Investigated Operating Conditions 64
5.3 Control Experiments: Loudspeaker as Actuator 65
5.3.1 Loudspeaker and Gain-Delay Control 65
5.3.2 Loudspeaker and $\mathcal{H}_\infty$ Control 67
5.4 Control Experiments: Fuel Injector as Actuator 69
5.4.1 Effect of Fuel Injector Offsets on Pressure Spectrum 69
5.4.2 Effect of Fuel Injector Control on Flame Structure 70
5.4.3 Fuel Injector and Gain-Delay Control 71
5.4.4 Fuel Injector and $\mathcal{H}_\infty$ Control 76
5.4.5 Fuel Injector: Controller Comparison and Robustness Study . . 81
5.4.6 Fuel Injector and CMA-ES Optimization 88

6 Summary and Conclusions **101**

A Additional Fuel Injector Controllers **103**
A.1 Fuel Injector and Manual Loop Shaping Control 103
A.2 Fuel Injector and Complex Lead-Lag Control 105
A.3 Fuel Injector and Peak Filter Control 106

B Historical Notes on Gas Turbines **107**
B.1 From Early Developments to the Steam Turbine 107
B.2 The Gas Turbine 108

C Thermodynamic Analysis of Gas Turbines **109**
C.1 Definitions and Characterization 109
C.2 Working Principles of Gas Turbines 110

D Combustion Systems **112**
D.1 Combustor Technology 112
D.2 Laminar and Turbulent Flames 113
D.3 Emissions 114

E A Note on Newton's Exclamation **115**

Bibliography **116**

Publications **128**

Curriculum Vitæ **129**

Main Achievements

An ihren Taten sollt ihr sie erkennen.

Mat 7:16

The main achievements reported in this thesis are the following:

Modeling:

- The $L-\zeta$ burner model is validated over the whole range of operating conditions.
- The extended $n-\tau$ flame model is verified for all flame types encountered.
- The transfer function from a loudspeaker input to a microphone pressure reading is modeled based on a network. The constituent blocks are described by physical principles — relevant parameters are identified experimentally.
- A new closed-loop identification method for the plant is proposed, when the fuel injector is used as actuator. It is straightforward, safe, robust, and easy to implement in an industrial setting.

Control:

- Passive control strategies based on Helmholtz resonators are investigated.
- A high-bandwidth fuel injector is implemented to provide significant control authority.
- Model-based $\mathcal{H}_\infty$ controllers are designed. Their flexibility and superiority over standard controllers are clearly demonstrated.
- A novel approach of improving controllers online with the combustor running is elaborated using evolutionary algorithms (CMA-ES). It is applied to an industry-relevant Gain-Delay controller as well as to a robust $\mathcal{H}_\infty$ controller.

Thanks, y'all!

Non omnia possumus omnes.

Vergil, "Bucolica" 8,63

My advisor Prof. Dr. Lino Guzzella initiated this project with Prof. Dr. Oliver Paschereit, Dr. Bruno Schuermans and Dr. Peter Flohr from ALSTOM Ltd. It is embedded in the Center of Energy Conversion CEC, a partnership between ETH and ALSTOM. Thanks to their generous support, I was able to work on an exciting topic and complete this thesis. Lino in particular gave me the freedom to live the true PhD experience, with its rough times and scientific breakthroughs (at least for me).

Dr. Chris Onder and Dr. Esfandiar Shafai took their time to talk about control systems with me.

I had many discussions about research and other crucial things in life with my colleagues from IMRT. I would like to mention my office mates Dres. Simon Frei, Peter Spring, Thomas Böhme, as well as Daniel Brand and Theo Auckenthaler.

Dr. Daniel Fritsche, Captain of HMS test rig, steered our vessel in the lab through roaring thunderstorms (and around windy Greek islands) and made sure we got out the lab alive.

Dr. Niko Hansen coded the CMA-ES algorithm in such a way that it could be easily used on the test rig. Dr. Marc Füri helped to run experiments.

Christoph Merz and Bob Rollinger completed their semester theses on the topic of self-tuning regulators, and helped me with the evaluation thereof.

Our skilled technicians Oskar Brachs and Hans-Ueli Honegger helped with welding and other more important repairs. The secretaries Brigitte Rohrbach and Claudia Wittwer made sure that my publications achieved a slight reminiscence of the English language and got properly published.

My instructors of automatic control, Profs. Dominique Bonvin, Denis Gillet and Roland Longchamp from EPFL, as well as Profs. William Messner from CMU, Oscar Crisalle from UF and Hans Peter Geering from ETHZ have instilled me with a sense of the beauty of research.

Kevin P. Coleman and Robert Arrighi from the NASA Glenn Research Center in Cleveland provided videos about combustion instability research at the Rocket Engine Test Facility.

Caroline made sure I did not drown in the engineering world. Thanks to her view vector being an element of the nullspace of mine, we can span more of the vector space commonly called world. She also provided the technical illustrations in this thesis and designed the cover.

"Was gid äs einisch us Diär?", my parents Irène and Ernst have been asking repetitively and are probably still not sure. My brother Dominik has given me inspirations and assistance.

My former Greek teacher Johann Brülisauer has helped to introduce some classical education into this thesis, and Urs Zihlmann took care of the New Testament. Cory Edwards, besides being a great roomie, assisted with the mapping $f : \mathcal{G} \to \mathcal{E}$.

The students' sports association ASVZ looked after the latter part of "mens sana in corpore sano", in areas like ski tours, mountaineering, spelunking, swimming, scuba diving, sailing, and juggling.

Finally, this thesis also features a few wisecracker quotes:
"Quidquid latine dictum sit, altum videtur".

I really had a kewl time with you guys. Thanks, y'all!

Outline of this Dissertation

Each equation in the book would halve the sales.

Stephen Hawking, in "A Brief History of Time"

The thesis at hand treats modeling, identification and control of thermoacoustic pressure oscillations in gas turbine combustors. The company ALSTOM Ltd. has sponsored a project to study the origin as well as the control of these oscillations. To that end, a test rig has been built at ETH Zürich to carry out experimental research. Two PhD theses have been written as a result, namely Daniel Fritsche's [101] and mine.

This thesis is organized as follows:

Chapter 1 introduces the reader to thermoacoustic instabilities. It explains the setting of the problem and mitigation attempts. The particularities of swirl-stabilized burners are highlighted.

Chapter 2 presents an extensive literature review. It shows that many research groups around the world investigate this topic, and their achievements are screened for control contributions.

Chapter 3 describes the test rig built at ETH. Its operating conditions and corresponding flame types are characterized. Data acquisition and treatment for the acoustic analysis is discussed. Reflection coefficients and impedances are defined.

Chapter 4 explains how a model of the combustor has been developed. The modeling approach adopted here is based on a network consisting of different blocks. They are described by physical principles and compared with measurements. The validity of this procedure is demonstrated over a wide range of operating conditions. In particular, the flame model and its parameters are found to correlate well with optical measurements and derived flame types. Moreover, transfer functions from a loudspeaker input to a microphone pressure reading are assembled and validated with measurements.

A new way of obtaining a model of the plant is suggested. It is based on closed-loop identification with various simple controllers. This approach is particularly appealing in an industrial setting, as the combustor is run in a controlled fashion, which does not compromise security.

Chapter 5 presents the results of passive and active control experiments. Passive control strategies are investigated with various Helmholtz resonators. Their effects are evaluated at positions both up- and downstream of the burner. Fundamental limits for feedback control are discussed, and $\mathcal{H}_\infty$ controllers are introduced.

A loudspeaker actuator is used to reduce the pressure oscillations in the combustor. This is done first with a simple Gain-Delay controller, but also with an $\mathcal{H}_\infty$ controller, and the superiority of the latter evident.

However, actuator saturation is a serious constraint for a loudspeaker, and therefore fuel actuation is a more viable option for industrial-scale gas turbines. Several kinds of controller structures are investigated. For an instability with a distinct peak in the pressure spectrum, Gain-Delay control is found to perform reasonably well. However, for more complex cases, this approach is outperformed by a model-based $\mathcal{H}_\infty$ controller. Moreover, it is shown that more flexibility is conferred to the designer, and robustness to changing operating conditions is assured.

A new method of improving controllers in an online fashion is presented. An evolutionary algorithm called CMA-ES monitors the performance of various controllers and changes them so as to minimize a given cost function. This not only improves steady-state performance, but also helps to cope with changing operating conditions. A Gain-Delay and an $\mathcal{H}_\infty$ controller are subjected to the CMA-ES optimization algorithm.

The appendices contain extra material for the interested audience. Additional fuel injector controller experiments are discussed. For the historically inclined reader, a few noteworthy and interesting facts are described in Appendix B. The thermodynamics people will find some treats in the analysis of gas turbines, and combustion systems are discussed last.

The author hopes that a few ideas from this thesis may spark improvements in gas turbines.

Zusammenfassung

It is no use saying, 'We are doing our best.'
You have got to succeed in doing what is necessary.

Sir Winston Churchill

Die vorliegende Doktorarbeit befasst sich mit der Modellierung und Regelung von thermoakustischen Druckschwankungen in Gasturbinenbrennkammern. Die Firma ALSTOM Ltd. unterstützte ein Projekt zur Untersuchung der Ursachen und Regelung derselben. Zu diesem Zweck wurde ein Prüfstand an der ETH Zürich gebaut und zwei Doktorarbeiten geschrieben, diejenige von Daniel Fritsche [101] und die vorliegende. Prof. Dr. Lino Guzzella, Prof. Dr. Oliver Paschereit, Dr. Bruno Schuermans und Dr. Peter Flohr haben dieses Projekt initiiert und betreut, ihre grosszüge Hilfe sei hiermit verdankt. Dr. Marc Füri und Dr. Niko Hansen haben ebenfalls bei der Ausführung der Arbeiten mitgeholfen.

Die folgenden Punkte kommen in dieser Arbeit zur Sprache:

Kaptiel 1 stellt das Problem der thermoakustischen Instabilitäten in Brennkammern vor. Involvierte Mechanismen werden diskutiert, speziell für drallstabilisierte Brenner.

Kapitel 2 präsentiert eine Literaturrecherche. Besonders wird dabei auf Berichte über Regelstrategien geachtet.

Kapitel 3 geht auf den ETH Prüfstand ein. Betriebspunkte und Flammtypen werden klassifiziert. Die Datenerfassung für die akustische Analyse wird vorgestellt. Reflektionskoeffizienten und Impedanzen werden definiert.

Kapitel 4 erklärt den Modellierungsansatz. Die Idee ist, dass man ein Netzwerkmodell aus verschiedenen Blöcken (Rohrungen, Brenner, Flamme etc.) zusammenbaut. Jeder Block beinhaltet ein physikalisches Modell, das mit Messungen verglichen wird. Die Gültigkeit dieses Ansatzes wird über einen breiten Bereich von Betriebsbedingungen gezeigt. Speziell die Flammenparameter stimmen sehr gut mit optischen Resultaten überein. Weiter werden Übertragungfunktionen von einem Lautsprechereingang zu Druckmessungen zusammengebaut und mit Messungen verglichen.

Eine neue Idee zur Bestimmung eines Modells im geschlossenen Regelkreis wird vorgestellt, das auf der Druckspektrumreduktion beruht. Dies ist interessant auch für

Industrieanwendungen, da die Brennkammer geregelt betrieben ist.

Kapitel 5 befasst sich mit der passiven und aktiven Regelung von Verbrennungsinstabilitäten. Passive Regelstrategien basierend auf Helmholtzresonatoren werden für verschiedene Betriebspunkte untersucht. Grundlegende Grenzen der klassischen Regelung mit Rückführung und der $\mathcal{H}_\infty$-Regler werden diskutiert.

Ein Lautsprecher ist als Aktor für einen proportionalen Regler mit variabler Totzeit und einen $\mathcal{H}_\infty$-Regler im Einsatz. Als Sensoren werden Mikrophone eingesetzt. Die Überlegenheit des modellbasierten Ansatzes tritt klar zutage.

Doch es stellt sich das Problem der Aktorsättigung, weshalb ein Gasinjektor im nächsten Schritt verwendet wird. Die chemische Energie des Erdgases erlaubt einen grösseren Wirkbereich, doch ergeben sich Probleme mit veränderten Flammenstrukturen. Verschiedene Reglerarchitekturen werden betrachtet, dabei schneidet der proportionale Regler mit variabler Totzeit für Fälle mit ausgeprägter Druckspektrumspitze zufriedenstellend ab, doch der $\mathcal{H}_\infty$-Regler arbeitet noch besser. Die Flexibilität und Leistungsfähigkeit dieses modernen Reglers zeigt sich vollends im Falle von drei Druckspektrumspitzen, wo es möglich ist in all diesen Frequenzbereichen eine Reduktion zu erreichen. Robustheit gegenüber sich ändernden Bedingungen wird sichergestellt.

Ein neuer Ansatz zur Verbesserung von Reglern bei direkter Anwendung auf dem Prüfstand wird vorgestellt. Es handelt sich um den CMA-ES Algorithmus, der die Minimierung eines Gütekriteriums erlaubt. Dieser Algorithmus kommt auf zwei Reglerstrukturen zum Einsatz.

Der Anhang enthält zusätzliches Material für die interessierte Leserschaft. Weitere Reglerarchitekturen werden diskutiert. Für den historisch geneigten Leser finden sich ein paar Lesestellen im Anhang; und auch thermodynamisch wissensdurstige Leute dürfen sich auf ihr Kapitel freuen.

Der Autor hofft, dass ein paar Ideen aus dieser Arbeit einen kleinen Niederschlag in der Form von verbesserten Gasturbinen finden mögen.

Notation

What's in a name? That which we call a rose
by any other name would smell as sweet.

William Shakespeare, in "Romeo and Juliet"

Symbols

ζ	loss factor in $L - \zeta$ burner model
λ	air/fuel equivalence ratio
ρ	density [kg/m^3]
σ_τ	time delay spread in $n - \tau$ flame model [s]
τ	time delay in $n - \tau$ flame model [s]
ω	frequency [rad/s]

a	duct radius [m]
A	area [m^2]
c	speed of sound [m/s]
C	Controller
f	frequency [Hz]
f_1	Riemann invariant
F_s	sampling frequency [Hz]
g_1	Riemann invariant
i	imaginary unit, $i^2 = -1$
k	wave number, ω/c
L_{down}	length of downstream duct [m]
L_{eq}	averaged sound-pressure level, or equivalent continuous level [dB re 20 μPa]
$L_{ps}(f)$	sound-pressure spectrum level [dB re 20 μPa]
L_{red}	reduced length in $L - \zeta$ model [m]
L_{up}	length of upstream duct [m]
M	Mach number
n	interaction factor in $n - \tau$ model
N	number of points in FFT
p'	acoustic pressure fluctuation [Pa]
P	Plant
R	reflection coefficient
s	Laplace variable, $s = i\omega$
S	sensitivity, $S = (1 - CP)^{-1}$ (positive feedback)
T_s	sampling time [s]
T^b	transfer function matrix of burner
T^f	transfer function matrix of flame
T^{bf}	transfer function matrix of burner and flame
T^{Inj}	transfer function from voltage at fuel injector to spool position
$TF^{P,LS}$	transfer function of the plant with loudspeaker as actuator (from voltage at loudspeaker amplifier to pressure reading) [dB Pa/V]
$TF^{P,Inj}$	transfer function of the plant with injector as actuator (from voltage at fuel injector amplifier to pressure reading) [dB Pa/V]
u'	acoustic velocity fluctuation [m/s]
$\bar{u}$	mean flow [m/s]
V	volume [m^3]
x_i	axial position [m]
Z	impedance

Abbreviations

2MM	Two-Microphone Method
CMA-ES	Covariance Matrix Adaptation Evolutionary Strategy
CO	Carbon Oxide
Dres.	Doctores
Dr. sc. techn.	Doctor scientiarum technicarum
EV	EnVironmental burner, by ALSTOM Ltd.
FFT	Fast Fourier Transform
$\mathcal{H}_\infty$	Hardy space $\mathcal{H}_\infty$ norm
IMRT	Intensity Modulated Radiation Therapy; Institut für Mess- und Regeltechnik
Inj	Fuel injector
LHP	Left-Hand Plane
LMS	Least Mean Square (error)
ln	Logarithmus naturalis, with base e
log	Logarithm with base 10
LQG/LTR	Linear Quadratic Gaussian/ Loop Transfer Recovery
LS	Loudspeaker
$L-\zeta$	$L-\zeta$ burner model
MAVT	Multiple Attribute Value Theory; Multiple Audio-Visual Terminal; Departement Maschinenbau und Verfahrenstechnik
Mic	Microphone
MIPS	Million instructions per second
NARMAX	Non-Linear AutoRegressive Moving Average with exogenous input
NMP	Non-Minimum Phase
NO_x	Nitric Oxides
$n-\tau$	$n-\tau$ flame model
PhD	Philosophical Doctor
PLIF	Planar Laser-Induced Fluorescence
PM	Photomultiplier; Particulate Matter
ppmvd	parts per million by volume of dry exhaust gas corrected to standard pressure and temperature
RHP	Right-Hand Plane
STR	Self-Tuning Regulator
TF	Transfer Function
UHC	Unburnt Hydrocarbons

1

Thermoacoustic Oscillations

The Wolf: I'm Winston Wolf. I solve problems.
Jimmie: Good, we got one.

From "Pulp Fiction", by Quentin Tarantino

1.1 Abatement of Emissions: Solutions and Problems

Modern premixed gas turbines have to comply with continually more stringent emission regulations (NO_x, CO etc.), and traditional methods of reducing NO_x (water and steam injection) cannot reach those extremely low levels required. Therefore, the equivalence ratio (or mixture ratio, defined as the ratio of fuel/air used to stoichiometric fuel/air ratio) is reduced, which brings the combustion into a regime called "dry lean". This means that the combustors operate with excess air to cool down the combustion temperature. The Zeldovich mechanism states that the formation of NO_x is exponentially dependent on temperature, which shows the benefits of lean combustion.

However, this regime makes the combustor prone to thermoacoustic instabilities, blowout, and flashbacks. The flame becomes much more sensitive to disturbances of pressure, velocity, and equivalence ratio. Thus, the flame anchoring and fronts are perturbed; shear layers and recirculation zones are altered. The acoustic damping of the combustion chamber is reduced, because of lacking dilution air downstream.

If the heat release and pressure fluctuations are properly phased, the flame feeds energy into the acoustic field. This in turn influences the flame and closes a (potentially) unstable feedback cycle, called thermoacoustic instability or oscillations.

Combustion instabilities are the most common form of thermoacoustic instabilities, where energy is transferred from a heat source to a fluid causing oscillatory fluctuations in heat release and pressure.

This phenomenon occurs in lean premixed low emission gas turbines, jet engines, afterburners, liquid-fueled rocket motors as well as domestic burners. Practitioners call the resulting noise "rumble", "growl", "howl", and "humming".

Four modes of unstable combustion can be distinguished:

- bulk: also known as Helmholtz mode or called "buzz". In this case, the pressure varies only temporally but not spatially, the important parameter is the volume of the combustor. Unstable frequencies of less than several hundred Hz.

- longitudinal: also called "rumble". It is strongly dependent on the acoustic length of the combustor. Unstable frequencies of several hundred Hz but less than 1 kHz.

- circumferential: this mode depends on the circumference of the annular combustor with several burners.

- transverse: also called "screech", occurs mostly in afterburners.

The ensuing unsteady heat release and pressure oscillations lead to excessive vibrations resulting in mechanical failure, high levels of acoustic noise, high burn rates, and possible component melting [8, 198, 79]. In addition, higher heat transfer rates to the walls and increased emissions of pollutants such as unburnt hydrocarbons or oxides of nitrogen are observed. The pressure oscillations constitute between 1 and 10% of the mean operating pressure, and since today's combustors work with pressures up to 35 MPa, these fluctuations are of considerable amplitudes [239, 49]. However, pressure oscillations are desired in certain devices such as ramjet engines and pulsed combustors.

A number of passive and active strategies have been employed in the past to mitigate these problems. The installation of dampers, baffles, and vortex generators is aimed at increasing damping and disrupting the phasing between heat release and pressure. On the other hand, active control algorithms monitor the pressure or another performance signal and take action accordingly, through an actuator such as a loudspeaker or auxiliary fuel injection.

The term "instabilities" is often used interchangeably with "oscillations", as it is often difficult to determine whether the system is (linearly) unstable and saturated, or just lightly damped and noise driven. This slight abuse of notation should not cause any confusion.

1.2 Instability Mechanisms

At the core of thermoacoustic instabilities lies the coupling between the unsteady components of pressure and heat release rate. Atomization and vaporization play important roles for liquid-fueled combustors.

The often stated Rayleigh's criterion is as follows [256]: "If heat be periodically communicated to, and abstracted from, a mass of air vibrating in a cylinder bounded by a piston, the effect produced will depend upon the phase of the vibration at which the transfer of heat takes place. If heat be given to the air at the moment of greatest condensation or to be taken from it at the moment of greatest rarefaction, the vibration is encouraged. On the other hand, if heat be given at the moment of greatest rarefaction, or abstracted at the moment of greatest condensation, the vibration is discouraged". Mathematically stated, it is given by Eq. 1.1, from [79], with the pressure, density, heat-release rate per unit volume, particle velocity, speed of sound, and ratio of specific heat capacities denoted by $p, \rho, q, \mathbf{u}, c$ and γ, respectively. Mean and fluctuating values are denoted by an overbar and by a prime, respectively.

$$\frac{\partial}{\partial t}\int_V \Big(\underbrace{\frac{1}{2}\overline{\rho}\mathbf{u}^2}_{kinetic} + \underbrace{\frac{1}{2}\frac{p'^2}{\overline{\rho}\overline{c}^2}}_{potential}\Big)dV = \int_V \underbrace{\frac{\gamma-1}{\overline{\rho}\overline{c}^2}p'q}_{Rayleigh}\,dV - \int_S \underbrace{(p'\mathbf{u})}_{surface}\,d\mathbf{S} \tag{1.1}$$

The first two terms denote the kinetic and potential energies, and the first term on the right-hand side is Rayleigh's integral. It can be seen that if p' and q are in phase, the integral is positive. Finally, the last term describes the surface loss terms.

Thermoacoustic instabilities may be caused by fluctuations in the air supply to the burner, by aerodynamic (intrinsic) instabilities or by perturbations in the fuel supply, where the pressure waves interact with the fuel nozzle [120, 198, 49]. These equivalence ratio perturbations happen when a positive pressure excursion produces a decrease of the fuel supply at a later instant. Local extinction and re-ignition within the flame may be due to maldistributions in the fuel distribution. Large-scale structures such as vortices are also involved.

The periodic heat released by the flame gives rise to pressure fluctuations, which are reflected back to the flame. If they are coupled such that Rayleigh's criterion is fulfilled, this process is sustained. The flame may wrinkle and increase its surface area, and change its position.

Interestingly, this mechanism can also be reversed and used to build a thermoacoustic refrigerator [266, 167, 183, 297, 296]. A thermoacoustic Stirling heat engine is proposed in [16], and used in [252] to drive a pulse tube cooler (PTC), which reaches 80 K ($-193\,^{\circ}$C). Such devices contain no moving mechanical parts, no environmentally

hazardous substances, and reach high efficiencies. Potential applications are in space exploration (Space Shuttle mission STS-42 in 1992) and liquifying natural gas[1]. A "SoundsCool" freezer from ThermoAcoustics Corp. cools "Sweet & Sonic" ice cream at Ben & Jerry's in New York City, using a loudspeaker emitting 195 dB of sound [32].

1.2.1 Premixed Swirl-Stabilized Burners

The ETH combustor works in premix operation, so that fuel feed line dynamics and equivalence ratio fluctuations are of minor importance.

The installed lab-scale ALSTOM EV (EnVironmental) burner is discussed [222]. It has the unique property of flame stabilization in free space near the burner outlet utilizing the sudden breakdown of a swirling flow, called vortex breakdown.

Vortex shedding for dump combustors is studied in [274]. The shear layer develops instability waves in its initial region. When the amplified waves reach a certain energy level, they roll up into vortices. In the early phase of the vortex development, with the unburnt mixture on one side of an interface and the hot combustion products on the other side, mixing and burning are limited. When the vortex roll-up process is followed by interaction between vortices and/or side walls, a large interface between the air/fuel mixture and hot products develops, leading to fine-scale turbulence enhancement and sudden heat release. The associated acoustic velocity fluctuations then trigger the next cycle of vortex shedding [49].

Unsteady flame dynamics in a lean premixed swirl-stabilized combustor are addressed in [129, 128]. A central toroidal recirculation zone is established in the wake of the center body under the effects of the swirling flow (vortex breakdown). As a result of the sudden increase in combustor area, a corner recirculation zone is also formed downstream of the backward-facing step.

The flame can be anchored in the center or in both the center and outer recirculation zone. This depends on the flame speed, which is influenced by the preheat temperature and the equivalence ratio. Hysteresis is related to the heating of the combustor walls.

Large-scale vortex structures can influence the turbulent flame speed and the flame area [159].

More on the role of coherent large-scale structures can be found in [276, 231, 129, 226, 273, 244, 198, 153, 193, 82].

[1] And, just like in the Middle Age: "to give a small quantity of Beer &c. a moderate degree of coolness" [10].

1.3 Approaches to the Problem

Combustion instabilities became a serious issue in liquid-fueled rocket engines before and during World War II. However, the installation and cooling of pressure transducers was difficult. The first theoretical considerations were done in the 1950's on liquid-fueled rocket motors [65, 264], and the development of the F-1 engine for the Apollo space vehicle increased the efforts, see [214, 67] for a review. Active control of thermoacoustic oscillations was first applied to for Rijke tubes in the 1980's [37, 35, 300, 194, 34, 93]. Due to new environmental standards requiring more stringent emission levels both for aircraft and land-based gas turbines, the interest in modeling and active control grew steadily [181].

1.3.1 Passive Control

A number of passive ways to suppress instabilities exists [28, 84, 8]. They can be classified into two categories:

1. Reduction of the coupling between heat release and acoustics. Therefore, less energy is fed into the unstable acoustic modes by

   - changing flame anchoring point
   - affecting vortex shedding [234]
   - changing acoustic boundary condition
   - changing fuel line dynamics
   - changing fuel injection pattern [198]

2. Increase of (acoustic) energy losses in the combustor is achieved by

   - installing baffles
   - acoustic dampers
   - geometric changes of the combustion chamber

Reducing the coherence of large-scale vortices and generating axial vorticity is another passive approach [234, 228, 88, 240, 274]. This may be accomplished by extending the fuel injecting lance so that the vortices break down [222], or to install distributed vortex generators [234]. Changing the burner shape is also an option [225].

1.3.2 Active Control

Active control methods are becoming more promising with the introduction of new sensor, actuator, and computing technology.

Active control methods are advantageous because they can [8]:

- reduce pressure oscillations
- reduce pollutants (NO_x)
- increase combustion intensity
- operate combustors beyond their natural flammability limits
- be applied in a wider frequency band than passive control
- cope with changing operating conditions
- allow design changes, for example shorter combustors

Available sensors are piezoelectric and moving coil microphones to detect pressure fluctuations; photodiodes and OH/CH chemiluminescence to measure heat release rates. Radiometers measure CO and CO_2; NO_x can be determined, and Laser velocimetry and Schlieren photographs show the flame shape.

Actuators introduce perturbations in acoustic pressure, velocity, vorticity, fuel or air mass flow, or heat release. Mostly used are fuel stream oscillation devices and speakers; oscillating center bodies, moving flaps or airfoils, single or several stream-wise or cross-stream jets, swirl generators or heating elements are reported, too [8]. (Secondary) fuel injection uses small fractions of power generated in the system, whereas mechanical methods which use loudspeakers or moving bodies are less feasible due to the high energy density in the combustor [147, 105].

An active control algorithm has been applied to a Siemens-Westinghouse heavy-duty V94.3A 267 MW gas turbine in January of 1999. Two circumferential modes in a 24 burner configuration are controlled with secondary fuel injectors using a phase-shift strategy [181, 283].

Summary

This chapter has given an introduction to and classification of thermoacoustic instabilities. It explained mechanisms that are particular to swirl-stabilized burners, and laid out both passive and active control strategies.

2

Literature Review

Ἐν ἀρχῇ ἦν ὁ λόγος
Κατά Ιωάννην

2.1 Reported Control Concepts

In general, it is difficult to compare the achievements of the different controllers directly against each other, since the range of combustor setups used varies by a great degree (liquid, gaseous, laminar, swirl-, dump-, bluff body-stabilized, different power ratings). Moreover, various sensors and actuators are used (microphones and photomultipliers, loudspeakers and fuel injectors being the most common).

One more important distinction has to be made. Most of the researchers class their combustor behavior as "unstable" and as being in a limit cycle, except in [47, 20, 59, 48], which are rated as lightly damped. The reduction of the noise in an unstable combustor can usually be seen at all frequencies [263], and may be very large. Reducing the sound pressure is thus a task of stabilizing a plant. Conversely, making a stable combustor more silent is a problem of noise suppression.

The easiest and ubiquitous control strategy is **phase-shift** or **Gain-Delay** control [38, 154, 283], where the sensor signal is multiplied with a gain and delayed by a certain amount and sent to the actuator. This controller is easy to implement and often gives satisfactory results. Manual tuning is usually employed.

Subharmonic fuel injection is tried in [135, 140, 52]. Although it is found to work for some particular conditions, it can be conjectured that the flame is just locally enriched (yielding a different global equivalence ratio) and thus stabilized.

In an early paper [154], a swept-sine signal is used to find the transfer function of a combustor equipped with on/off fuel valves in a stable condition. The parameters of a second-order system are then adjusted so that an unstable plant can be described. In the Nyquist plot, the parameters of a phase-shift controller are found such that the

closed-loop plant is stabilized. A similar approach is followed in [59, 20], but here a stable system is fitted.

The **Least-Mean-Square** error method (LMS) and its derivations (x-LMS, u-LMS, leaky) have been used with mixed success—feedback loop instabilities and algorithm divergence occur [139, 33, 299, 4, 204, 11]. Furthermore, there are no theorems that guarantee global stability. An improvement is shown in [92, 90].

A so-called **Self-Tuning Regulator** (STR) [93, 90, 263, 262, 91] only needs knowledge of the time delay, and shows some robustness against changing operating conditions. In two semester theses [201, 265], it is concluded that for a combustor which is already stable, the STR does not offer advantages over a model-based controller. In particular, numerical problems may arise.

Loudspeakers controlling vortex shedding and cross-flow jets are implemented as actuators in [216, 215]. Optimization using a downhill-simplex algorithm is performed on the frequency of the loudspeaker control signal and the cross-flow strength. Note that this yields a *static* control system, not one with pressure feedback. The tradeoff between acquiring repeatable cost functions and short convergence times is highlighted.

In [19, 147], adaptive algorithms are presented. But only simulations are carried out in [147], and only the control phase is updated in [19]. Noise is identified as a problem, and questions about algorithm instability are raised.

A Rijke tube is controlled in [36] with loudspeakers and a neural network, which requires an identification procedure beforehand.

The fuel flow through different injection locations along the burner is optimized with an evolutionary algorithm in [237].

A range of **lead/lag** controllers are optimized with an evolutionary algorithm in [238, 275]. The influence of the noise is realized, the problem with resulting long evaluation times discussed, and a two-step evaluation proposed (short and long). The maximum number of iterations is fixed to 200.

A loudspeaker is used to control an unstable 1 kW rig in [7]. With an analytical model, an **LQG/LTR** and an $\mathcal{H}_\infty$ **controller** are designed. A linear model valid for the limit cycle of the unstable 114 kW swirl combustor is identified in [206]. About 8% of the total fuel are modulated with on/off injectors, using an LQG/LTR approach. The results are compared with a fixed gain/ variable delay phase-shift controller, which performs worse for one condition but just as well in a one-mode dominated case.

Only simulation studies with an $\mathcal{H}_\infty$ **controller** are reported in [126, 57]. A loudspeaker is used as actuator together with an on/off fuel injector operated open-loop at 400 Hz in a swirl-stabilized 125 kW spray combustor [48]. A stable network model valid between 100–300 Hz is identified and used to design an **LQG/LTR** and $\mathcal{H}_\infty$ **controller**. Small delays are added during the experiments to obtain maximum

attenuation. Only the phase is varied for the phase-shift controller. It turns out that LQG/LTR works best, followed by $\mathcal{H}_\infty$ and phase-shift.

Fuel is modulated in a swirl-stabilized premix combustor [47]. It is identified as a stable but lightly damped noise-driven network model. Two kinds of $\mathcal{H}_\infty$ controllers are tried, and found to work better than phase-shift. However, pollutant emissions can rise for some conditions.

2.2 Work of Various Research Groups

The work of various research groups is presented here, along with more references to publications.

ALSTOM (Switzerland), Ltd, Baden, Switzerland

The structure of instabilities is examined in [229, 230, 228, 233, 275], coherent structures are explained in more detail in [231]. The model of a burner and flame is laid out in [248, 29, 239, 276]. The network model is presented in [279, 223, 277, 278, 236]. A phase-shift controller is implemented in [229, 230, 228, 232, 224]. An evolutionary algorithm working on controller parameters is discussed in [238], while the injection pattern is influenced with such an algorithm in [237, 235]. An $\mathcal{H}_\infty$ controller is shown in [47, 278, 112]. Passive approaches are evaluated in [88, 240, 222, 225, 226, 227], and further in [234, 26, 28, 27]. The ALSTOM EV burner is discussed in [222]. Power Plant CO_2 emissions are treated in [190, 113].

Massachusetts Institute of Technology, Cambridge, USA

Good overviews are given in [8, 9]. This group presents a model based on the acoustic equation with a one- or two-mode Galerkin expansion [8, 5, 6, 121, 99, 119, 118, 110]. A model for a laminar premixed flame similar to a $n-\tau$ model is presented in [98, 6, 220, 221]. Stability of the combustor depends on the position of the flame (Rayleigh's criterion), the first mode is stable and the second unstable. This model is stabilized with a self-tuning phase-lead controller and compared to an LMS algorithm [4, 91]. LQG/LTR and $\mathcal{H}_\infty$ are used in [7, 220, 206], and open-loop control is discussed in [251].

Cambridge University, Cambridge, UK

An excellent review on feedback control of combustion oscillations is [79]. A general overview of the problem is [77], and of the acoustics [80]. A flame model similar to the $n-\tau$ model and further experiments are described in [153, 39]. Yet more modeling is found in [74, 75, 76, 78, 308, 42, 290, 14, 289, 18], passive approaches are considered

in [84, 130]. Simulations with a controller can be found in [56]. A movable centerbody is commanded by a phase-shift controller in [38], this alters the upstream boundary condition of the 250 kW test rig. The unstable frequency lies at 88 Hz. On the same setup, automotive on/off fuel valves are used [154]. The LMS algorithm and a self-tuning regulator are presented in [90, 93, 91, 92, 262, 94, 263]. Robust controllers are discussed in [57].

Georgia Institute of Technology, Atlanta, USA

The Galerkin method in conjunction with combustion instability problems is first mentioned in [309]. Equivalence ratio fluctuations are considered in [182, 180], and limit cycles investigated in [170, 169]. Further statistical analysis is done in [177, 174, 176]. Fuel injection tests are described in [210, 209, 208, 24]. Control using a set of second-order filters is reported in [211], with a prior sweep identification in [134], and phase-shift in [272, 133, 64, 310]. Interactions between flames and acoustic waves are studied in the review paper [173], as well as in [168, 161, 175, 171, 179, 178, 162, 253, 172, 54, 55, 25, 254, 255, 310], and the lean blowout limit in [205].

Centre National de la Recherche Scientifique, and CERFACS, France

Good overviews are [49, 198, 73, 82, 51], and a tutorial [50]. Further investigations are [267, 58, 295, 281, 137, 156, 280, 155, 31, 282, 17]. The role of vortices is discussed in [244, 11], Helmholtz behavior in [307]. Algorithms based on the LMS principle are discussed in [33, 204, 11], more adaptive control is reported in [36, 37, 191]. Flame transfer functions are measured in [81, 30, 81, 298], and the reflection coefficient of a flame is investigated in [243].

United Technologies Research Center, East Hartford, USA

A stable second-order model with delay is fitted to an experimentally found transfer function between valve command and microphone signal in [59, 21, 20]. An analytic model is presented in [241, 147, 63]. A transfer function is evaluated in [12], the effect of Helmholtz resonators in [115]. A phase-shift controller is described in [61, 13, 62], an adaptive controller in [22, 19]. A spinning valve actuator is developed in [23].

NASA Glenn Research Center, Cleveland, USA

NASA's efforts are described in [69, 144, 143, 142, 160, 60]. Models and algorithms adjusting phase-shift controllers are laid out. The importance of the background noise is discussed.

ALSTOM Technology Center, Whetstone, UK

An industrial focus on the problem is reported in [138]. A neural-network predictor is presented in [187], and a controller based on a sine decomposition in [185], emissions are taken into account in [186].

Technische Universität München, Germany

The application of a controller in a heavy-duty gas turbine is reported in [283]. Modeling is done in [218], the $n-\tau$ flame model is extended in [247, 217, 219, 108, 150, 109], a network model described in [148, 158, 249], numerical considerations in [245]. Stability is addressed in [271, 270, 246, 102, 188]. A phase-shift controller and fuel feed line dynamics are discussed in [15].

Deutsches Zentrum für Luft- und Raumfahrt DLR, Stuttgart, Germany

Very detailed investigations of flame structures are reported in [302, 111]. PLIF of OH and CH radicals shows inner and outer recirculation zones in their combustor.

Imperial College of Science, Technology and Medicine, London, UK

Part of the fuel supply is modulated with a phase-shift controller in [284, 250, 68, 87], models of combustion are presented in [136], flame models in [117, 189, 159].

The Pennsylvania State University, University Park, USA

A simulation of a modeled combustor with a PI controller is done in [105, 104, 145]. Subharmonic fuel injection is tried in [135, 140], mechanisms of instability explained in [301, 164, 163]. Especially [129, 127, 128] show the stabilization of the flame in two regions resulting in a stable and an unstable case, similar to the transition observed in the ETH test rig. An $\mathcal{H}_\infty$ controller is simulated in [126].

US Department of Energy, Morgantown, USA

Open-loop injection is reported in [260, 257], passive approaches in [259], general low-emission issues in [258].

Virginia Polytechnic Institute and State University, Blacksburg, USA

Several theses treat modeling of combustors [184, 261, 95], and subharmonic injection [52]. The LMS algorithm is tried in [299], passive control in [89], and adaptive in [300].

Naval Air Warfare Center, China Lake, USA

The importance of coherent flow structures is emphasized in [274, 273]. Lead-lag controllers are applied in [120], phase-shift in [306, 305].

Stanford University, Stanford, USA

A downhill simplex algorithm is used in [215, 216], and the LMS strategy in [139].

California Institute of Technology, Pasadena, USA

A good overview of the problem is given in [66], hysteresis is investigated in [141, 131], experimental studies in [44, 194, 193], and modeling in [3].

Japan Aerospace Exploration Agency, Japan

Steady injection of fuel close to the flame increases the equivalence ratio and stabilizes the flame (causing a diffusion flame), at the expense of higher emissions [293, 269, 122].

Other groups

A general paper is [287]. The gas turbine manufacturer General Electric presents a phase-shift controller [114] and a voice-coil driven fuel injector [197]. An $\mathcal{H}_\infty$ controller is tried in [48, 46]. Helmholtz resonators are also examined in [71, 70, 123, 199, 311, 207]. A NARMAX model is identified in [45, 40] and simulated with a neural controller in [96]. Another nonlinear model is identified in [83]. The Rijke tube is treated in [35, 34, 268]. Characterizations of unstable combustors can be found in [157, 146, 149, 85, 294]. A neural network controller is suggested in [106]. Flame transfer functions are measured in [192], and the choice of actuator/sensor location is studied in [1].

Summary

This chapter has given an overview of relevant contributions to the control of thermoacoustic instabilities, and the work of various research groups has been summarized. The most promising approaches seem to be with secondary fuel injectors as actuators, and model-based controllers.

Der Worte sind genug gewechselt.
Lasst mich auch endlich Taten sehn!
Indes ihr Komplimente drechselt,
Kann etwas Nützliches geschehn.

JWvG

3

Experimental Setup and Characterization of the Test Rig

Sunt facta verbis difficiliora.

Cicero, "ad Quintum fratrem" 1,4,5

3.1 Experimental Setup

A picture of the test rig built at ETH Zürich is shown in Fig. 3.1(a). It belongs to the class of premixed swirl-stabilized combustors with a sudden expansion region. The whole structure visible on the picture stands about 2 meters tall.

The air enters the combustor through the red pipe on the right-hand side and is heated up by an electrical heater. It is premixed with natural gas (CH_4), guided through mixers and flow straighteners into the upstream[1] plenum chamber duct. Fig. 3.2(a) shows the lab-scale ALSTOM EV swirl burner which stabilizes the flame in recirculation regions near the burner outlet plane; the burning flame can be monitored through quartz glass windows. For control purposes, a secondary fuel valve injects natural gas into the burner, see Fig. 3.2(b). The combustion gases are guided through a cooled downstream duct. Various end plates can be installed at the end of this duct, to change the reflection coefficient. A hood covers the end of the downstream duct and guides the hot gases to the exhaust pipe.

A schematic illustration of the test rig is shown in Fig. 3.1(b). The pressure signal is detected by water-cooled microphones (Mic) distributed along both ducts up- and downstream of the burner. For identification purposes, loudspeakers (LS) can be mounted there, too. They are placed in housings and connected by flanges (length 68 mm upstream and 50 mm downstream, diameter 30 mm) to the combustor duct.

[1] the term "up- and downstream" are always to be understood relative to the burner location, and in the direction of the flow.

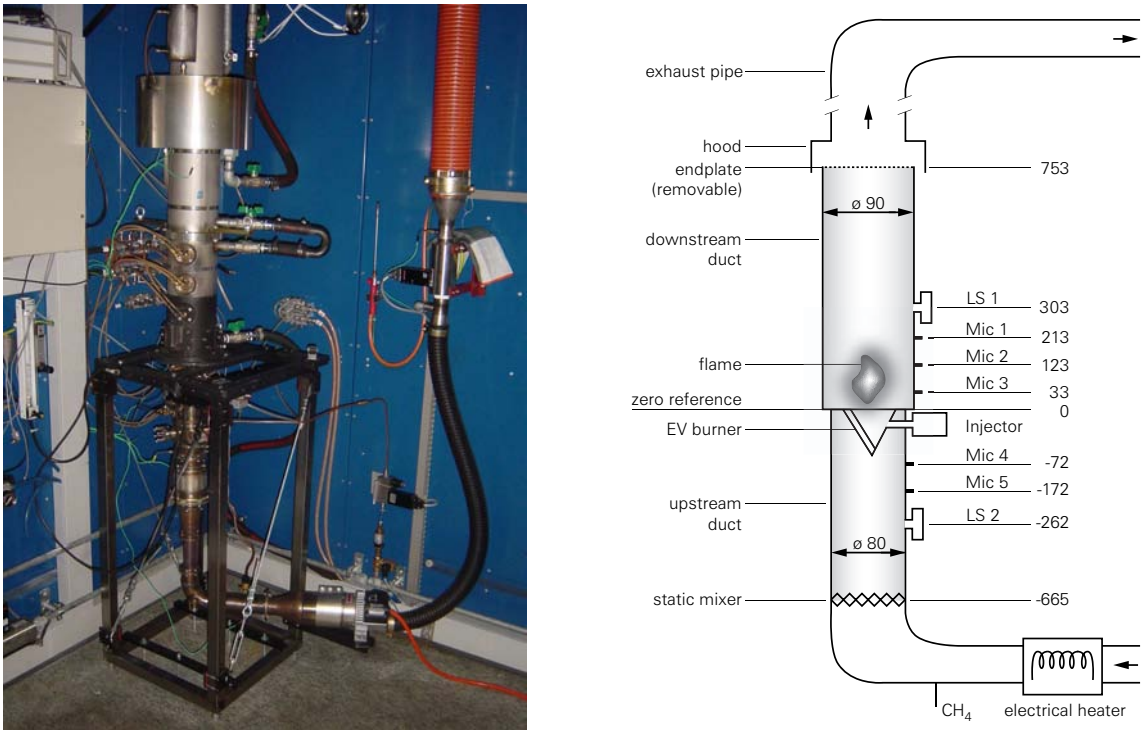

(a) An illustration of the ETH combustor.

(b) The ETH combustor setup.

Figure 3.1: *The ETH combustor. It works in lean premixed mode, burning natural gas in the lab-scale ALSTOM EV burner. A fuel injector is installed for control purposes, loudspeakers (LS) for system identification. Acoustic pressures are sensed with several microphones (Mic). All dimensions in mm.*

The housings and flanges are flushed with cooling air to protect the loudspeaker membrane.

The loudspeakers are also used as actuators for control, but offer only limited actuation power of 30 W each. On the other hand, natural gas has a heating value of 40 MJ/m^3. A secondary fuel injector is therefore installed close to the burner to achieve better results. About 10% of the total methane flow of 1 g/s are modulated, leading to an actuation power (density of methane 0.68 kg/m^3) of about 6000 W.

Fig. 3.2(b) displays the mounted fuel injector on the right-hand side, seen from slightly below. It is water cooled, the natural gas is delivered by a copper pipe, the red wire at the back of the injector carries the spool position signal. The two brass inserts in the upstream combustor duct are water-cooled microphone holders. The flanges at the bottom of the picture can be used to mount loudspeakers.

An HP-9000 system (built 1988, 25 MHz, 8 MB RAM, upgraded to 33 MHz and 24 MB RAM in 1990, 8 MIPS) is used to acquire transfer functions. This is done with

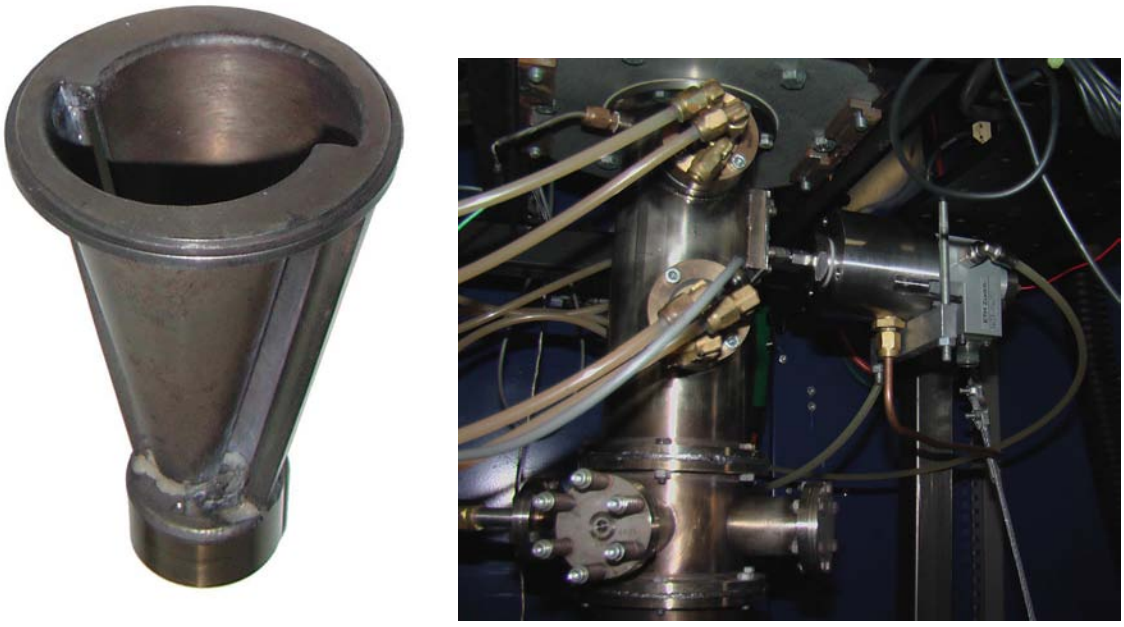

(a) ALSTOM's lab-scale EV burner. (b) MOOG's fuel injector, installed on the test rig.

Figure 3.2: *Photographs of ALSTOM's lab-scale EV burner; and MOOG's fuel injector installed on the test rig.*

swept-sine signals that are sent to an amplifier driving either the loudspeaker or the fuel injector. The output of the plant is usually the pressure read by microphones.

In order to assess the quality of the transfer function measurements, variances and distortions are evaluated. Depending on the noise levels (flame/ no flame), longer integration times are needed to get satisfactory variance levels. Linearity is also confirmed, with the obvious drawback that lower excitation signals require longer acquisition times. Overall, the repeatability is very good. The acquisition time for one frequency sweep (50–1500 Hz, 200 points) for the ETH study is about 20–30 minutes, compared with 15 h reported in [97].

For controller implementation, a dSPACE DS1103 real-time board in conjunction with the MLIB/MTRACE package from Mathworks is used, making direct logging of data to the Matlab workspace possible. Furthermore, controller parameters are directly manipulated on the real-time board from an m-file running on the host computer.

The spectra acquired with a sampling frequency of 200 kHz have shown that higher frequency components are weak compared to frequencies below 5 kHz. Therefore, the sampling frequency is chosen as 10 kHz and no analog anti-aliasing filter is necessary.

A more thorough presentation of the ETH test rig is laid out in [101].

3.2 Acoustics: Techniques and Definitions

3.2.1 Multi-Microphone Method

The acoustic field in the combustor is treated as purely longitudinal, because the cut-off frequency is higher than the frequency range of interest (0–1500 Hz). This cut-off frequency is given by $\omega = 1.841c/a$, c being the speed of sound and a the duct radius [242]. For a temperature of 300 K with a duct radius of 90/2 mm, this gives a cut-off frequency of about 2000 Hz.

Moreover, the geometrical extents of the burner and the flame are small compared to the wavelengths of the frequencies involved, which allows to take only plane waves into account. In this case, the pressure and velocity fluctuations $p'(t)$ and $u'(t)$ are described by the Riemann[2] invariants (characteristic variables) $f(t)$ and $g(t)$ in the following way, with ρ being the density:

$$p'(t) = \rho c[f(t) + g(t)] \tag{3.1}$$

$$u'(t) = f(t) - g(t) \tag{3.2}$$

The two-microphone method [18, 243, 298, 132] is based on the property of the Riemann invariants that at given positions x_i and x_j with mean flow $\bar{u}$ the following relationship applies ($s = i\omega$):

$$f(x_j) = f(x_i)e^{-s\frac{x_j - x_i}{c+\bar{u}}} \tag{3.3}$$

This makes it possible to determine the acoustic velocity and pressure at any position in the duct using only two pressure measurements via the bias of the Riemann invariants.

Problems are expected to occur if the distance between two microphones becomes equal to half the wavelength of interest. In the ETH test rig, this happens for ambient conditions at 1600 Hz, and for hot conditions at 4000 Hz. Another problem may occur if a microphone is placed in a pressure node, but this did not cause any difficulties in the present study. The multi-microphone method uses more than two pressure sensors, such that an overdetermined system has to be solved for the Riemann invariants. In this study, the improvements are not significant and the two-microphone method is applied.

[2] named after Georg Friedrich Bernhard Riemann (1826–1866)

3.2.2 Reflection Coefficients and Impedances

With the aid of Riemann invariants, reflection coefficients at various positions are defined as a function of frequency.

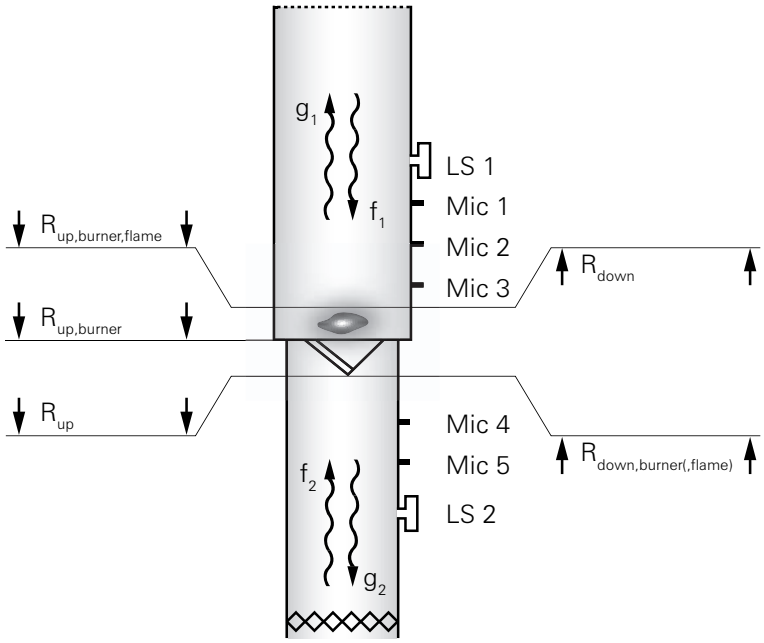

Figure 3.3: *The definition of various reflection coefficients.*

A variety of them are shown in Fig. 3.3. In particular, the *upstream* reflection coefficient R_{up} is measured at a location just *upstream of the burner*. It is defined as the ratio of the Riemann invariant f_2 returning from the upstream end divided by the Riemann invariant g_2 leaving the upstream burner location:

$$R_{up}(i\omega) = \frac{f_2(i\omega)}{g_2(i\omega)} \tag{3.4}$$

The reflection coefficients "looking" *upstream* $R_{up,burner}$ and $(R_{up,burner,flame})$ including the burner (and the flame) are defined for a location just *downstream* of the burner. They provide information about the influence of the burner and the flame.

Similarly, reflection coefficients "looking" *downstream* are defined as R_{down}, $R_{down,burner}$ and $(R_{down,burner,flame})$. The latter two again contain the effects of the burner and the flame, because they are located *upstream* of the burner:

$$R_{down}(i\omega) = \frac{f_1(i\omega)}{g_1(i\omega)} \tag{3.5}$$

Moreover, (scaled) impedances are defined as the ratio of acoustic pressure and velocity:

$$Z(i\omega) = \frac{p'(i\omega)/\rho c}{u'(i\omega)} \tag{3.6}$$

And lastly, reflection coefficients and impedances are related by the following properties:

$$Z = \frac{1+R}{1-R} \qquad R = \frac{Z-1}{Z+1} \tag{3.7}$$

3.2.3 Averaged Sound-Pressure Level and Spectral Density of Pressure

The averaged sound-pressure level or equivalent continuous level L_{eq} of a pressure (fluctuation) signal $p(t)$ is defined relative to a reference pressure[3] $p_{ref} = 20$ μPa. Thus following [124] with T being the time window of interest

$$L_{eq} = 10 \log_{10} \frac{1}{T} \int_0^T \frac{p^2(\tau)}{p_{ref}^2} \, d\tau \tag{3.8}$$

or equivalently, $(p^2)_{av}$ being the mean squared pressure [242]

$$L_{eq} = 10 \log_{10} \frac{(p^2)_{av}}{p_{ref}^2} \tag{3.9}$$

On the other hand, the spectral density $L_{ps}(f)$ is a function of the frequency f. It is defined as a sound-pressure spectrum level [242]

$$L_{ps}(f) = 10 \log_{10} \frac{p_f^2(f)(\Delta f)_{ref}}{p_{ref}^2} \approx 10 \log_{10} \frac{(p_b^2)_{av}(\Delta f)_{ref}/(\Delta f)_b}{p_{ref}^2} \tag{3.10}$$

where $p_f(f)$ is the spectral density of $p(t)$, $(\Delta f)_{ref}$ is a reference bandwidth (taken to be 1 Hz), and $(p_b^2)_{av}$ is the contribution to the mean squared pressure from a band of width $(\Delta f)_b$ centered at the frequency f. Since this process involves an averaging process for each frequency bin, the height of sharp peaks depends crucially on the choice of the Fourier Transform parameters. The frequency resolution is given by $\Delta f = \frac{2\pi}{N \cdot T_s}$, N being the number of points considered and T_s the sampling time. Increasing N thus leads to better frequency resolution Δf at the expense of less averaging per bin, creating a fluffier and furrier look of the Fourier transform, see Fig. 3.4. When the Fast

[3] The decibels of sound quantities in this thesis are always relative to $p_{ref} = 20$ μPa, unless otherwise stated.

Fourier Transform is carried out using 2^{15} points, the highest peak measures nearly 8 dB more than the one calculated with 2^{10} points. Therefore, it should be kept in mind that reductions of the peak spectrum value are afflicted with this uncertainty. The averaged sound-pressure level L_{eq} on the other hand does not suffer from this shortcoming.

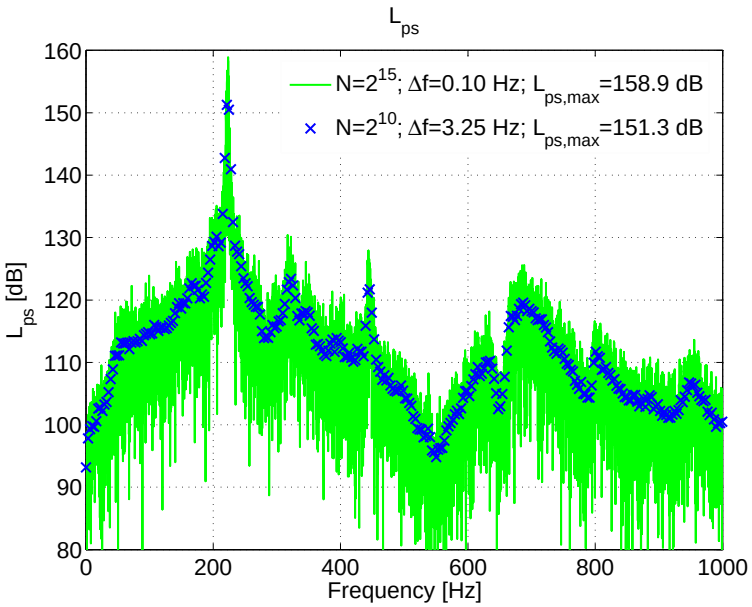

Figure 3.4: *The influence of the number of points N used in the Fast Fourier Transform on the frequency and amplitude resolution of the spectrum. Taking more points yields a better resolution Δf and sharper peaks at the expense of more noise.*

3.3 Operating Conditions, Coding Conventions

Investigations are carried out for various operating conditions, guided by the identification of the flame types in [101]. They are characterized by the air mass flow in g/s, the air preheat temperature in K and the fuel equivalence ratio λ, giving a triple for each operating condition. In order to facilitate the notation, the units are omitted and only the numerical values are written down.

For instance, 36/700/2.1 refers to the case with an air mass flow of 36 g/s, an air preheat temperature of 700 K and a λ of 2.1. This case features a strong instability with a distinct peak at 218 Hz, it is identified as flame type IIb, see Fig. 3.5(a). A similar flame type is 34/600/1.9. In contrast, the leaner type Ib case 36/700/2.4 is more stable. The slightly cooler case 36/650/2.1 is similar to 40/550/1.9, both are of

the more stable type IIa. Finally, 40/700/1.9 is a flame type IIIa. The various flame types are exemplified in Fig. 3.5(b). Flames of type Ia and Ib are burning only in the inner recirculation zone. By contrast, flame types IIb and IIIa are characterized by the flame moving into the outer recirculation and burning there as well.

The pressure spectra L_{ps} read with a microphone downstream at 123 mm are shown in Fig. 3.6(a), where the pressure data has been sampled at F_s=25 kHz. Fig. 3.6(b) shows the same data downsampled with a factor of 12, yielding a sampling frequency F_s of 2.08 kHz. Note that some aliasing effects are noticeable for the case 36/700/2.4, but the other cases benefit from the higher frequency resolution (the peak at 218 Hz for the case 36/700/2.1 is higher, see Fig. 3.4, where this effect is discussed). The spectra of the pressure read upstream at −172 mm are shown in Figs. 3.6(c) and 3.6(d) for a sampling frequency of 25 kHz and 2.08 kHz, respectively. In general, the levels are about 10 dB lower than in the downstream part, where the flame is burning.

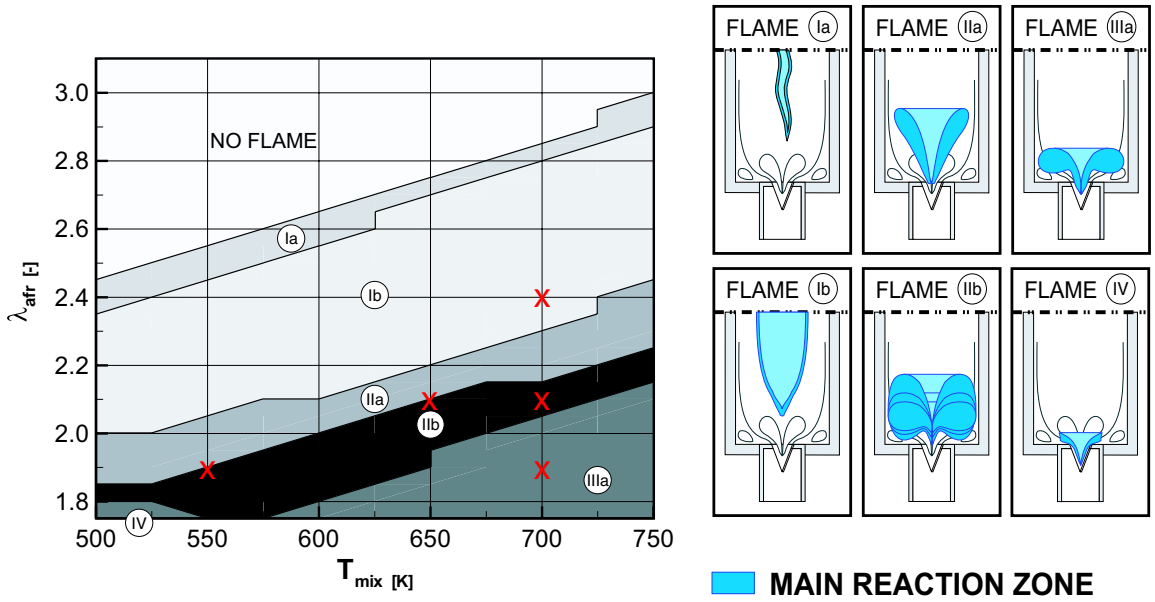

(a) The map of operating conditions. Red crosses indicate cases investigated more closely.

(b) Various flame types.

Figure 3.5: *The map of operating conditions and identified flame types. From [101].*

A second harmonic at 436 Hz is clearly visible in the microphone spectrum for 36/700/2.1. At first, it was suspected that this is due to microphone distortion [43], but further analysis showed that it also exists in the upstream duct, where the noise level is lower, see Fig. 3.6(d). The current understanding therefore suggests that flame saturation is involved.

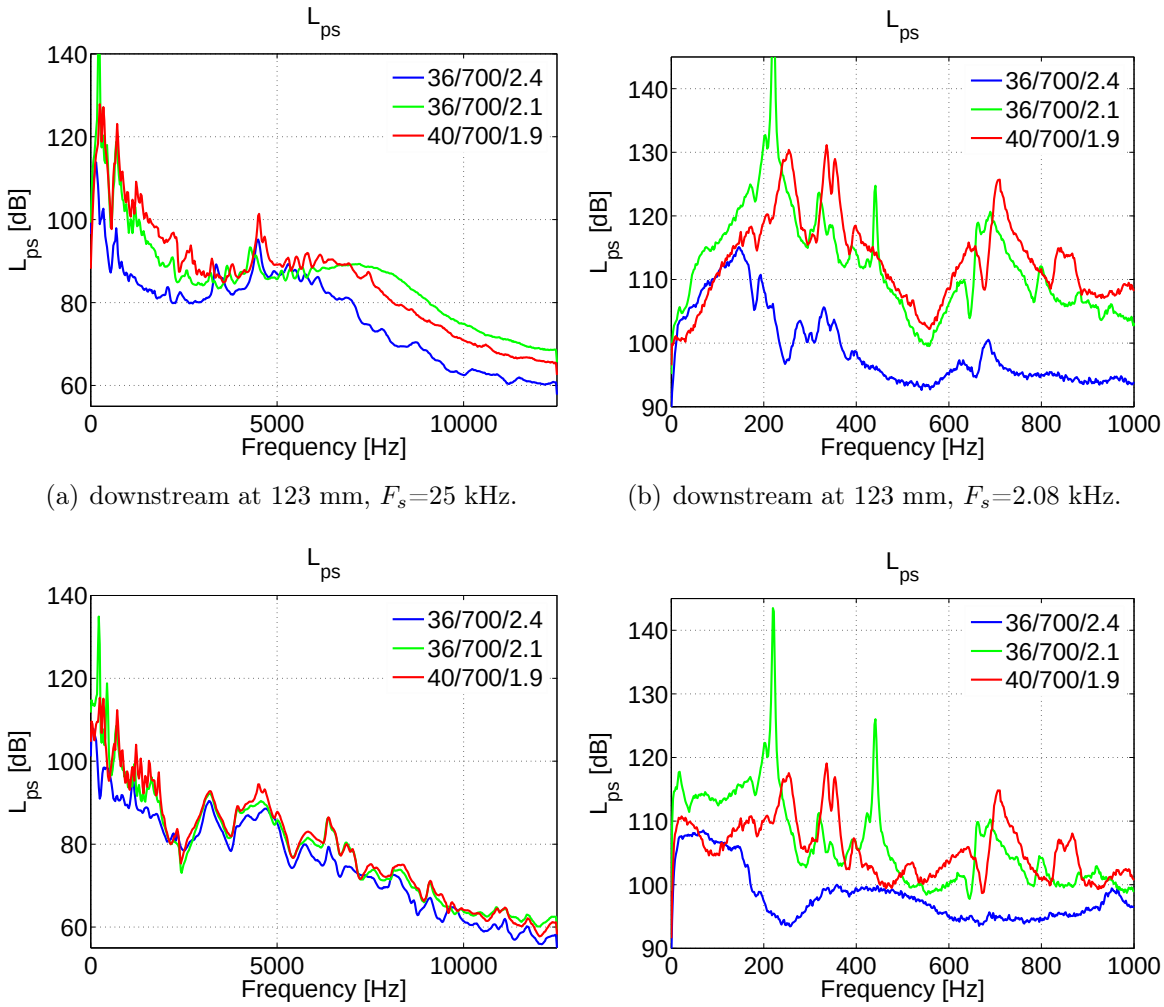

(a) downstream at 123 mm, F_s=25 kHz.

(b) downstream at 123 mm, F_s=2.08 kHz.

(c) upstream at −172 mm, F_s=25 kHz.

(d) upstream at −172 mm, F_s=2.08 kHz.

Figure 3.6: *The spectrum of the pressure read downstream at 123 mm and upstream at −172 mm for various operating conditions. Sampling frequencies F_s=25 kHz and 2.08 kHz.*

Summary

This chapter has presented the test rig built at ETH Zürich. The flame is swirl-stabilized with a lab-scale ALSTOM EV burner. The operating conditions are categorized as different flame types. The definition of acoustic quantities is given, and some identification techniques are explained.

4

Network Modeling and Identification

Bene diagnoscitur, bene curatur.

4.1 Physics-Based Network Modeling

4.1.1 The Network Model Setup

The analytic model of the combustor is based on a network of different blocks. Each block represents a part of the combustor which is analytically modeled, and experimentally identified [47, 275, 279, 277, 278, 236]. This modular approach offers insight into the intricacies of thermoacoustic oscillations, because the behavior of the blocks can be easily studied.

More specifically, referring to Fig. 4.1(b), the network model consists of an upstream end condition, where the air enters the upstream plenum chamber duct, followed by the lab-scale ALSTOM EV burner and the flame. The hot gases leave the combustion chamber duct through a downstream end condition. An actuator (loudspeaker or fuel injector) introduces acoustic velocity fluctuations into the system, and microphones sense pressure fluctuations.

The signals connecting the blocks are acoustic pressure and velocity fluctuations. More precisely, according to Eq. 3.1, the pressure signal is a *scaled* pressure fluctuation $p'_{sc}(t) = \frac{p'(t)}{\rho c}$. For ease of notation, the subscript is dropped in Fig. 4.1(b). The blocks contain transfer functions relating the outputs to the inputs. They are found analytically based on physics, and relevant parameters are identified experimentally. This is done with a dynamic signal analyzer which sends a swept-sine signal to the loudspeaker and monitors the pressure output of the microphones located up- and downstream. As laid out in Section 3.2.1, the two-microphone method is used to calculate the acoustic velocity and pressure at any location in the duct. Once they are known on both sides of a network element, it is easy to extract the transfer function.

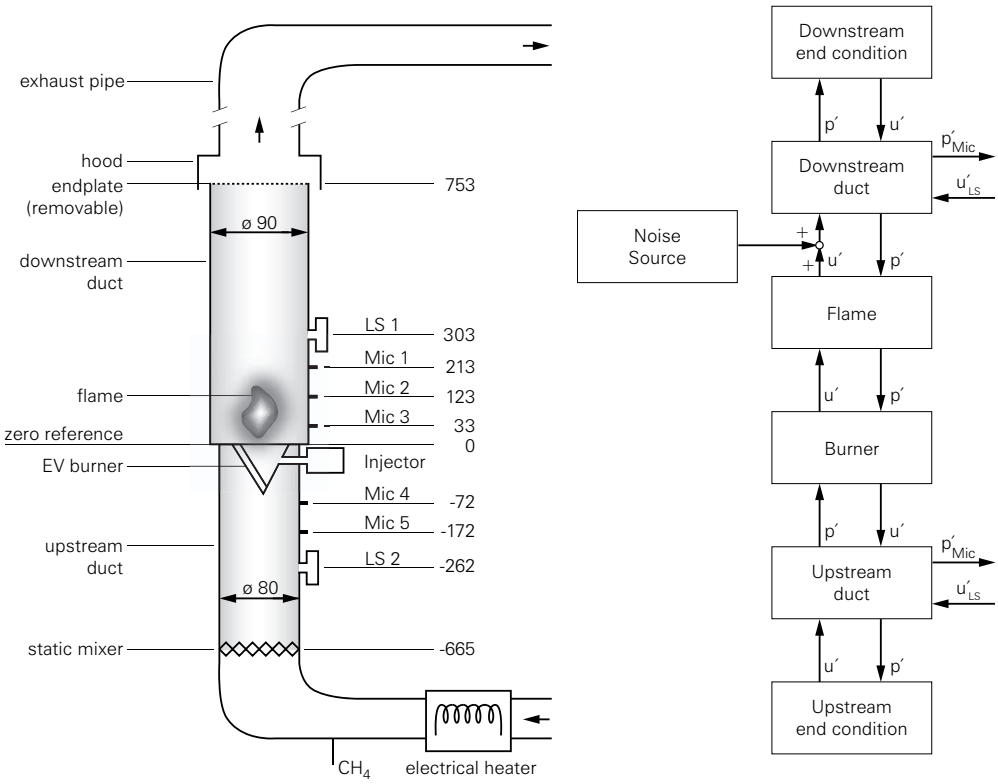

(a) The ETH combustor. (b) The network model.

Figure 4.1: *An illustration of the ETH combustor and the network model. It consists of blocks that are modeled analytically and identified experimentally. The signals connecting the blocks are acoustic pressure and velocity fluctuation.*

In order to determine the transfer matrix of the burner $T^b(s)$, the combustor is run without the flame, and excited with the loudspeakers upstream and then downstream. This assures two independent forcing setups, necessary for the determination of the four elements of this matrix. The transfer function of the flame by itself $T^f(s)$ cannot be measured. Instead, the *combined* transfer function of the burner and the flame $T^{bf}(s)$ is determined as before with the flame burning. Knowing the burner transfer matrix $T^b(s)$, the flame block can easily be extracted: $T^f(s) = T^{bf}(s)\big(T^b(s)\big)^{-1}$.

4.1.2 The Up- and Downstream Ducts and End Conditions

A modal expansion method of the acoustic equation is presented in [278, 275], where a velocity input $u'(t)$ occurs at x_j and the pressure $p'(t)$ is read out at x_k, yielding the following state-space representation for one mode n:

$$\dot{x}(t) = A_n x(t) + B_{nj} u'(t) \tag{4.1}$$

$$\frac{p'(t)}{\rho c} = C_{nk} x(t) + D_n u'(t) \tag{4.2}$$

where

$$A_n = \begin{pmatrix} -\alpha_n & -\omega_n \\ \omega_n & -\alpha_n \end{pmatrix} \quad B_{nj} = \begin{pmatrix} 0 \\ \psi_n(x_j) \end{pmatrix}$$
$$C_{nk} = \begin{pmatrix} 0 & \frac{cA_k}{\Lambda_n}\psi_n(x_k) \end{pmatrix} \quad D_n = \begin{pmatrix} 0 \end{pmatrix}$$

The eigenvector of the duct for mode n is $\psi_n(x)$, the eigenvalue is ω_n, modal damping is α_n, speed of sound c, $\Lambda_n = \int \psi_n^2 dV$, A_j and A_k are the input and output areas, respectively. It is straightforward to increase the number of modes. The pressure can be read out at an arbitrary position inside the duct by manipulating the matrix C_{nk}, and velocity inputs (for instance from the loudspeaker) can be added by changing the matrix B_{nj}.

An important parameter is the length of the duct which determines the modes; and the speed of sound, which is dependent on the temperature. Because of cooling by the walls and mixing effects, it is difficult to find the correct value for the length of the downstream duct with combustion. Therefore, this length is determined without flow at room temperature, and the temperature in the preheated cases is found on the basis of the length determined previously. The linear phase drops ($\angle R(\omega) = -2L\,\omega/c$) of the reflection coefficients R_{up} and R_{down} (see Section 3.1) in Fig. 4.2 are used to find the correct values for the lengths L_{up} and L_{down}.

Upstream Reflection Coefficient R_{up} and Impedance Z_{up}

Fig. 4.2 shows that the upstream reflection coefficient R_{up} depends on the flow, and that more flow is correlated with more damping (less reflection). Moreover, the reflection coefficient is not a constant value but depends on the frequency. The phase of R_{up} decays linearly and identically for all flows, indicating that the length of the duct model has been chosen correctly (and does not depend on the flow).

The measured peaks of the impedances Z_{up} indicate an acoustically closed-closed duct, because they are located at

$$f = n\frac{c}{2L_{up}} \qquad n \in N^+, \tag{4.3}$$

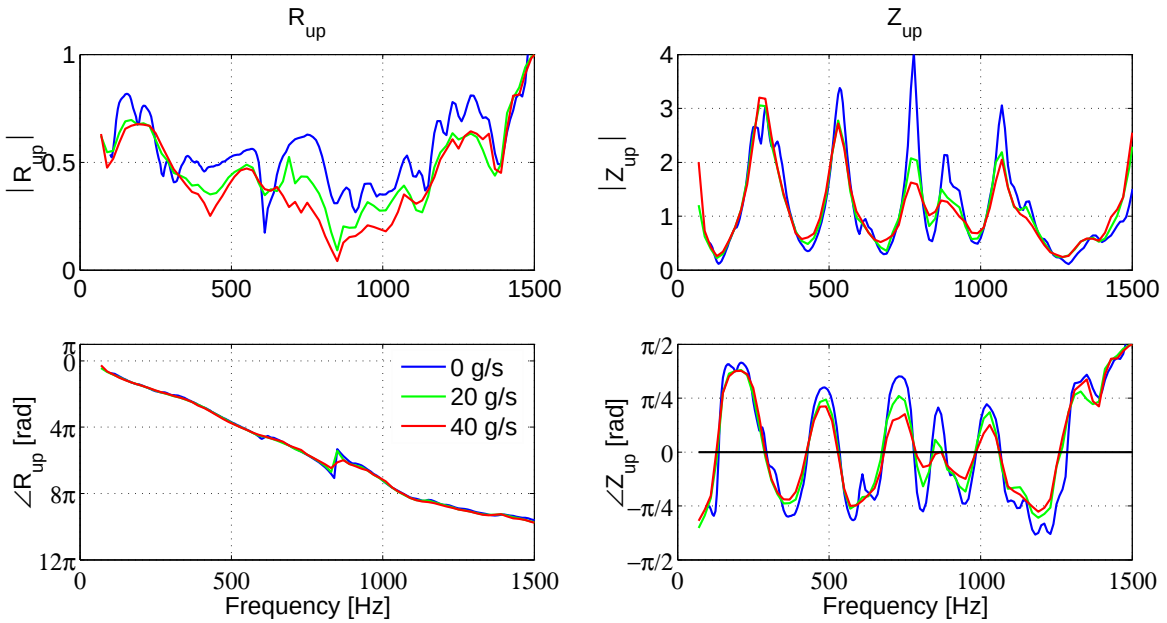

Figure 4.2: *Effect of the flow on R_{up} and Z_{up}. More flow increases the dissipation of acoustic energy and thus decreases R_{up}. The location of the impedance peaks is not affected, but their height is. Ambient conditions.*

and since the phase of Z_{up} stays within $\pm\frac{\pi}{2}$ rad, it is a passive end.

The effect of the preheat temperature on R_{up} and the impedance Z_{up} is exemplified in Fig. 4.3. Three cases are considered, namely 300 K, 450 K, and 700 K. For a set preheat temperature of 700 K, the actual value relevant for the acoustics is 620 K, due to cooling at the combustor walls.

It can be seen that higher temperatures shift the resonances of Z_{up} to higher frequencies. Conversely, the phase of R_{up} also decreases faster, since the speed of sound increases for higher temperatures.

Table 4.1 summarizes the calculated frequencies of the first four upstream modes for preheat temperatures of 300 K, 450 K, and 700 K, respectively.

Table 4.1: *The calculated frequencies of the first four upstream modes for three preheat temperatures. Compare with Fig. 4.3.*

T_{up} [K]	c [m/s]	1st [Hz]	2nd [Hz]	3rd [Hz]	4th [Hz]
300	347	261	522	783	1044
450	425	320	639	959	1278
700	499	375	750	1125	1500

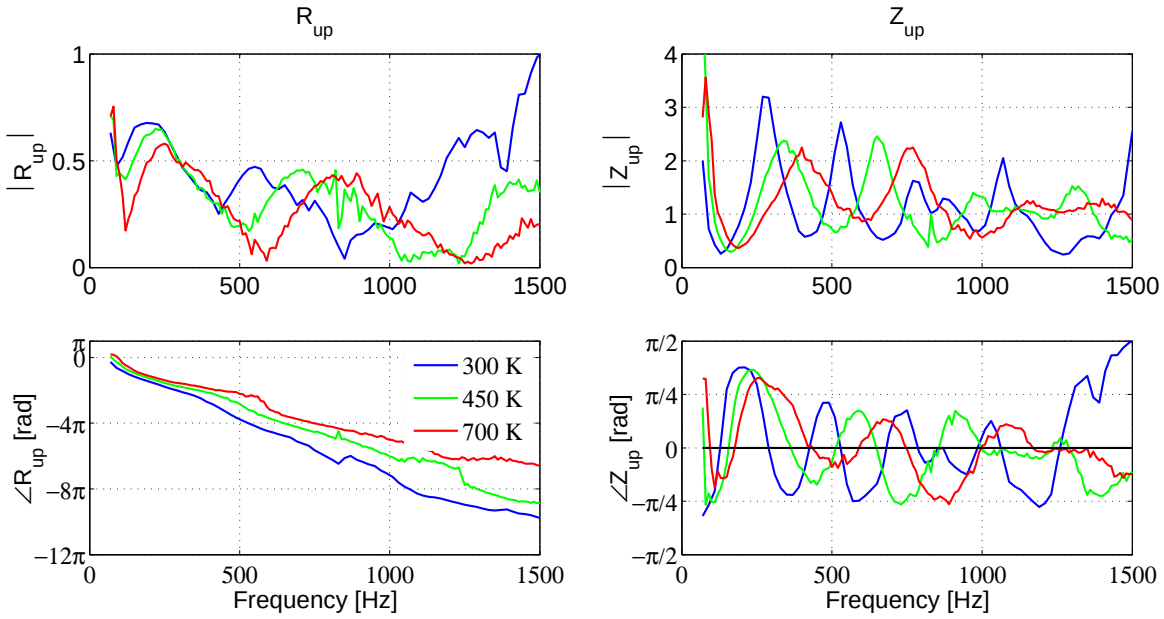

Figure 4.3: *Effect of the preheat temperature on R_{up} and Z_{up}. The phase of R_{up} decays faster at higher temperatures, and the impedance peak locations are shifted to higher frequencies. Compare with Table 4.1.*

Downstream Reflection Coefficient R_{down} and Impedance Z_{down}

The downstream reflection coefficient R_{down} seen from the burner is investigated and the results are shown in Fig. 4.4. The usual combustor configuration is with the exhaust gas hood mounted after the downstream duct, see the schematic of the experimental setup in Fig. 3.1(b). The values of R_{down} are in this case characterized by a regular pattern of low and high values, generally decreasing with frequency (plotted in blue). This is in accord with the theory by Levine and Schwinger [86], plotted in black for the absolute value of R_{down} only.

The green graph shows R_{down} when the exhaust gas hood is removed, which now exhibits a more pronounced spiky behavior. A smoother curve is obtained when the downstream duct is blocked (shown in red), and the absolute value and phase of Z_{down} now show the expected behavior for a closed-closed pipe. The end condition is now changed from an acoustically open to a closed one, as indicated by the impedance Z_{down}; and R_{down} also approaches 1.

It is conjectured that the origin of the spiky behavior lies in the exhaust pipe, which is mounted after the downstream duct, see Fig. 3.1(b). When this pipe is blocked (exhaust blocked) while the downstream duct remains open, the spikes disappear, see the cyan plot in Fig. 4.4.

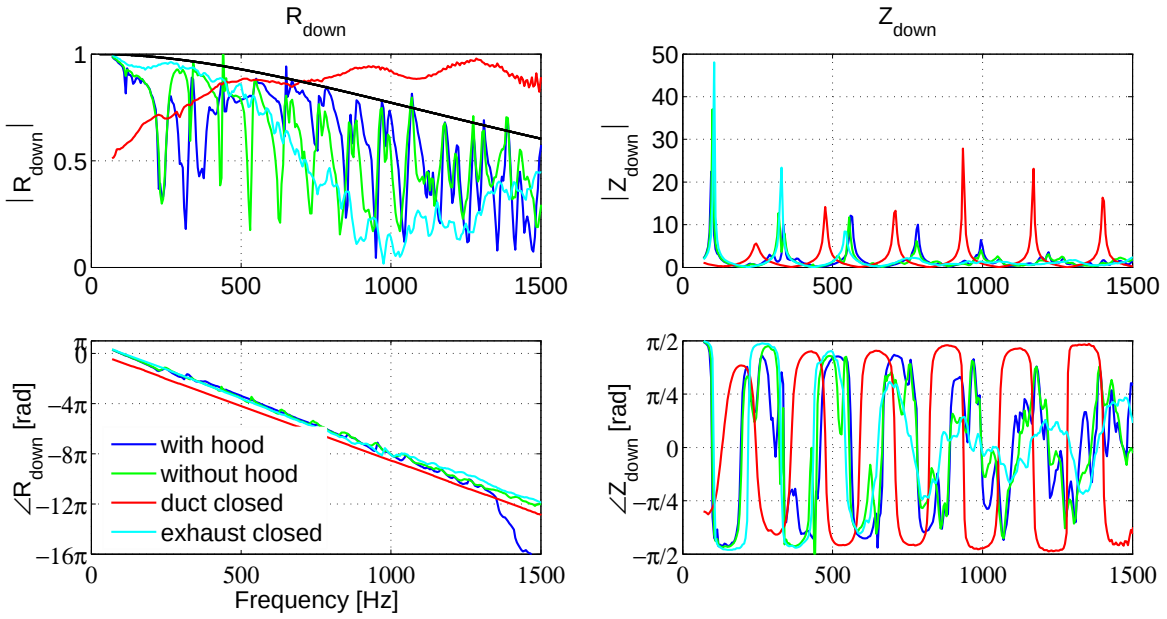

Figure 4.4: *The effect of the hood and the exhaust pipe on R_{down} and Z_{down}. The black graph in the upper left plot shows R_{down} calculated with the theory by Levine and Schwinger. Ambient conditions, no flow.*

The reflection coefficient in the presence of an expansion chamber and multiple echoes is treated in [97]. In particular, an expansion chamber of length l and area A_2 is inserted between two pieces of a duct with area A_1. If the downstream end of the second duct is assumed to be anechoic, the reflection coefficient of a duct in the presence of an expansion chamber $R_{down,ec}$ can be derived (speed of sound c, $\alpha = A_2/A_1$, $\beta = \frac{1-\alpha}{1+\alpha}$, $k = \omega/c$):

$$R_{down,ec} = \frac{\beta(1 - e^{-2ikl})}{1 - \beta^2 e^{-2ikl}} \tag{4.4}$$

The frequency response of $R_{down,ec}$ is plotted in Fig. 4.5. It looks very much like the experimentally observed coefficients R_{down} shown in Figs. 4.4 and 4.6. This analysis thus shows that the exhaust pipe is responsible for the spiky behavior seen in the downstream reflection coefficient.

An improvement could be obtained if the exit reflection coefficient of the second duct is modeled using a Levine-Schwinger end condition [86], and if dissipation is assumed for the area changes in the duct.

Some authors have suggested to install different end plates at the downstream end to decrease pressure oscillations. The influence of such plates as well the effect of the exhaust hood is investigated here. End plates with varying degrees of constriction

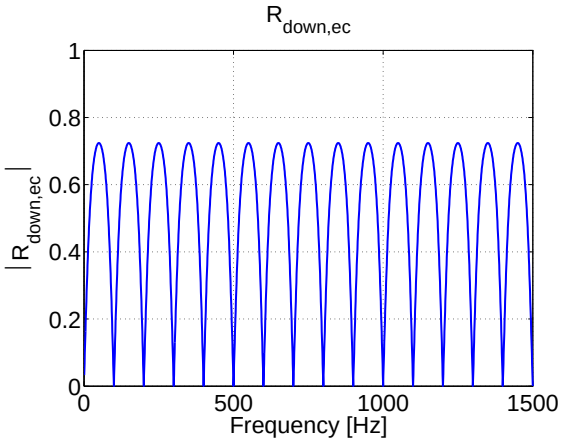

Figure 4.5: *The frequency response of R_{down} with an expansion chamber, given by Eq. 4.4.*

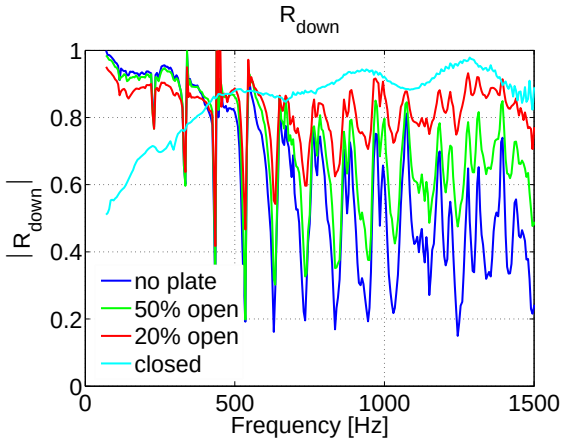

Figure 4.6: *Effect of various downstream end conditions on R_{down}. Ambient conditions, no flow.*

are installed at the end of the downstream duct. Perforated plates with holes of diameter 3 mm and an overall constriction of 50% and 65% are tried, and annular plates featuring one large opening in the middle, constriction is 50% and 80%. The R_{down} is plotted in Fig. 4.6, for the plates with annular constrictions, as well for the case when the downstream end is closed. The effect is confined to frequencies above 400 Hz, but the most amplified frequencies for the operating conditions studied are in the 200 Hz range. The perforated plates feature generally lower reflection coefficients than the annular plates (not plotted). As a comparison, the downstream duct is also closed, giving the highest reflection coefficient (cyan). The influence of the exhaust duct is again seen in all non-closed cases.

In the literature, the standard modeling approach assumes a constant reflection coefficient both up- and downstream. The analysis above shows that such a simplifying assumption may not always be accurate.

In practice when the combustor is running, the endplates do not have a decisive effect on the reduction of the pressure spectrum in the 200 Hz range, so other (active) strategies are pursued. Moreover, the pressure and flow field inside the combustor changes with the addition of such plates, thus altering the operating conditions.

4.1.3 The Burner and the $L - \zeta$ Model

ALSTOM's EV burner features flame stabilization in free space near the burner outlet due to sudden vortex breakdown of a swirling flow. The burner represents an obstacle to the flow, and an area change from A_1 to A_2 occurs at the dump plane. Linearizing

the unsteady Bernoulli and the continuity equations and introducing an acoustic loss factor ζ and a reduced length L_{red} (accounting for capacitance effects) yields in matrix form [248, 275]:

$$\begin{pmatrix} p_2' \\ u_2' \end{pmatrix} = T^b(s) \begin{pmatrix} p_1' \\ u_1' \end{pmatrix} \tag{4.5}$$

where $T^b(s)$ is a 2×2 matrix

$$T^b(s) = \begin{pmatrix} 1 & \rho c\left(M\left(1-\zeta-\left(\frac{A_1}{A_2}\right)^2\right) - i\frac{\omega}{c}L_{red}\right) \\ 0 & \frac{A_1}{A_2} \end{pmatrix} \tag{4.6}$$

The subscripts 1 and 2 denote conditions up- and downstream of the element, respectively, M is the Mach number, c the speed of sound, and $i^2 = -1$.

It is hard to indicate a priori values for the loss factor ζ and the reduced length L_{red}, so they are identified experimentally. The measured value of 0.2 m for L_{red} is very close to the physical length of the burner, and ζ=60. Note that two independent excitation experiments (up- and downstream) are necessary to determine all four elements of the matrix [248, 275].

The four elements of the burner transfer function for the case 36/700/noFlame are shown in Fig. 4.7. Measured values are plotted as red graph, and the frequency response of Eq. 4.6 in blue. The absolute value and the phase of the frequency response for the static element T_{11}^b are plotted in the upper left corner. The lower left corner depicts the element T_{21}^b, and the agreement is also good between theory and experiment. The lower right corner displays the element T_{22}^b, which should be equal to the area ratio A_1/A_2, according to the theory. This is indeed accurately the case. The dynamic element T_{12}^b is plotted in the upper right corner of Fig. 4.7. It relates the upstream velocity to the downstream pressure fluctuations, and the model and measurement agree very well, both in the phase and the absolute value.

The $L-\zeta$ burner model successfully predicts the change in phase between a no-flow and a flow case for ambient temperatures, see Fig. 4.8. The left plot shows the measured and modeled frequency response of the burner matrix element T_{12}^b for ambient temperatures and no flow, while the right plot represents teh case with 20 g/s flow. The absolute value is not influenced much by the flow, but the phase is susceptible to it.

The model of the burner has been found to work well over a very large range of operating conditions. Mass flows from 0–44 g/s, and temperatures from ambient to 700 K have been successfully validated.

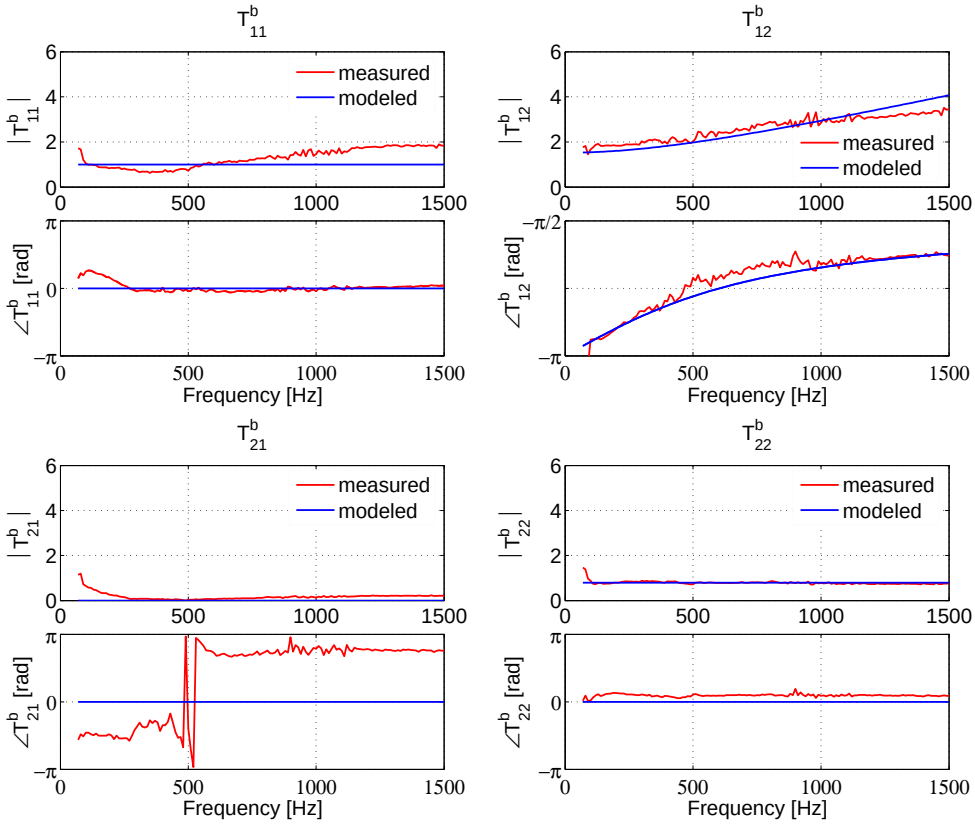

Figure 4.7: *The four elements of the burner transfer function $T^b(s)$, given by Eq. 4.6 for 36/700/noFlame. Very good agreement between theory and experiment.*

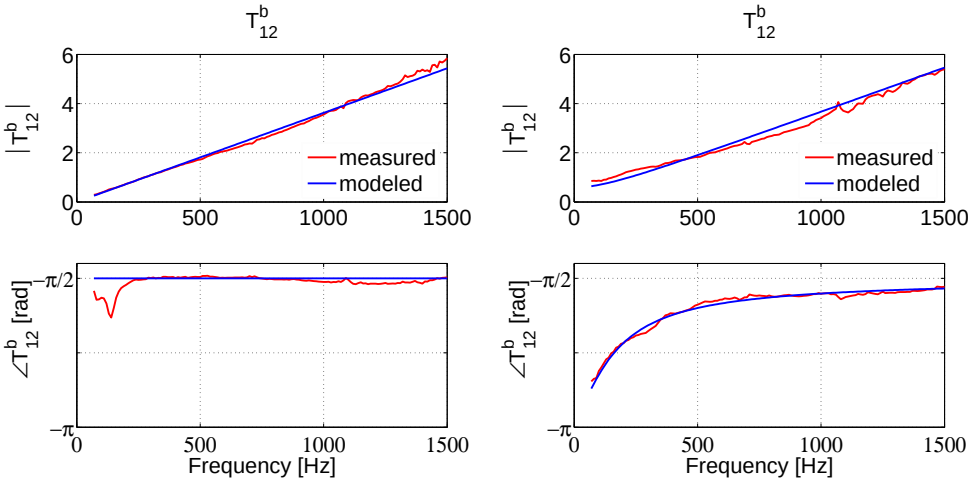

(a) 0/300 (b) 20/300

Figure 4.8: *The dynamic element T^b_{12} of the burner transfer function. Comparison between no flow and a flow of 20 g/s. The model successfully predicts the behavior of the phase.*

4.1.4 The Flame and the $n - \tau$ Model

A vast body of literature about flame modeling exists [98, 198, 275, 152, 82, 247, 55, 81, 30, 217, 219, 108, 150, 54, 14, 290]. For this study, the flame is modeled as an acoustically compact element causing a jump in the acoustic velocity due to heat addition, while continuity of pressure is assumed. The key assumption is that velocity fluctuations at the burner cause heat release fluctuations, after a time delay τ [276, 248, 223, 239]. In our premixed case, equivalence ratio fluctuations are not occurring, because the mixing happens so far upstream that pressure waves are unlikely to influence it. The extended $n - \tau$ model is given in matrix form [275, 278, 277, 29]:

$$\begin{pmatrix} p_2' \\ u_2' \end{pmatrix} = \underbrace{\begin{pmatrix} 1 & 0 \\ 0 & k + ne^{-i\omega\tau} e^{-\frac{1}{2}\omega^2\sigma_\tau^2} \end{pmatrix}}_{T^f(s)} \begin{pmatrix} p_1' \\ u_1' \end{pmatrix} \tag{4.7}$$

The time delay τ is associated with a convective transport lag. This value has a Gaussian distribution with a standard deviation σ_τ^2, which is represented by the term $e^{-\frac{1}{2}\omega^2\sigma_\tau^2}$. The value σ_τ^2 describes the geometrical shape of the flame, and it is indeed observed that visibly longer flames are modeled by higher values of σ_τ^2. Finally, n is an interaction factor, k is a value close to 1, $i^2 = -1$, and ω is the frequency.

The measured and modeled transfer functions of the flame expressed by Eq. 4.7 for the case 36/700/2.4 are displayed in Fig. 4.9. The upper left corner shows the absolute value and the phase of the element T_{11}^f, which is close to 1. The measured and modeled values agree well. The lower left corner depicts the element T_{21}^f, which should be close to 0. The element T_{12}^f is shown in the upper right corner, with a modeled value of 0. Noise is getting an issue at frequencies around 1100 Hz.

Finally, the dynamic element is T_{22}^f, which relates the upstream to the downstream velocity fluctuations. It is plotted in the lower right corner of Fig. 4.9, and again in Fig. 4.10(a), which is done for better comparison with other operating conditions. Both the absolute value and the phase of the frequency response of T_{22}^f are captured well by the model. The dynamic influence of the flame vanishes for frequencies higher than about 300 Hz.

Further cases are compared in Fig. 4.10, namely 36/700/2.4, 36/550/2.1, 36/700/2.1 and 40/700/1.9. As the flame becomes more unstable, the first dip of the absolute value of the frequency response moves to higher frequencies. In parallel, data acquisition becomes more difficult as there is more noise in the system.

The identified parameters of the $n - \tau$ model for various operating conditions are summarized in Table 4.2. The experimentally observed behavior that the flame becomes more compact from flame type Ib to IIb and IIIa is reflected by the decreasing

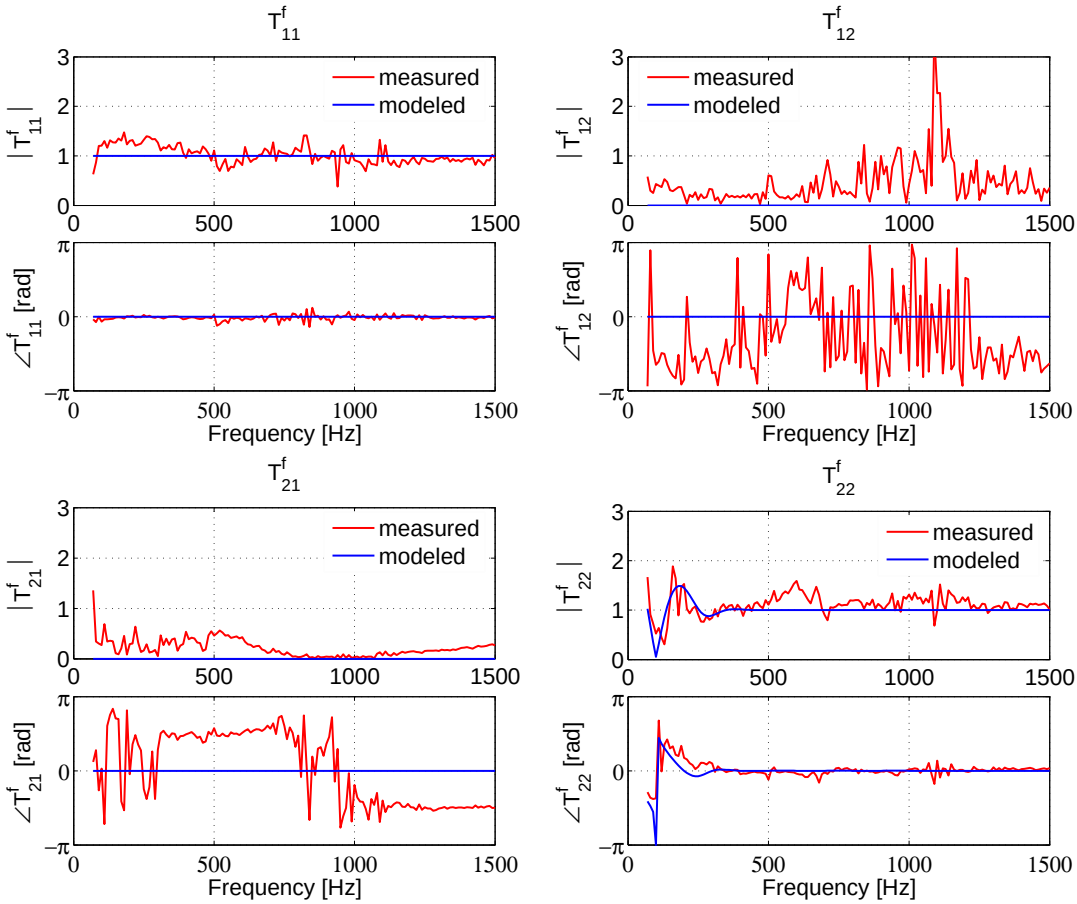

Figure 4.9: *The flame transfer function $T^f(s)$ for 36/700/2.4. The dynamic element T^f_{22} is in the lower-right corner.*

values for the distribution parameter σ_τ shown in Table 4.2. The fact that it retracts closer into the burner is seen in the decreasing value for the time delay τ. The product d of the flow velocity and the time delay is shown in the last column. These results correlate well with optical results indicating the flame size [101].

Table 4.2: *The identified parameters of the $n-\tau$ flame model for various flame types.*

case	flame type	n	τ [ms]	σ_τ [ms]	k	d [m]
36/700/2.4	Ib	1.4	5	1.2	1	0.18
36/550/2.1	Ib	1.3	5	1.0	0.9	0.15
36/700/2.1	IIb	1.2	1.4	0.4	0.8	0.05
40/700/1.9	IIIa	1.5	1	0.2	0.8	0.03

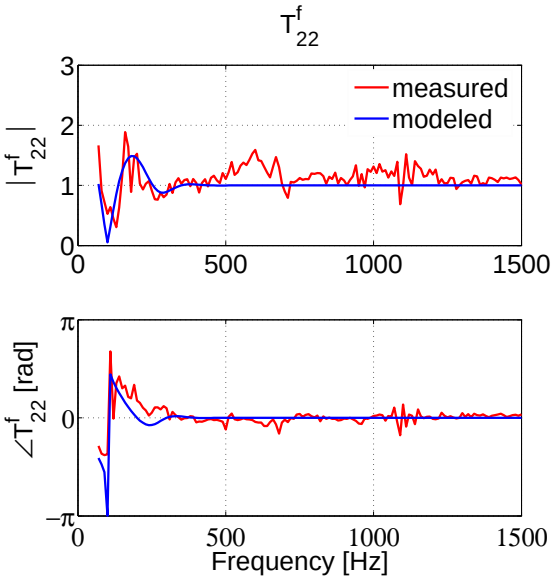

(a) 36/700/2.4, extracted from Fig. 4.9. Flame type Ib.

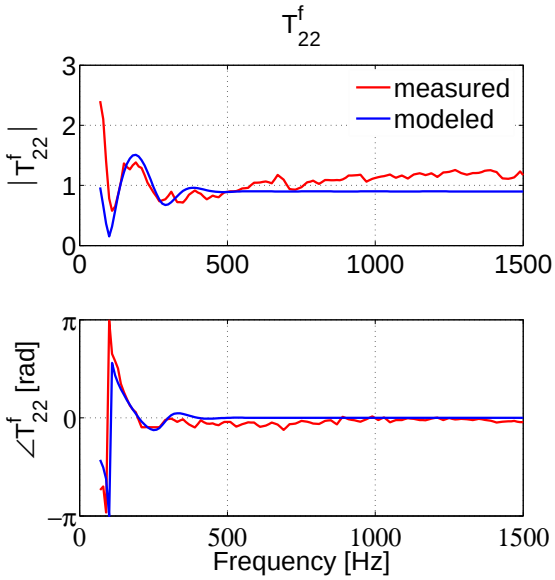

(b) 36/550/2.1. Flame type Ib.

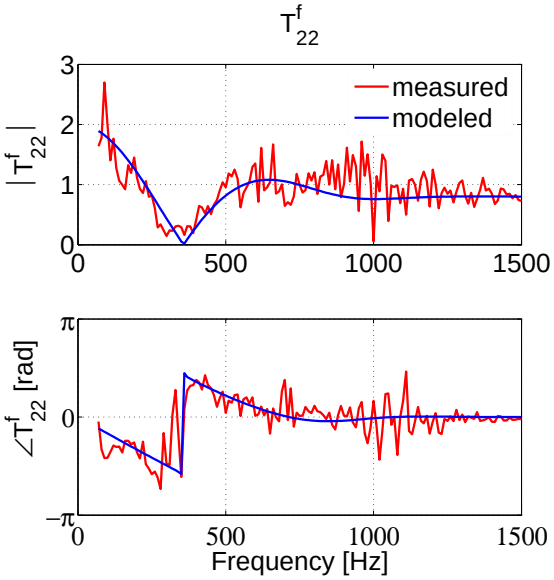

(c) 36/700/2.1. Flame type IIb.

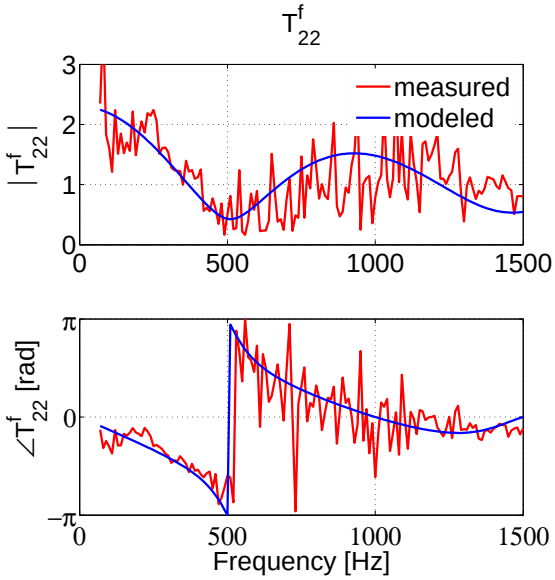

(d) 40/700/1.9. Flame type IIIa.

Figure 4.10: *The dynamic element T_{22}^f of the flame transfer function for various operating conditions. The model is able to capture the flame behavior at various operating conditions.*

4.1.5 The Noise Source Term

When a volume of gas expands at constant pressure, direct combustion noise arises, which is characterized as an acoustic monopole. Engine power is the most important factor for this kind of noise, which has a blunt peak in the 300–500 Hz range for large-scale engines [166]. But non-reactive flows also generate noise. The noise block is the source term of the network model. It will be possible to predict sound-pressure spectra when everything is assembled.

Effect of Flow and Temperature on Noise Source Term

Figs. 4.11(a) and 4.11(b) show the effect of the flow on the source term N_s. The intensity roughly doubles when the flow increases from 30 g/s to 44 g/s. When the temperature is raised to 700 K, the flow velocity increases for the same mass flow and yet more noise is generated, see Fig. 4.11(c). For these cases, a first-order system well approximates the measured behavior, plotted in blue.

Effect of the Flame on Noise Source Term

Figs. 4.11(c) and 4.11(d) show the influence of the flame on the noise source term, the preheat temperature being the same. Since 36/700/2.4 is a stable flame type Ib, this difference is not big. In contrast, 36/700/2.1 in Fig. 4.11(e) and 40/550/1.9 in Fig. 4.11(f) exhibit more noise. This is not surprising, since they are both type IIb flames. A second-order system is a good approximation for these cases.

Table 4.3 summarizes the identified parameters for various cases. The influence of the flame is that the noise source term is best approximated by a second-order system, compared with a first-order system for non-reactive cases.

Table 4.3: *The identified noise source term parameters for various cases.*

case	fit	gain	ω_n [Hz]	ζ
30/300/noFlame	1^{st}-order	0.0035	150	
44/300/noFlame	1^{st}-order	0.008	150	
36/700/noFlame	1^{st}-order	0.02	150	
36/700/2.4	2^{nd}-order	0.05	200	0.5
40/550/1.9	2^{nd}-order	0.15	160	0.02
36/700/2.1	2^{nd}-order	0.2	200	0.1

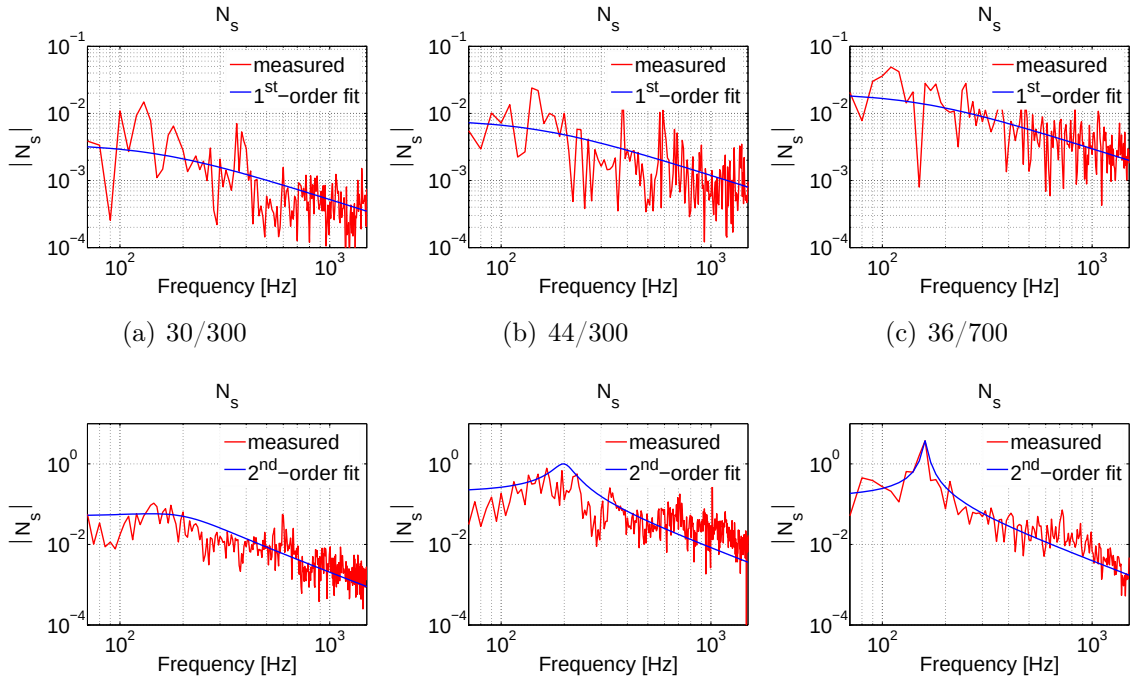

(a) 30/300 (b) 44/300 (c) 36/700

(d) 36/700/2.4 (e) 36/700/2.1 (f) 40/550/1.9

Figure 4.11: *The noise source term N_s for various operating conditions. More flow, higher preheat temperatures, and the flame all contribute to a stronger noise source term.*

4.1.6 The Loudspeaker

The loudspeaker is modeled taking into account both the mechanical and the electromagnetic dynamics [213]. Relevant physical parameters are found in the manufacturer's data sheet and in Table 4.4. The model has two inputs and two outputs: electric voltage and pressure at the membrane; and electric current and acoustic velocity of the membrane.

The membrane and mechanical damping are expressed as in [125]

$$S = \frac{A^2 \rho_a c_a^2}{V_{as}} \tag{4.8}$$

$$d = \frac{S}{w_s Q_{ts}} - \frac{Bl^2}{R_s} \tag{4.9}$$

Define the following terms:

$$G(s) = \frac{s}{ms^2 + ds + S} \tag{4.10}$$

$$H(s) = \frac{1}{L_s s + R_s + Bl^2 G} \tag{4.11}$$

Table 4.4: *The parameters relevant for loudspeaker (LS) modeling.*

Description	Symbol	Value
air density	ρ_a	1.16 kg/m^3
sound speed	c_a	347 m/s
resonant LS frequency	w_s	94 Hz
DC resistance	R_s	6.6 Ω
driving factor	Bl	2.8 Tm
inductance	L_s	0.6×10^{-3} H
membrane area	A	32×10^{-4} m^2
mech. Q-factor	Q_{ms}	4.55
electr. Q-factor	Q_{es}	1.21
total Q-factor	Q_{ts}	0.96
eq. air volume	V_{as}	1.7×10^{-3} m^3
membrane damping	S	
mech. damping	d	
el. voltage at LS	U_e	
el. current through LS	I_e	
acoustic pressure at membrane	p_m	
acoustic velocity at membrane	u_m	
Laplace variable	s	

This allows to write the transfer function of the loudspeaker

$$\begin{pmatrix} I_e \\ u_m \end{pmatrix} = LS \begin{pmatrix} U_e \\ p_m \end{pmatrix} \tag{4.12}$$

where

$$LS = H \begin{pmatrix} 1 & Bl \cdot A(L_s s + R_s) \\ G \cdot Bl & -G \cdot A(L_s s + R_s) \end{pmatrix} \tag{4.13}$$

In addition, the pressure input must be scaled with ρc to get the correct units.

The measured electrical impedance at the loudspeaker agrees well with the modeled impedance. The loudspeaker is connected to the combustor duct by means of a short flange, this is modeled as a short duct, and the area change as an $L-\zeta$ transfer matrix.

4.1.7 The Fuel Injector

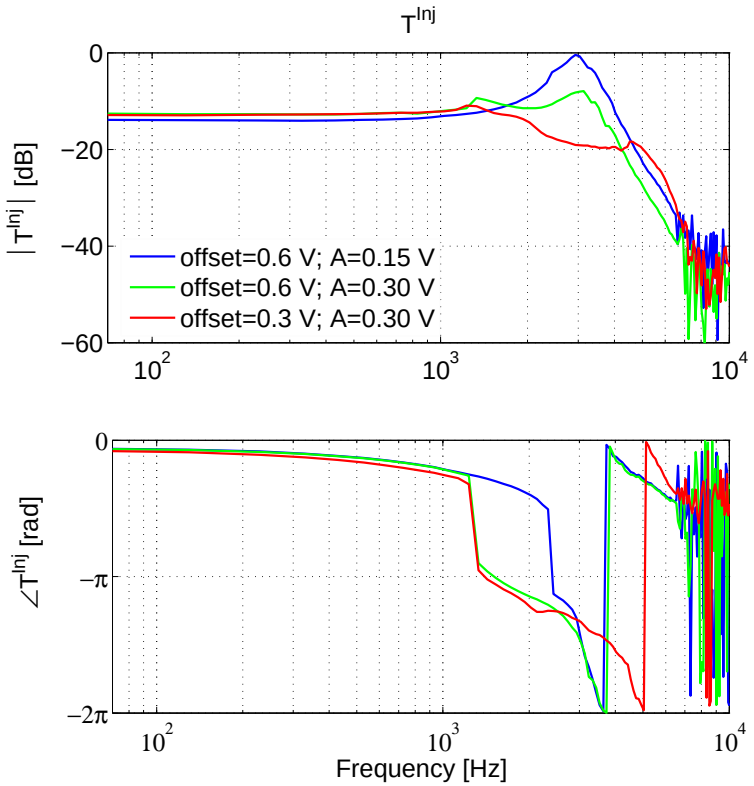

Figure 4.12: *The transfer function T^{Inj} of the injector from voltage to spool position for various offsets and amplitudes. The natural frequency is about 3.2 kHz.*

A MOOG magnetostrictive valve is used in the ETH setup to inject secondary fuel close to the flame, which offers more control authority than loudspeakers. The location of this injector has to be carefully chosen. If it is closer to the flame, less time delay is present, but the mixing of the fuel and air is less optimal and emissions rise.

The injector is operated around an offset, which causes a mean flow through the valve. More offset allows for higher control amplitudes, but again emissions rise and flame stabilization is altered. In the reported experiments, about 10% of the total fuel flow are modulated.

The transfer function from voltage to injector spool position T^{Inj} is shown in Fig. 4.12. For an offset of 0.6 V and an amplitude of 0.15 V, the resonant peak is 12 dB or a factor of 4 above DC. For higher amplitudes, this leads to saturation due to limited space available for the spool to move in the injector. The natural frequency of a second-order fit is 3.2 kHz, the damping ratio $\zeta = 0.25$, and the time delay is 0.08 ms.

The effective control bandwidth to exert pressure fluctuations in the combustor will be lower. This is because of convection, mixing, and combustion (remember that the flame acts as a low-pass filter, see Section 4.1.4). For the control experiments, the offset is fixed at 0.25 V, as explained in Section 5.4.1.

Compare this to a MOOG direct drive valve evaluated in [30], which offers a mechanical bandwidth of 400 Hz. The bandwidth from control signal to pressure is similar, but with a delay of 12 ms. Section 4.3.2 shows that in the ETH test rig the bandwidth from voltage to pressure is similar, but the time delay is around 2.5 ms.

The transfer function between command signal and position sensor for an actuator is shown in [30, 51]. However, the explanation of a variable delay does not hold if one models the actuator as a sixth-order system with break frequency 400 Hz and a delay of 0.03 ms. The transfer function from command signal to pressure in the combustor still has a comparable bandwidth of 400 Hz. The time delay is not taken into account in the second-order fit, and therefore the model is only valid around the unstable frequency [292].

4.2 Assembling the Model

Transfer Functions: Ambient Case 0/300/noFlame

The aforementioned and identified blocks are now assembled to yield the transfer function $TF^{P,LS}$. The input is the voltage applied to an amplifier connected to a loudspeaker; and the output is the pressure measured by a microphone. The loudspeakers and microphones can both be mounted up- and downstream.

For the ambient case 0/300, a comparison between the measured and modeled transfer function $TF^{P,LS}$ is shown in Fig. 4.13. The actuator is a downstream loudspeaker at 303 mm, and microphones at 213 mm, 123 mm and -72 mm are used as output signals. The qualitative behavior is matched very well, but the amplitudes are more difficult to predict accurately. Although only spaced apart by 90 mm, the transfer functions to the two microphones at 213 mm and 123 mm are quite different, and the model is able to match that. The phase plots exhibit slowly decreasing values. This is due to the time delay present between actuation and sensing, which increases with increasing distance between the two positions.

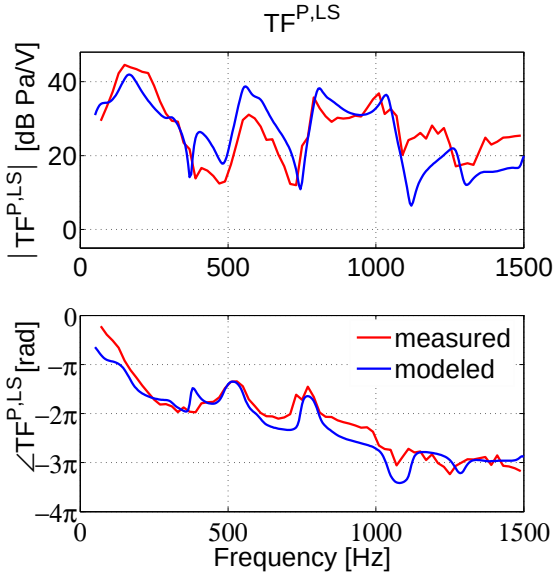

(a) Downstream at 213 mm.

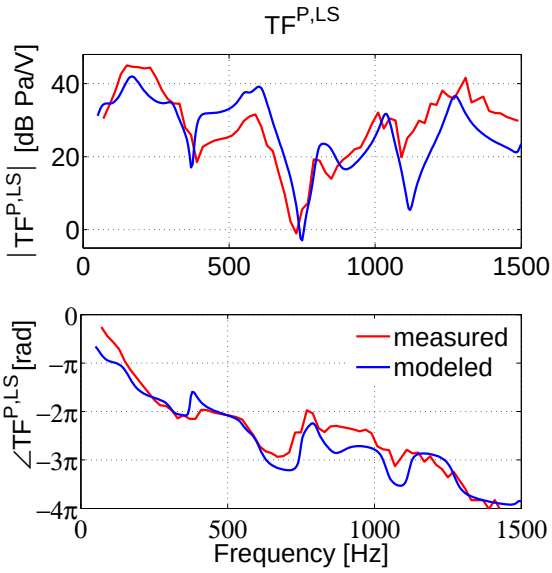

(b) Downstream at 123 mm.

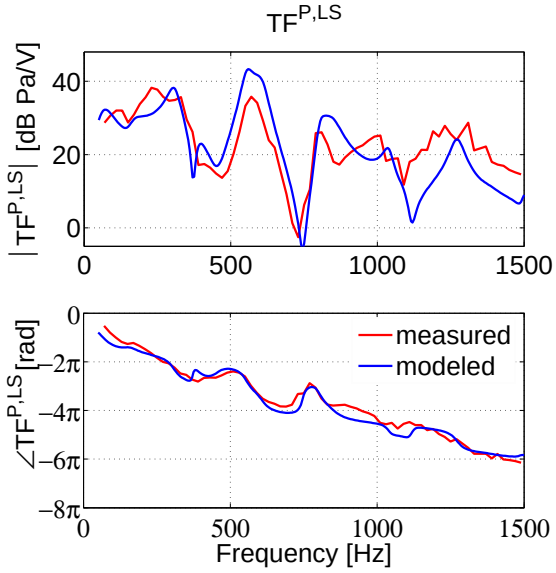

(c) Upstream at −72 mm.

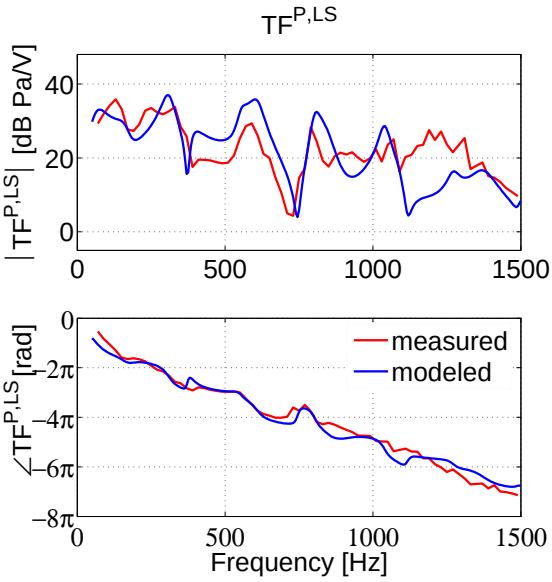

(d) Upstream at −172 mm.

Figure 4.13: *The transfer function $TF^{P,LS}$. The input is a loudspeaker downstream at 303 mm, and the pressure outputs are read at various locations down- and upstream of the burner. Ambient case 0/300/noFlame.*

Reflection Coefficients: Ambient Case 0/300/noFlame

This section evaluates reflection coefficients. Their definitions are explained in Section 3.2.2 and Fig. 3.3.

The *upstream* reflection coefficient *looking upstream* R_{up} as well as the impedance at a location just upstream of the burner Z_{up} are revealed in Fig. 4.14. The phase drop of R_{up} indicates the acoustic length of the upstream duct. The absolute value of R_{up} shows that the upstream end condition is not constant, but rather a function of frequency. The impedances have peaks where they are expected for the closed-closed case.

The reflection coefficient at a position *downstream* of the burner and *looking upstream* $R_{up,burner}$ is shown in Fig. 4.15. The model is able to accurately predict the saw-tooth like behavior. It also shows that the burner becomes acoustically more reflective for higher frequencies.

The reflection coefficient "looking" *downstream* R_{down} and impedance Z_{down} measured at a location *downstream* of the burner are depicted in Fig. 4.16. The length for the downstream duct is chosen correctly, the peaks of the impedances match. Like $\mid R_{up} \mid$, $\mid R_{down} \mid$ does not follow a simple curve.

When placing oneself *upstream* of the burner and evaluating the values in the *downstream* direction, $R_{down,burner}$ and $Z_{down,burner}$ are obtained, see Fig. 4.17. These values also give an appreciation of the effect of the burner. Again, the model is able to describe the measured behavior accurately. The absolute values of $R_{down,burner}$ are around 0.5 up to 400 Hz and increase to 0.8 for higher frequencies. This indicates that sound transmission from the upstream to the downstream part is weak.

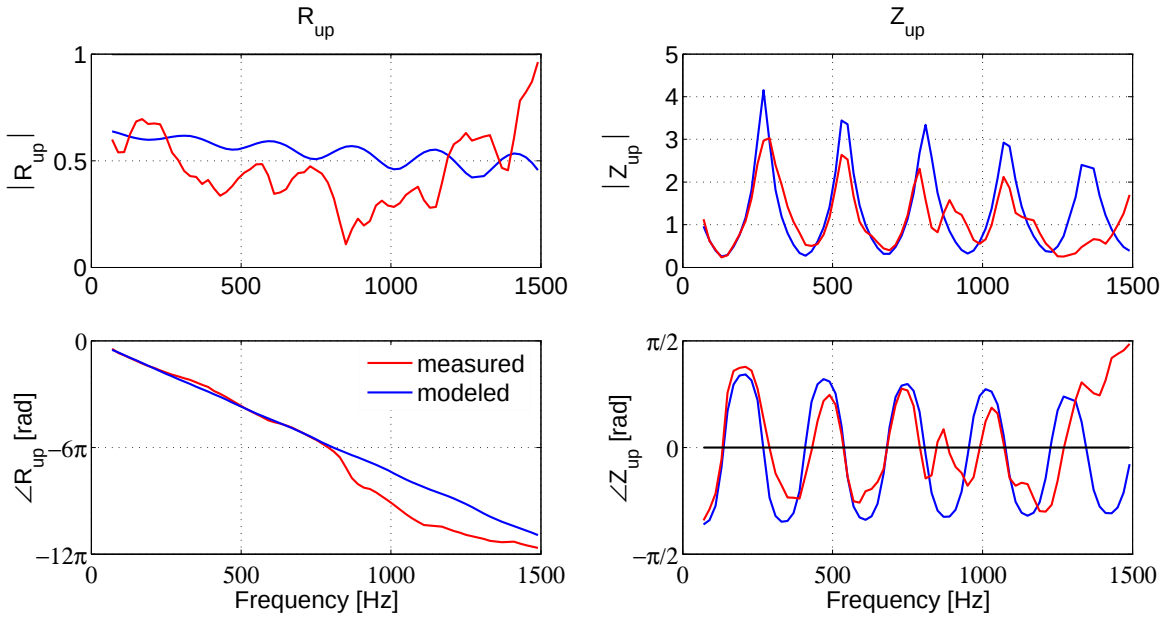

Figure 4.14: *The reflection coefficient of the upstream part R_{up} and the impedance Z_{up}, measured upstream of the burner. Ambient case 0/300/noFlame.*

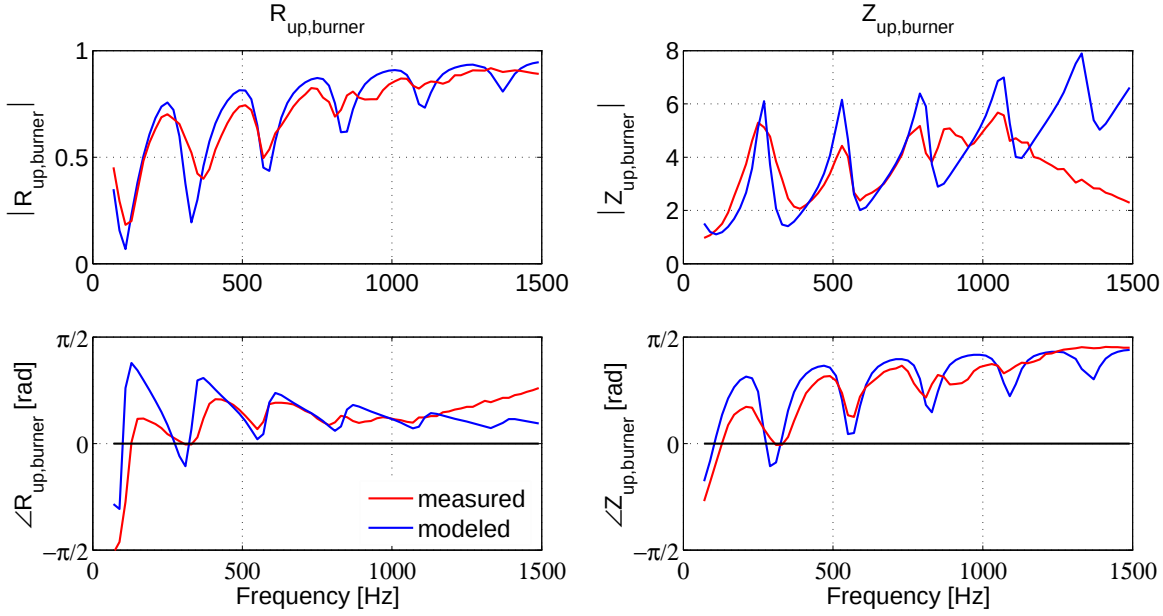

Figure 4.15: *The reflection coefficient $R_{up,burner}$ of the upstream part including the burner; and the impedance $Z_{up,burner}$, measured downstream of the burner. Ambient case 0/300/noFlame.*

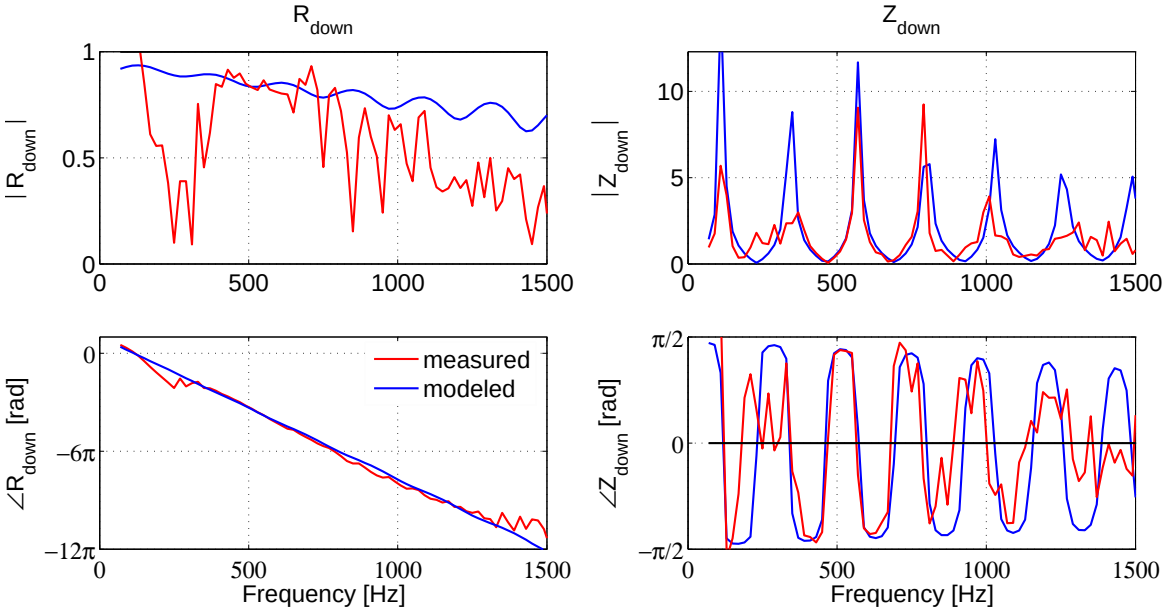

Figure 4.16: *The reflection coefficient R_{down} and impedance Z_{down}. They are measured at a location* downstream *of the burner. Ambient case 0/300/noFlame.*

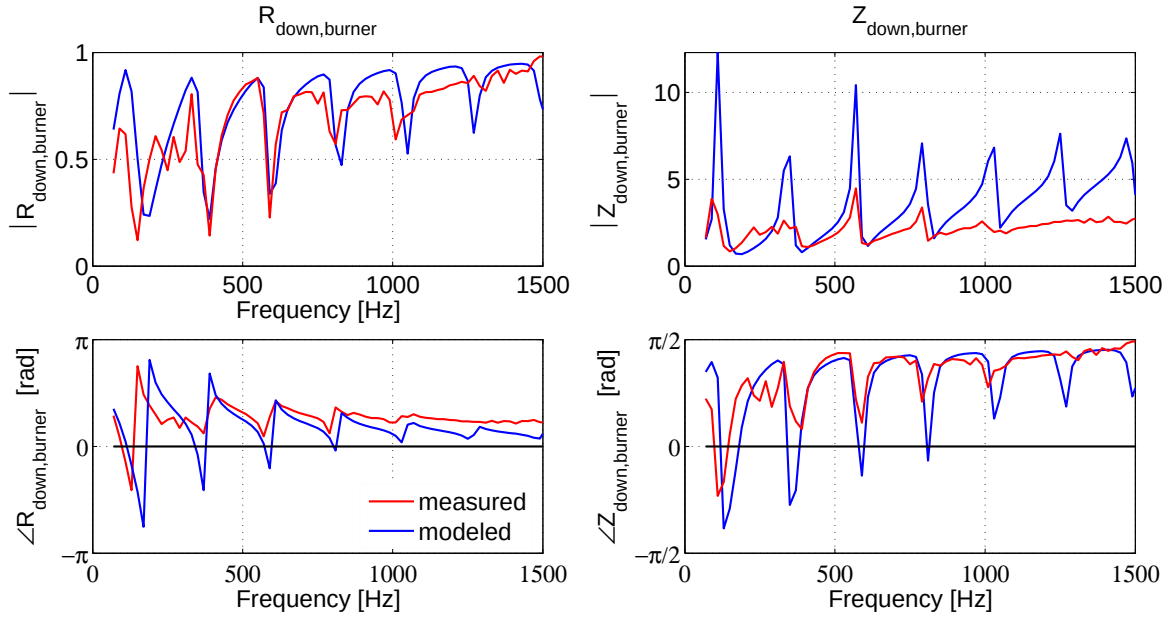

Figure 4.17: *The reflection coefficient $R_{down,burner}$ and impedance $Z_{down,burner}$. They are measured* upstream *of the burner and include the influence of the burner and the downstream part. Ambient case 0/300/noFlame.*

Transfer Functions: Preheated Case 36/700/noFlame

The transfer function $TF^{P,LS}$ for the 700 K preheated case is shown in Fig. 4.18 for microphone positions at 213 mm, 123 mm, −72 mm and −172 mm. Loudspeaker forcing happens downstream at 303 mm. The match between the values predicted by the network model and the measured values is also very good.

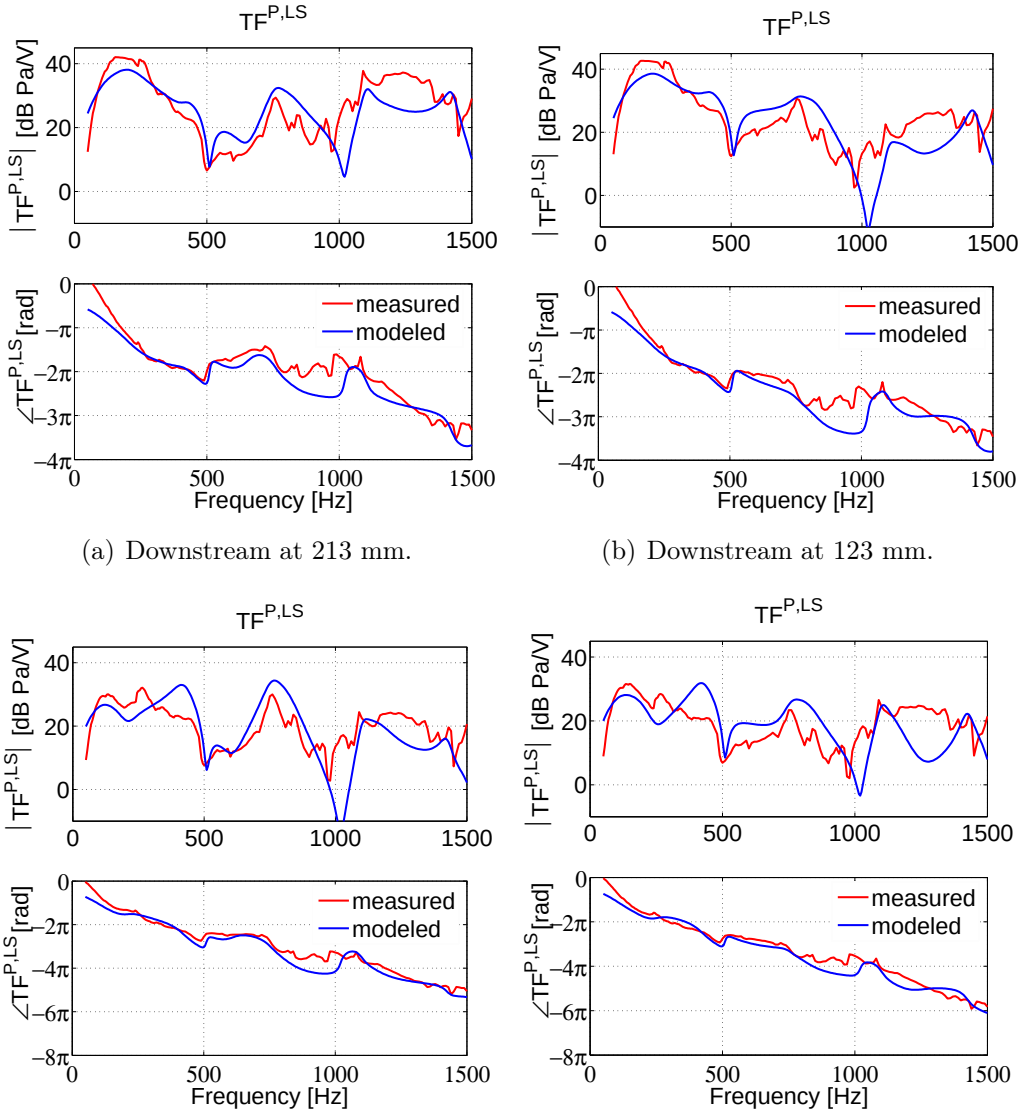

(a) Downstream at 213 mm.

(b) Downstream at 123 mm.

(c) Upstream at −72 mm.

(d) Upstream at −172 mm.

Figure 4.18: *The transfer function $TF^{P,LS}$ from a loudspeaker input downstream at 303 mm to pressures read at various locations down- and upstream of the burner. Preheated case 36/700/noFlame.*

Transfer Functions: Flame Type Ib versus IIb: Cases 36/700/2.4 and 2.1

This section examines the effect of the flame on the transfer function. Figs. 4.19(a) and 4.19(b) reveal the transfer function from the voltage at the loudspeaker to a pressure measurement at 213 mm and −72 mm for the flame type Ib case 36/700/2.4.

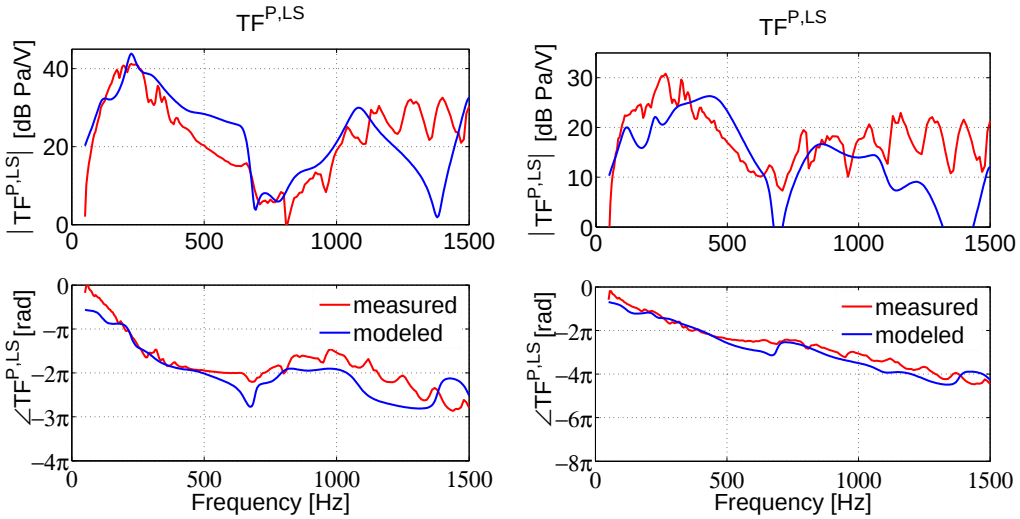

(a) Downstream at 213 mm.

(b) Upstream at −72 mm.

Figure 4.19: *The transfer function $TF^{P,LS}$ from the loudspeaker downstream at 303 mm to the pressure read down- and upstream of the burner. Flame type Ib case 36/700/2.4.*

Figs. 4.20(a) and 4.20(b) show the transfer functions for flame type IIb case 36/700/2.1. The agreement between model and measurement is still good, even in the presence of a complicating element, namely the flame. However, the frequency of the highest peak is a little bit overestimated. When comparing the two cases, it is revealed that the 36/700/2.1 case has a higher resonance around 200 Hz. This is consistent with the observation that the power spectrum also exhibits a higher peak for this more unstable case.

Prediction of the Sound-Pressure Spectrum

The sound-pressure spectrum is modeled in this section. The identified noise term acts as a source to the network model. The pressure signal spectrum is simulated and compared with measured values. The sound-pressure spectrum for the flame case 36/700/2.1 is shown in Figs. 4.21(a) and 4.21(b). In Fig. 4.21(a), the analytical fit of the noise source term is used, whereas for Fig. 4.21(b) the identified noise model is used. The latter gives a slightly better prediction in the 300 Hz, 700 Hz, and 1200 Hz

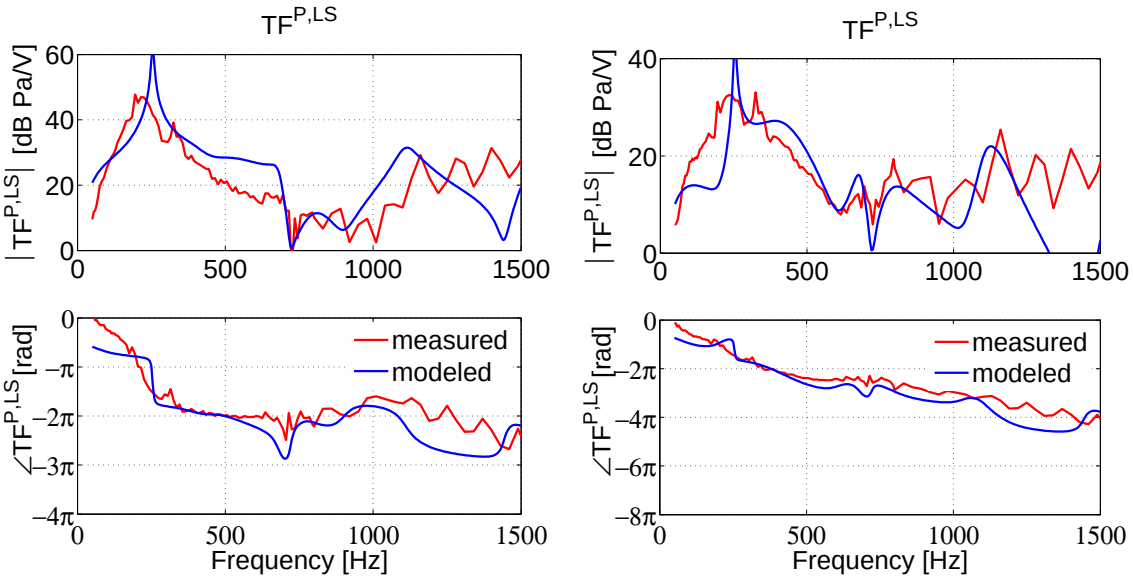

(a) Downstream at 213 mm. (b) Upstream at −72 mm.

Figure 4.20: *The transfer function $TF^{P,LS}$ from the loudspeaker downstream at 303 mm to the pressure read down- and upstream of the burner. Flame type IIb case 36/700/2.1.*

range. The agreement between the model and the measurement is nevertheless very good.

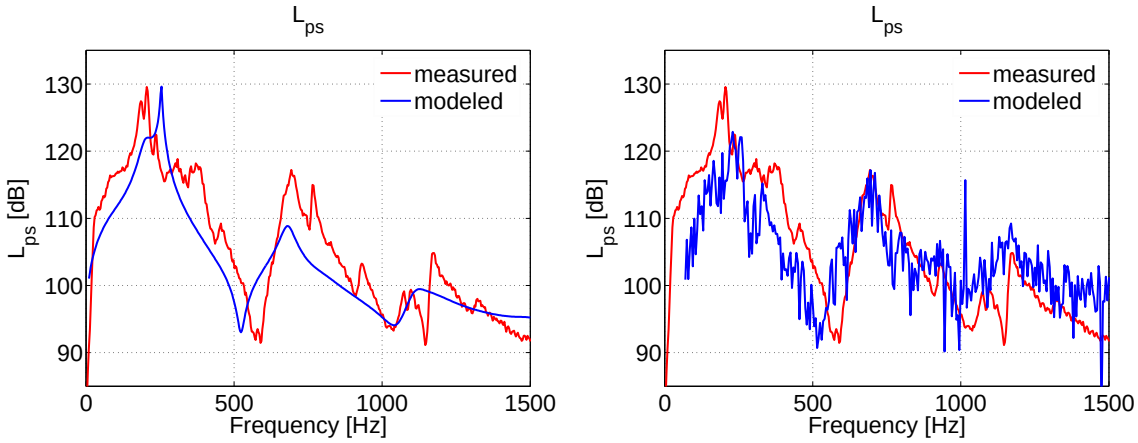

(a) fitted noise source term (b) identified noise source term

Figure 4.21: *A comparison of the measured and modeled sound-pressure spectrum. The left plot uses the fitted noise source term; the right the identified term. Flame type IIb case 36/700/2.1.*

Reflection Coefficients Upstream Including the Flame

This section examines the reflection coefficients $R_{up,burner,flame}$ for various cases. Remember that it is defined as the ratio of the Riemann invariants, being just downstream of the flame and looking toward the upstream end. The four plots in Fig. 4.22 display the modeled and measured $R_{up,burner,flame}$ for the same flame type cases that have been the subject of the flame study in Section 4.1.4.

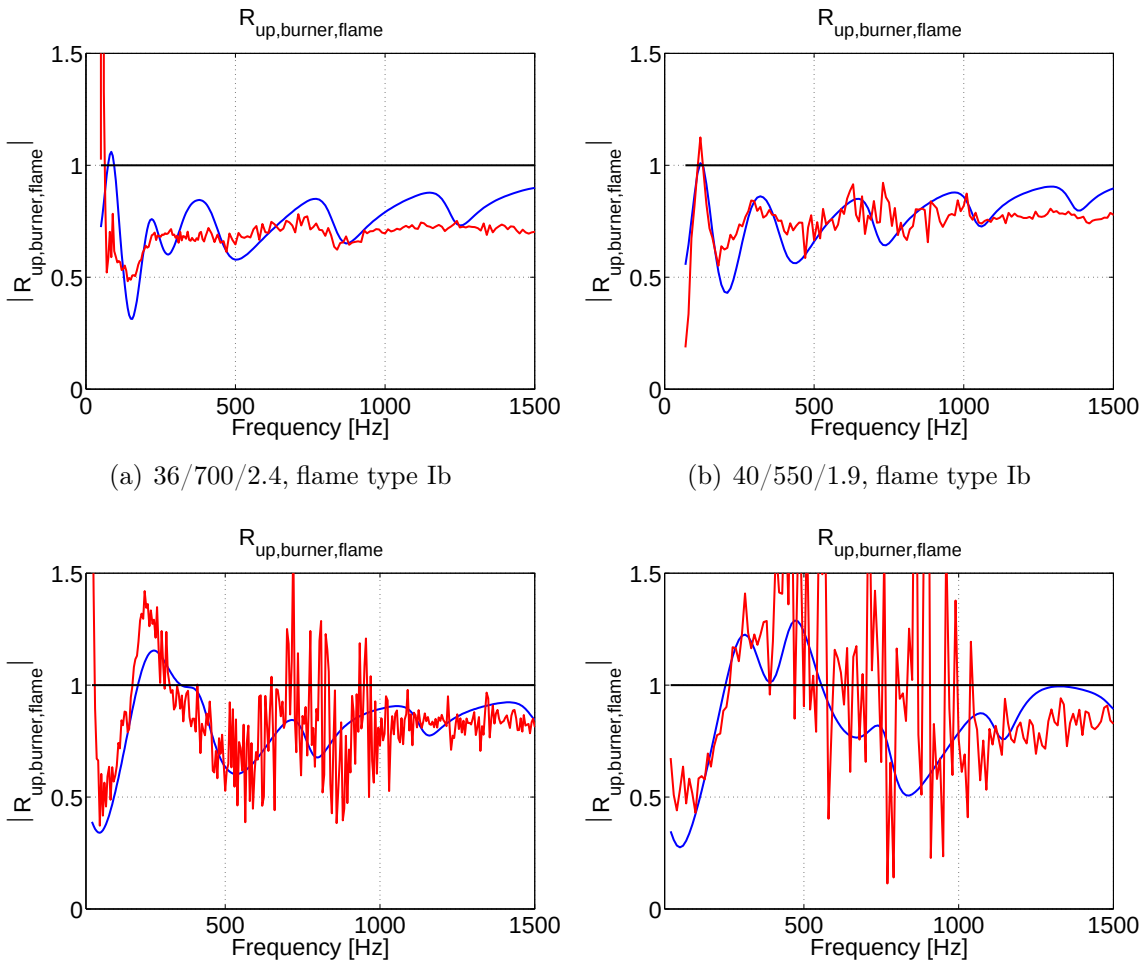

(a) 36/700/2.4, flame type Ib

(b) 40/550/1.9, flame type Ib

(c) 36/700/2.1, flame type IIb

(d) 40/700/1.9, flame type IIIa

Figure 4.22: *The reflection coefficients of the upstream part including the flame for various flame types. They show that the flame can act as an active element feeding energy into the acoustic field, a prerequisite to thermoacoustic instabilities. This is the case whenever the absolute value of the reflection coefficient exceeds 1.*

The stable type Ib flame case 36/700/2.4 features low values of $R_{up,burner,flame}$, like 40/550/1.9. For the type IIb case 36/700/2.1, values larger than 1 occur between 200 and 300 Hz. A similar amplifying behavior is recognized in the IIIa case 40/700/1.9 at frequencies between 260 and about 500 Hz. This shows that the flame acts as an active element in certain frequency ranges, and can thus lead to an unstable behavior of the combustor. Indeed, the amplification is due to the flame, because the upstream reflection coefficients (excluding the burner and the flame) are similar. Data acquisition becomes more difficult as the noise floor rises.

The pressure spectra of the four cases discussed are shown in Fig. 4.23, the right plot zooms in onto the 0–500 Hz range. They show that more unstable flames exhibit a higher noise floor and higher peaks in the pressure spectrum, and their locations in the frequency range correlate well with the regions of amplification explained before in Fig. 4.22.

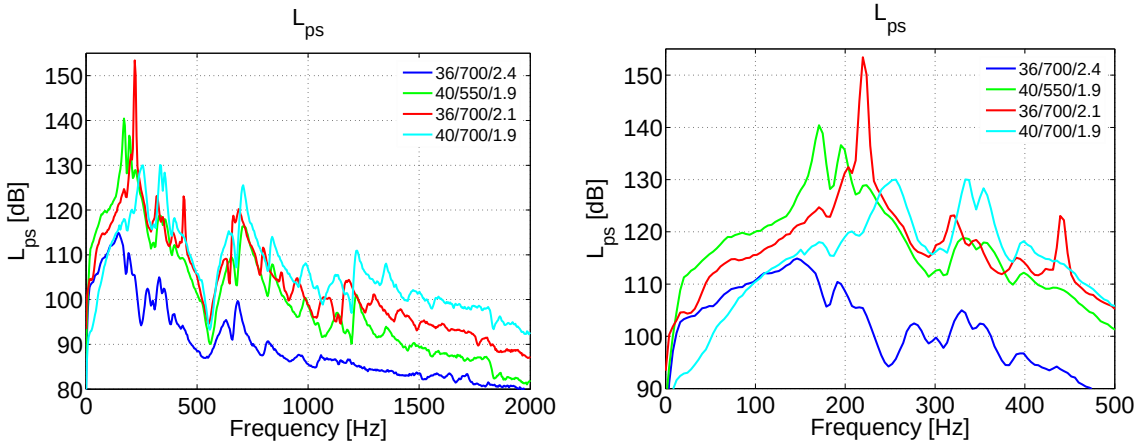

(a) 2000 Hz (b) 500 Hz

Figure 4.23: *The pressure spectrum at 123 mm for various cases. Left: up to 2000 Hz, right: up to 500 Hz. High values are observed in regions where the flame feeds energy into the acoustic field, see Fig. 4.22.*

4.3 Identification for Control

4.3.1 Loudspeaker as Actuator

The system obtained by the physical modeling process offers a lot of insight into the mechanisms of thermoacoustic interactions, but is not accurate enough to be used for controller design purposes. For instance, the heights of the first peak around 200 Hz in the measured and modeled transfer functions differ by about 10 dB, see Fig. 4.20(a). Therefore, the *measured* transfer function from the voltage applied to the loudspeaker to the pressure signal is utilized.

In order to find a state-space representation of an acoustic system, the subspace identification technique [196, 195] is well suited. The algorithm is kindly provided by Andrew Fleming from the University of Newcastle, Australia[1].

In our case, the loudspeakers are connected through flanges to the ducts, causing an actuation time delay τ_{act}. It is preferable to include as much prior knowledge about the plant as possible into the identification step, and therefore the time delay is estimated in the following way: Bode's gain-phase relationship [285] expresses the idea that a minimum-phase system is uniquely determined by its amplitude response:

$$\angle G(j\omega_0) = \frac{1}{\pi} \int_{-\infty}^{\infty} \underbrace{\frac{d\ln|G(j\omega)|}{d\ln\omega}}_{N(\omega)} \ln\left|\frac{\omega+\omega_0}{\omega-\omega_0}\right| \frac{d\omega}{\omega} \tag{4.14}$$

Therefore, one fits a stable minimum-phase system to the absolute value of the transfer function only. The phase of the identified minimum-phase system and the measured one will differ. The actuation time delay τ_{act} is then the amount of phase difference divided by frequency, which should be constant. At higher frequencies, the phase loss contributed by the time delay is much higher than a possible phase mismatch from the fitting procedure, so the identification of the time delay is more robust there, see Fig. 4.24. The identified value for the actuation time delay τ_{act} between the loudspeaker at 303 mm and the microphone at 213 mm is about 0.45 ms, which corresponds to a distance of 20 cm. This is close to the length of the flange that connects the loudspeaker to the combustor duct.

The subspace identification technique can now be applied to the transfer function which is corrected for the time delay. In Fig. 4.25, the blue dots represent the measured data points, and the red line is the Bode plot of the transfer function identified with the subspace technique. The agreement is very good for low frequencies, and still acceptable up to 1000 Hz. Control action will be required mostly in the low-frequency range up to 400 Hz.

[1] http://www.eng.newcastle.edu.au/eecs/

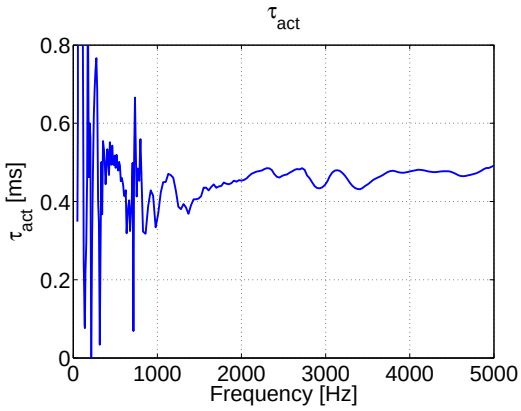

Figure 4.24: *The estimated time delay τ_{act} between the loudspeaker at 303 mm and the microphone at 213 mm, when Bode's gain-phase relationship is used.*

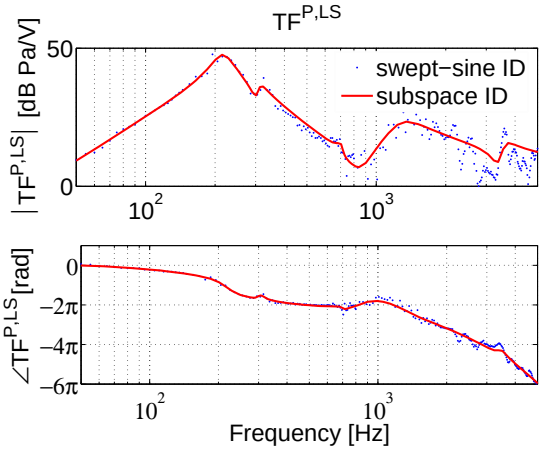

Figure 4.25: *The transfer function of the plant identified with a swept-sine signal; and the result of the subspace identification. Flame case 36/700/2.1.*

4.3.2 Fuel Injector as Actuator

When a frequency sweep like in the loudspeaker as actuator case is applied to the fuel injector, the resulting pressure peaks are so high that saturation occurs and the flame stabilization process is disturbed, see Fig. 4.26. In this experiment, a swept-sine signal is applied to the fuel injector. The pressure spectrum L_{ps} shows that a forcing signal with a frequency of 50 Hz and an amplitude A of 0.12 V has negligible influence on the main instability at 218 Hz. A higher amplitude of 0.24 V disrupts the flame stabilization and removes the harmonic at 436 Hz, too. The picture is similar with a forcing frequency of 60 Hz. Note that harmonics of the fundamental of 50 Hz and 60 Hz are present. It is conjectured that they are due to saturations of the heat release process.

If the forcing amplitude is lowered, the flame anchoring is not altered, but the signal to noise ratio greatly deteriorates. The identified transfer function from the voltage at the injector to the pressure signal at 123 mm is shown in Fig. 4.27, which is obtained with two different forcing amplitudes of 0.12 V and 0.24 V, respectively. It shows that the higher forcing amplitude A of 0.24 V fails to correctly capture the resonant peak at 218 Hz. Thus, the identified plant does not correctly represent the true dynamics.

As a remedy, an attempt could be made to work with lower and frequency-dependent amplitudes, but a different approach proposed in the following. The combustor is run in a closed-loop fashion with simple controller structures, and the ensuing change of the sound spectrum (with respect to the uncontrolled case) is recorded. But one has

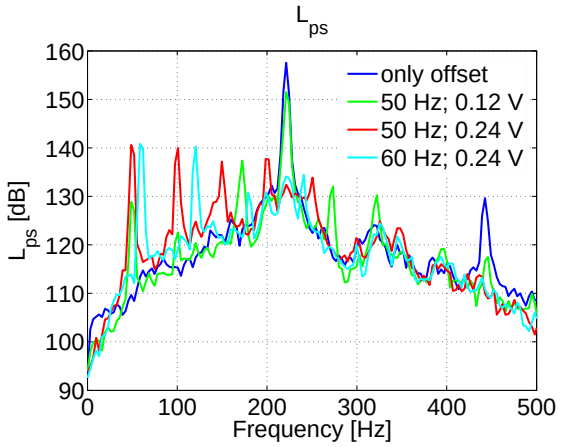

Figure 4.26: *The pressure spectrum L_{ps} when a sine sweep is applied to the fuel injector. Forcing frequencies are 50 Hz and 60 Hz, two amplitudes. An amplitude of 0.24 V changes the flame anchoring process and the instability at 220 Hz vanishes. Flame case 36/700/2.1.*

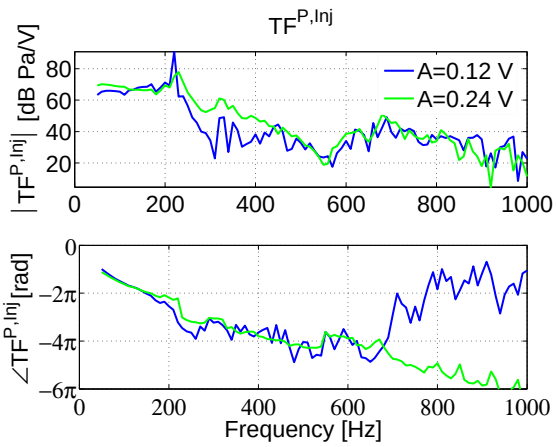

Figure 4.27: *The transfer function from the voltage at the fuel injector to the pressure at 123 mm for two different forcing amplitudes. The identification is difficult and uncertain. Flame case 36/700/2.1.*

to be careful: several controllers have to be used in order not to fall prey to identifying the negative inverse of the controller. The difference between the uncontrolled and controlled pressure spectrum is the sensitivity in control speak. It is defined as $S = 1/(1 - CP)$, where P is the plant and C is the controller in positive feedback; it highlights the effect of added noise at the plant output on the sum of the two. The different controllers are known, and so the plant can be identified point-by-point in the frequency domain. Finally, a stable model is derived from this information.

This procedure is used to find the transfer function $TF^{P,Inj}$ from the voltage at the fuel injector to the pressure at 123 mm. This is done for two flame cases (36/700/2.1 and 36/700/1.875), where 42 and 27 controllers (Phase-Delay, complex lead-lag, peak filters) are employed, respectively.

The result of this identification for the case 36/700/2.1 is presented in Fig. 4.28 (as blue dots), together with the swept-sine identification (in green), which fails to correctly identify the sharp and high peak around 218 Hz. The red graph shows the frequency response of the derived model, approximating the blue dots. The errors of the optimization defined as the difference between the pressure spectrum reduction measured and the sensitivity modeled stay around 3 dB. For higher frequencies, the identification is less certain, this is due to decreasing control authority in this range.

The outcome of the identification for the case 36/700/1.875 is shown in Fig. 4.29. The fit is very good up to a frequency of 400 Hz, and the errors stay around 2 dB. It is of course important to dispose of controllers that excite the frequency range of interest.

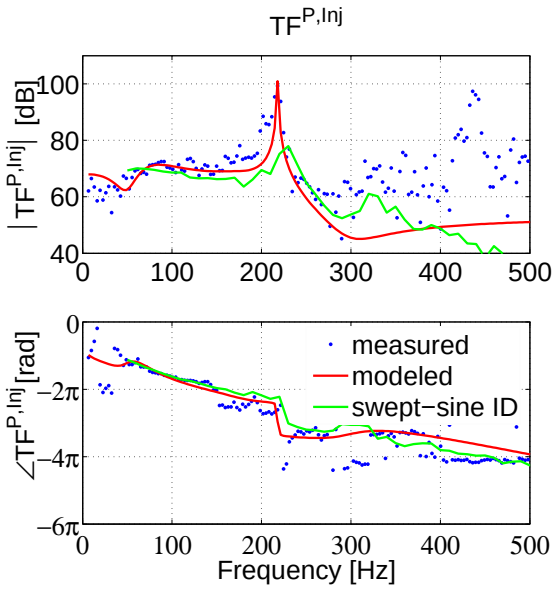

Figure 4.28: *The frequency response $TF^{P,Inj}$ of the identified plant for the flame case 36/700/2.1. The blue dots represent the outcome of the identification, and the red line is a fit to these points. The result of the swept-sine identification is also shown in green, which fails to identify the sharp peak around 218 Hz.*

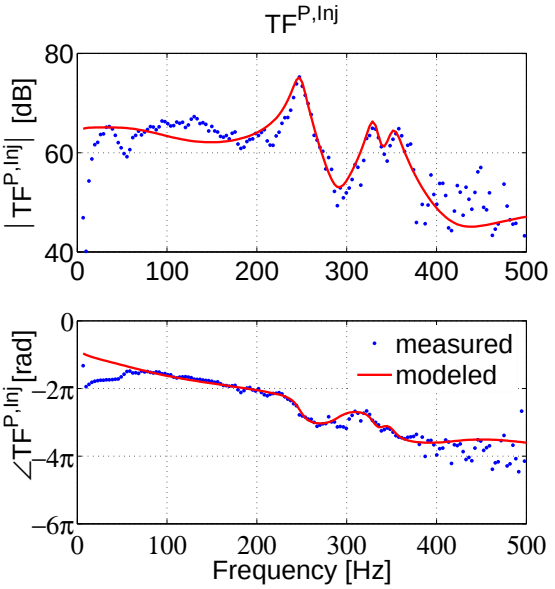

Figure 4.29: *The frequency response $TF^{P,Inj}$ of the identified plant for the flame case 36/700/1.875.*

Summary

This chapter has introduced the network modeling approach. The blocks are physically modeled and experimentally verified. The $L-\zeta$ burner model and the $n-\tau$ flame model are confirmed over a wide range of operating conditions. Finally, the model is assembled and found to correspond well to measurements. A new technique to obtain the transfer function of the combustor is introduced. It works in a closed-loop manner and yields excellent results.

5

Passive and Active Control

Fast cars, fast women, fast algorithms...
what more could a man want?

Joe Mattis

5.1 Passive Control and Helmholtz Resonators

In order to mitigate combustion oscillations, passive strategies are usually preferred, because they are less complex and failure-prone. Section 1.3.1 has presented some general ideas.

For the ETH test rig, various downstream end plates of varying constrictions are tried, as well as Helmholtz resonators. The loudspeakers which are used for identification are placed in housings to protect them from the hot combustion gases, see Section 3.1. It turns out that these boxes also act as Helmholtz resonators.

Helmholtz resonators are studied in [27, 28, 130, 84, 115, 307, 71, 70, 123, 199, 311, 207]. The resonant frequency of a simple volume V with a neck of length L_n and area A_n, speed of sound c, is given by $\omega_r = c\sqrt{\frac{A_n}{VL_n}}$. In the ETH case, loudspeaker housings with a size of 80×80×50 mm are used. They are connected with flanges of length 68 mm and diameter 30 mm to the combustor ducts. The Helmholtz equation thus yields a resonant frequency of about 300 Hz. If the loudspeakers are installed in the housings, the effective volume is a little bit smaller, increasing the resonant frequency. Moreover, honeycomb structures are inserted in the connecting flanges, decreasing the neck opening area. In summary, the predictions of this simple calculation agree well with the experimental results reported in the following section.

It makes no difference in the pressure spectrum whether the loudspeakers are electrically shunted or not, see Fig. 5.8. Because of the constricted connecting flanges, too little coupling occurs between the two acoustic fields in the combustor and the housing. However, it could be worth checking this idea out on other rigs, see [213].

5.1.1 Effect of Helmholtz Resonators

Effect on Spectrum of Two Loudspeakers at −282, 213, 303 mm.

Two loudspeakers in their housings are placed upstream, downstream, and at both locations. Then the loudspeakers are removed, and only the housing is connected to the combustion duct. This gives two different resonant volumes.

The Helmholtz effect of the loudspeakers (LS) and the loudspeaker housings (boxes) at various positions is evidenced in Fig. 5.1. The pressure spectra measured by a microphone placed downstream at 123 mm are shown in Fig. 5.1(a); and measured by a microphone upstream at −172 mm in Fig. 5.1(b). The air is not preheated, but the flow velocity of 44 g/s results in a temperature of 320 K.

The loudspeakers and boxes mounted *downstream* at 213 mm have an effect on the *downstream* microphone at 123 mm in the frequency range 100–300 Hz, consistent with the Helmholtz resonator equation. This fact is plotted as red and green graphs in Fig. 5.1(a). The loudspeaker housing box (with the loudspeaker removed) has a higher resonating volume and thus a lower resonant frequency (green). The loudspeakers *upstream* have virtually no influence on the *downstream* microphones at 123 mm (cyan).

The influence on the *upstream* microphone at −172 mm is shown in Fig. 5.1(b). The *downstream* loudspeakers and housings have virtually no effect on the *upstream* pressure. Only the upstream loudspeakers reduce the pressure spectrum between 100 and 250 Hz, at the expense of more noise at higher frequencies (cyan and pink graphs).

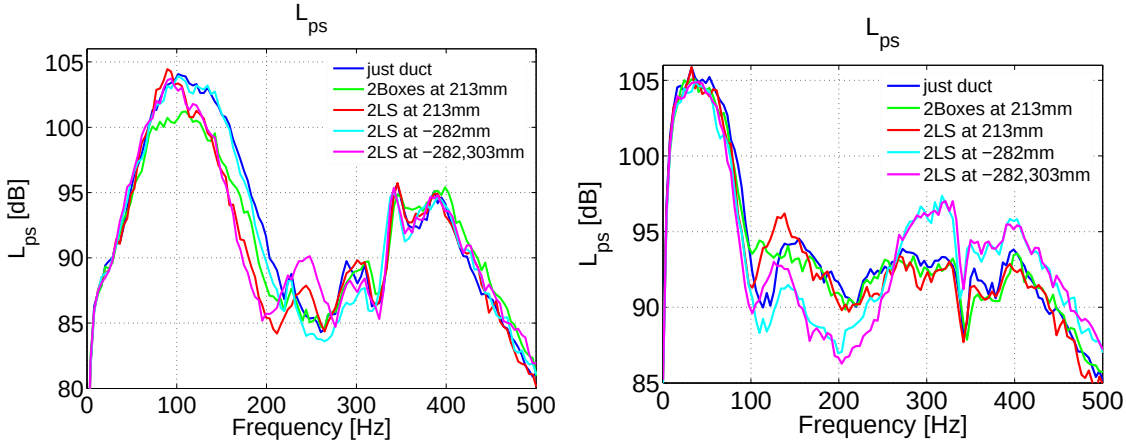

(a) downstream at 123 mm

(b) upstream at −172 mm

Figure 5.1: *Passive control with Helmholtz resonators for 44/320. The effect on microphones upstream and downstream is shown.*

Effect on R_{down} of Two Boxes/LS at Various Downstream Positions.

To make things more lucid, the downstream reflection coefficient as seen by the flame R_{down} is displayed in Fig. 5.2 for ambient conditions and no flow. It shows the effect of two loudspeakers at various downstream positions. When they are mounted at 123 mm, their effect is negligible. The loudspeaker positioned at 213 mm reduces R_{down} in the frequency range from 100 to 300 Hz. When it is mounted at 303 mm, the highest reduction is obtained.

The Helmholtz behavior rests on the dissipation of acoustic velocity in the neck. With the given configuration (closed-open duct), a pressure antinode exists at the burner location, and one would expect that the Helmholtz resonators placed close to the flame would work best. However, this is not the case. A possible explanation is that the flow interacts with the Helmholtz neck tubing, creating turbulence and favoring the dissipation of acoustic energy. This could explain why the loudspeaker at 303 mm offers the most reduction of R_{down}.

Fig. 5.3 displays the effect of different kinds of Helmholtz resonators, namely one or two boxes/loudspeakers. As shown in the analysis above, boxes have a higher volume and thus are effective at lower frequencies. Two pieces of resonant volumes are also more effective than just one (red vs. green; pink vs. cyan). Loudspeakers are better at reducing R_{down} in the 100–300 Hz frequency range than loudspeaker housings (green vs. cyan; red vs. pink).

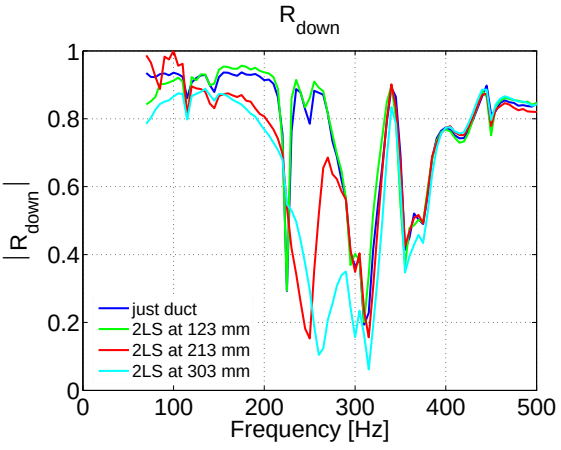

Figure 5.2: *R_{down} for two loudspeakers mounted at various downstream positions. Ambient case 0/300/noFlame.*

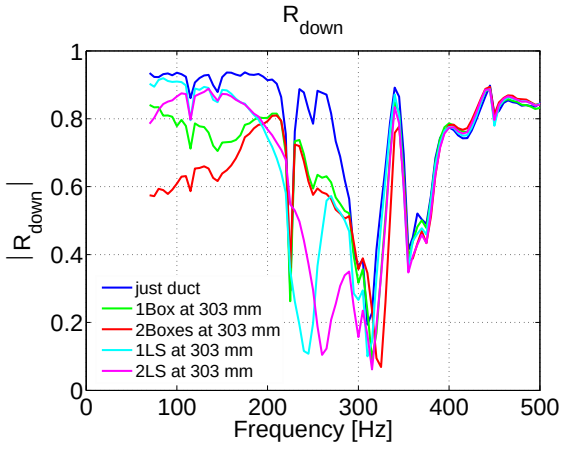

Figure 5.3: *R_{down} for one/two box/LS at 303 mm. Ambient case 0/300/noFlame.*

Effect on R_{down} of Two LS at 303 mm; Comparison of Different Measurement Setups

The downstream reflection coefficients R_{down} are usually measured by exciting with a loudspeaker upstream at -282 mm and measuring with two microphones downstream. This section compares the standard approach with one where forcing happens downstream at 123 mm, and the microphones at 213 mm and 303 mm are used for the two-microphone method to determine R_{down}.

The calculated R_{down} with the standard method is shown in Fig. 5.4. Various flames and operating conditions are investigated. Moreover, it compares two setups: one with two additional damping loudspeakers downstream at 123 mm, and the other with none downstream. The results show two things: Firstly, the Helmholtz behavior of the downstream loudspeakers in the 150–300 Hz range (blue vs. the other colors). Secondly, R_{down} does not depend strongly on the operating condition, since all three cases with downstream loudspeakers show similar values for R_{down}.

To confirm the Helmholtz behavior of the downstream loudspeaker, two forcing loudspeakers are mounted downstream at 123 mm. Microphones at 213 mm and 303 mm are used to determine R_{down}. Now forcing also happens downstream. This is compared with a case where two loudspeakers acting as Helmholtz resonators are mounted downstream at 303 mm (forcing is applied upstream at -282 mm).

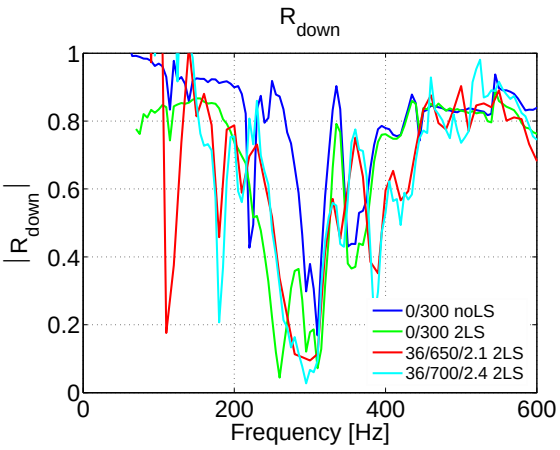

Figure 5.4: *R_{down} for no/two LS at 303 mm. Forcing upstream at -282 mm. R_{down} only depends on the presence of a downstream loudspeaker at 303 mm, but not on the operating condition.*

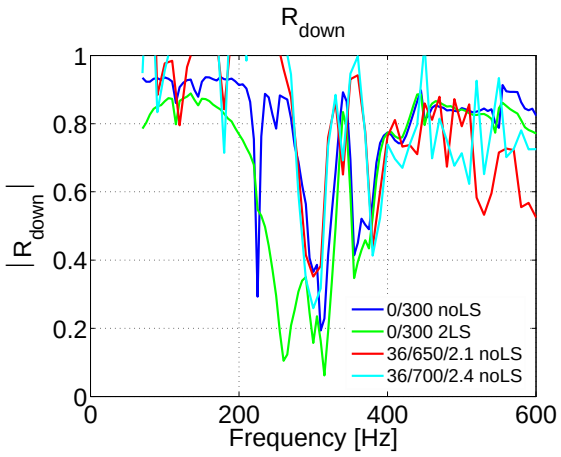

Figure 5.5: *R_{down} for no/two LS at 303 mm. Forcing downstream at 123 mm. The results are similar to Fig. 5.4, and show the Helmholtz behavior of a downstream loudspeaker.*

The effect of these two loudspeakers downstream is clearly seen in Fig. 5.5. The case where downstream loudspeakers are present (green graph) stands out from the other measurements, which are all similar. The observed behavior confirms the findings in Fig. 5.4: loudspeakers act as Helmholtz resonators; and the two-microphone method is a reliable technique.

Effect on the Spectrum with Flame of One/Two Box/LS at 303 mm.

Having realized that loudspeakers and their housings (or boxes) act as Helmholtz resonators and are thus able to suppress pressure oscillations, their effect on the pressure spectrum is investigated here.

Fig. 5.6 shows how much one and two boxes and loudspeakers reduce the pressure spectrum at two microphone locations. The effect on the downstream microphone at 123 mm is mostly noted between 150 Hz and 300 Hz, at the expense of more noise around 320 Hz, see Fig. 5.6(a). Loudspeakers are more efficient at the frequency of the main instability at 218 Hz; two loudspeakers are more efficient than one, but more waterbed effect is a side effect.

A similar behavior is seen for the upstream microphone at −172 mm, see Fig. 5.6(b). It shows that *downstream* Helmholtz resonators have a comparable effect on upstream as on downstream microphones, in particular they can decrease the main peak considerably.

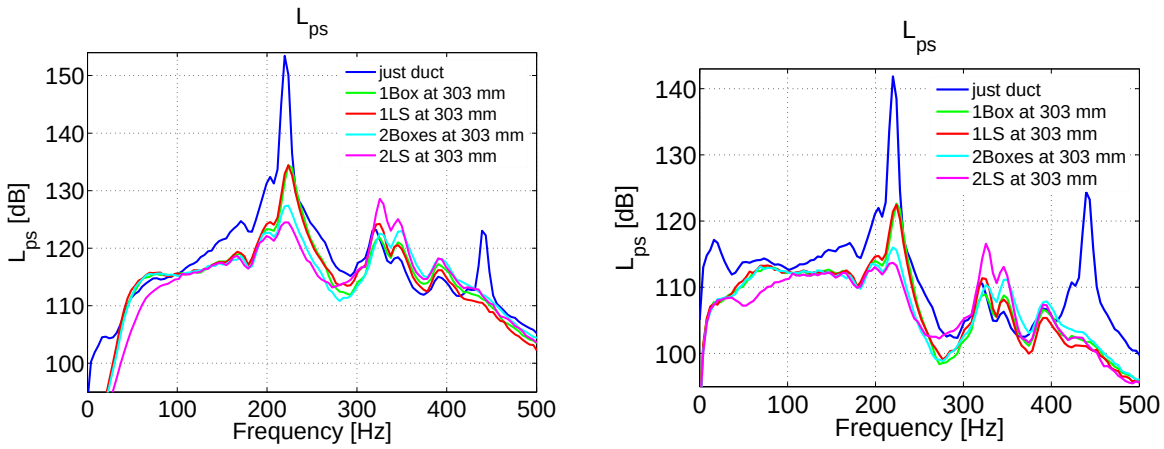

(a) downstream at 123 mm

(b) upstream at −172 mm

Figure 5.6: *The pressure spectrum up- and downstream in the presence of various Helmholtz resonators at 303 mm. Flame case 36/700/2.1.*

This investigation has been extended to other operating conditions and shows the potential of Helmholtz resonators. If they are properly tuned, they can significantly

decrease pressure levels. For this study, the effects of the Helmholtz resonators are confined to a narrow frequency band of roughly 150 Hz to 300 Hz. This shows the need for active control strategies, to suppress the pressure oscillations more effectively.

5.1.2 Effect of Electrically Shorted Loudspeaker

In order to investigate passive control strategies that alter the electrical impedance at the loudspeaker terminals, a damping loudspeaker is mounted downstream at 303 mm; and the electrical terminals are shorted or left open.

Fig. 5.7 shows the transfer function from the upstream loudspeaker at −282 mm to a microphone at 123 mm for the ambient case without flow. It shows that virtually no difference occurs because when the damping loudspeaker mounted at 303 mm is electrically shorted or not. However, the addition of the damping loudspeaker shows a Helmholtz resonator effect.

Fig. 5.8 shows that no change in the pressure spectrum for a flame case 36/700/2.1 occurs whether the damping loudspeaker is electrically shorted or not. This precludes the use of electrical impedance based control strategies, which would have the advantage of not requiring a microphone as sensor [213].

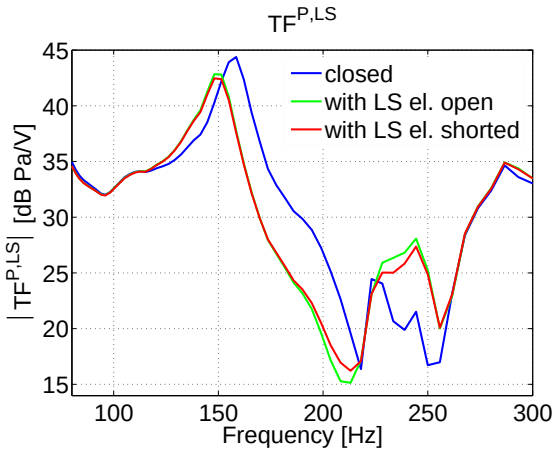

Figure 5.7: *Transfer function $TF^{P,LS}$ from the loudspeaker at −282 mm to a microphone at 123 mm. Only a Helmholtz effect is noticeable, but nearly no difference between cases when the damping loudspeaker is electrically shorted and not. Ambient case 0/300/noFlame.*

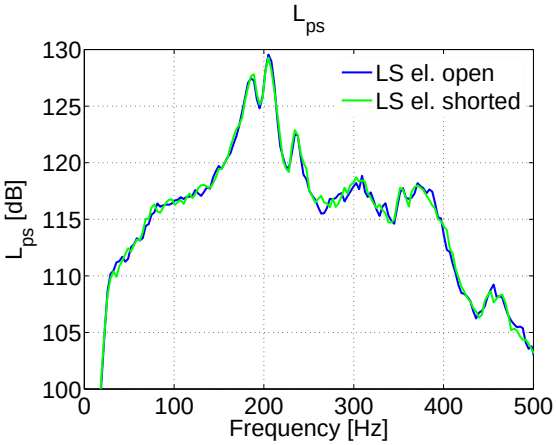

Figure 5.8: *Pressure spectrum read at 123 mm when the damping loudspeaker at 303 mm is electrically shorted and not. Nearly no difference occurs, therefore electrical impedance based passive strategies are not applicable. Flame case 36/700/2.1.*

5.2 Active Feedback Control

Active feedback control measures a state of the system to be controlled and takes action accordingly by means of an actuator. In particular, the ETH setup is equipped with microphones that sense the acoustic pressure inside the combustor. A control algorithm uses this input signal and generates a control signal, which is sent to the actuators. For this study, two types of actuators are used: loudspeakers introduce acoustic waves; and a secondary fuel injector is implemented to change the combustion behavior of the flame. The task of the control engineer is the design of the controller, respecting the constraints imposed by the plant.

5.2.1 Fundamental Limits of Active Control

Ignorantia iuris nocet—Ultra posse nemo obligatur.

Justinian, "Digesten" 22,6,9 pr.—anonymus

Limits to active feedback control arise from a range of sources:

- unstable plants
- non-minimum phase (NMP) zeros in the plant
- time delays in the control loop
- limited actuator and sensor bandwidth
- actuator saturation

As pointed out by many authors (see for instance [285]), a real NMP zero z limits the achievable bandwidth for feedback control to $\omega_c \lesssim z/2$. The plant can again be robustly controlled for higher frequencies ω_{c2} satisfying $\omega_{c2} \gtrsim 2z$. On the other hand, right-hand-plane (RHP) poles require a minimum bandwidth $\omega_c \gtrsim 2p$ for real RHP poles p. It is clear that a real RHP pole p and a real NMP zero z have to satisfy $z \gtrsim 4p$ for acceptable controller performance.

Time delays also pose fundamental problems. The "ideal" complementary sensitivity function for a time delay τ is $T = e^{-\tau s}$ [285], so the sensitivity function is $S = 1 - T = 1 - e^{-\tau s} \approx \tau s$ by a Taylor series expansion. The sensitivity S crosses the 0 dB line for the first time at about $\omega = 1/\tau$, which determines the bandwidth. Another way of looking at it is to consider the first-order Padé approximation of a time delay $e^{-\tau s} \approx \frac{1-\tau/2s}{1+\tau/2s}$, which has a NMP zero at $2/\tau$, yielding again a bandwidth constraint of $\omega_c < \frac{z}{2} = \frac{2/\tau}{2} = 1/\tau$.

Another fundamental constraint to controller design is the so-called waterbed effect for systems with pole excess of at least two. The famous Bode integral states that

$$\int_0^\infty \ln |S(j\omega)| \, d\omega = \pi \sum_{i=1}^{N_p} Re(p_i) \tag{5.1}$$

where N_p represents the number of RHP poles p_i and $Re(p_i)$ is their real part. This equation says that a sensitivity decrease over a frequency band always has to be compensated for with an equal (or even greater for unstable plants) increase in sensitivity at other frequencies. If actuator bandwidth constraints or model uncertainties exist, the sensitivity increase cannot be spread over an infinite frequency range—sensitivity peaks necessarily occur [288].

If the system has a NMP zero z, another "waterbed" formula is derived, which takes into account that the sensitivity increase and decrease have to happen over a limited frequency range $\omega < z/2$, yielding peaks for $|S|$. As pointed out in [100], a sensitivity decrease as well as an increase have to be completed within the actuator bandwidth. In other words, there must be a decrease in performance within a certain frequency band, when feedback action is present. Effects limiting controller performance for combustors in terms of the Bode sensitivity integral can also be found in [59, 20].

Another important constraint is actuator saturation. This may be involved whenever a plant cannot be stabilized in reality—even though in simulations, a linear controller can stabilize it. Actuator bandwidth is often overlooked in controller design.

For the present study, the plant is stable, minimum-phase but a time delay is present, and periodic disturbances are assumed. This means that disturbance attenuation can only be achieved over a limited frequency range, and that the waterbed effect will be present. This is not a serious problem, as there are only a few distinct peaks in the pressure spectrum that one would like to decrease. What turns out to be more restraining is actuator saturation. In the case of loudspeaker control, the output is limited to 2×30 W. With the fuel injector, the electrical amplifier is driven into saturation.

5.2.2 Control Setup

The combustor is modeled as *stable but lightly damped, and driven by persistent noise.* This leads to the control setup shown in Fig. 5.9.

The noise input block models the uncontrolled combustor generating the pressure signal p_n. The plant P is the block that relates the control signal input u to the pressure p_c generated by altered combustion (in case of fuel injection), or by the action of the

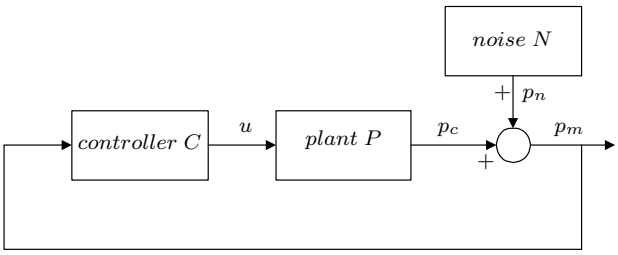

Figure 5.9: *A schematic diagram of the control setup.*

loudspeaker. The sum of these two is the measured pressure signal p_m, which is to be minimized. This signal is used by the controller C to generate the control signal u.

It is clear that the noise and plant blocks share some characteristics. Reducing p_m now amounts to finding a controller C such that the sensitivity function (positive feedback!) $S(j\omega) = 1/(1 - CP)$ from p_n to p_m is lower than 1 in the frequency bands where noise suppression is desired. In the evaluation of the controllers, the achieved pressure spectrum reduction will be compared to the sensitivity obtained with the model and the controller. With the chosen setup, they should coincide if the model is correct.

5.2.3 Actuators

Loudspeaker

Two Visaton SC8 30 W loudspeakers are used primarily for identification purposes, but also for control. They have to be protected from very hot exhaust gases. In the ETH test rig, this has been accomplished by placing them in cooled housings which are connected through flanges to the combustor ducts. The housings and flanges are purged with air, to prevent hot exhaust gases from entering and burning the membrane. This tendency is more marked when they are mounted closer to the flame.

Loudspeakers exert control by introducing acoustic waves directly into the combustor ducts. The main problem is their limited control authority—saturations invariably occur. In pressurized large-scale combustors, this shortcoming exacerbates, and they are not a viable option for industrial applications.

For control purposes, the loudspeaker is placed downstream at 213 mm. It could not be installed closer to the flame because the membrane would melt. It is mounted downstream because the pressure levels are higher, and it can control the oscillations more effectively. In order to minimize time delays in the control loop, the microphone is placed as close as possible to the actuator. The microphone noise level is higher the closer it is to the flame, so a position of 303 mm is chosen.

Fuel Injector

Fuel injectors rely on the intrinsic energy of fuel to achieve control. Section 3.1 shows that the installed fuel injector has a power of roughly 6000 W, compared with 2×30 W from the loudspeakers. Five problems associated with controllers acting on the fuel modulation in combustion chambers are listed in [304]:

- distributed actuation arising from the burning of injected fuel
- time lags
- intensive noise
- time variations of mean flow conditions
- model uncertainties and parametric errors

It is stressed in [59] that the actuator must be able to interfere with the coupling process, i.e. that the fuel is properly injected, mixed, and burned. If the mixing is bad, local rich spots may attenuate oscillations, but raise emissions, as it happened in [292]. Moreover, high shear flows and feed line dynamics could reduce actuator authority [69].

The fuel injector installed on the ETH test rig is a MOOG magnetostrictive high-bandwidth valve. It modulates a maximum of 1 g/s of natural gas and injects it into the lips of the EV burner to ensure good mixing and low convective delays. The microphone for this control setup is placed at 123 mm to minimize time delays and reduce noise.

5.2.4 Controllers

When it comes to control design,
there are only two choices: PID or Ph.D.

David Bayard

Section 2.1 highlighted some of the controller designs reported in the literature. The simplest strategy is Gain-Delay (also known as phase-shift), but better results can be achieved with model-based approaches such as $\mathcal{H}_\infty$ controllers. In addition, the Covariance Matrix Adaptation Evolution Strategy CMA-ES with Noise-Handling is used to improve both control concepts online. Other evaluated strategies include a manual loop shaping process, whereby simple elements are assembled to meet certain criteria, this is done with the help of Nyquist diagrams. Complex lead-lag controllers

are an extension of the classic lead-lag element, except that they offer steeper slopes [202]. Finally, peak filters concentrate the energy in a narrow frequency band—it is hoped that saturation issues are less severe. The last three structures are presented in the appendix.

$\mathcal{H}_\infty$ control

The $\mathcal{H}_\infty$ method is a powerful design tool allowing the control engineer to define bounds on the sensitivity and the complementary sensitivity by means of weighting functions added to the plant G_s and controller K to form an augmented plant. Fig. 5.10 shows a setup known as $S/KS/T$ [107], where W_e weights the sensitivity, W_u the control signal, and W_y the complementary sensitivity. The control variables are represented by u, the measured variables by y, exogenous signals by w, and error signals by z.

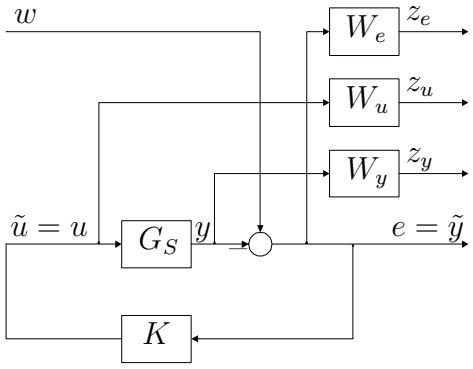

Figure 5.10: *A schematic diagram of the S/KS/T setup used to design an $\mathcal{H}_\infty$ controller*

The $\mathcal{H}_\infty$ control synthesis procedure now consists of finding a controller K that stabilizes the closed-loop system and yields $\|T_{zw}(s)\|_\infty < \gamma = 1$. For the suggested $S/KS/T$ weighting scheme, the matrix T_{zw} is given by

$$T_{zw} = \begin{bmatrix} W_e S_e \\ W_u K S_e \\ W_y T_e \end{bmatrix} \tag{5.2}$$

which allows to weight the sensitivity S_e with W_e, the complementary sensitivity T_e with W_y, and the control signal energy KS_e with W_u.

The designer now shapes the bounds according to the performance criteria. For this study, noise reduction is the primary objective, so the important bound is S_e, while keeping an eye on control signal saturation weighted by W_u.

CMA-ES optimization

Gain-Delay control is convenient because there are only two parameters to adjust. Its performance is often satisfactory if the spectrum of the instability only features one dominant peak. Model-based $\mathcal{H}_\infty$ controllers on the other hand offer more design freedom and perform generally better. However, their often complex nature with many parameters makes online optimization difficult. Moreover, thermal transients during start-up change the location and height of the pressure peaks, and the (steady-state) model of the process is not accurate. Therefore, the combination of a model-based controller and online optimization is well suited. More specifically, the $\mathcal{H}_\infty$ controller is shifted in the frequency domain by multiplication of the A and B matrix, and thus coping with the thermal transients. The gain is also adjusted, giving two parameters to optimize by the evolutionary algorithm. Optionally, a third parameter to be optimized is added, namely an additional time delay.

The evolutionary algorithm proposed here has been written by Niko Hansen, ICOS, ETHZ. It is a population based stochastic evolutionary algorithm [116], and features a noise-dependent cost function evaluation time. The cost function taken for this study is the averaged sound-pressure level L_{eq}.

5.2.5 Investigated Operating Conditions

The case 36/700/2.4 is of flame type Ib and does not exhibit large pressure oscillations, so the need for control is not given.

The flame type IIb cases 36/650/2.1 and 40/550/1.9 are both controlled by a loudspeaker commanded with a Gain-Delay and an $\mathcal{H}_\infty$ controller. The results for the two cases are similar, so only 36/650/2.1 is shown. The $\mathcal{H}_\infty$ controller performs much better than the Gain-Delay and offers more flexibility.

For fuel injection, 40/550/1.9, 36/700/2.1 and 36/700/1.875 are investigated. Problems with flame stabilization arise with the case 40/550/1.9. The flame type IIb case 36/700/2.1 has a very distinct peak at around 218 Hz, about 30 dB above background noise levels. The second harmonic is also present at 436 Hz, which is caused by flame saturation. Gain-Delay is very effective here, because the gain and phase can be tuned optimally with respect to this frequency. However, $\mathcal{H}_\infty$ control still performs better.

In contrast, the flame type IIIa case 36/700/1.875 exhibits three peaks of about equal amplitude. Gain-Delay control is not promising, because the optimal gain and delay for suppressing one peak will increase the other peaks. An $\mathcal{H}_\infty$ controller is able to decrease all peaks simultaneously, or to target a single peak, at the designer's will.

The loudspeaker housing also acts as a Helmholtz resonator. This should be kept in mind when comparing the spectra controlled with a loudspeaker and a fuel injector.

5.3 Control Experiments: Loudspeaker as Actuator

5.3.1 Loudspeaker and Gain-Delay Control

Gain Delay: 36/650/2.1

This operating condition is a flame type IIb. It is subjected to Gain-Delay control, with a loudspeaker as actuator. The value of the peak in the pressure spectrum $max(L_{ps})$ as

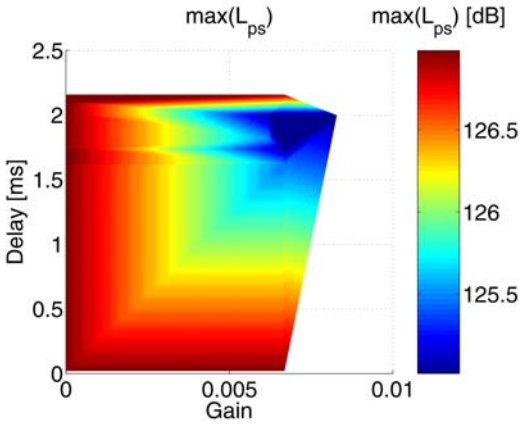

Figure 5.11: *The peak of the pressure spectrum $max(L_{ps})$ as a function of various Gain-Delay parameters for the case 36/650/2.1 with a loudspeaker as actuator. An optimum value of gain 6.5×10^{-4} and 1.9 ms delay is identified.*

a function of the gain and delay of the controller can be seen in Fig. 5.11. A minimum is discerned around a gain of 6.5×10^{-4} and 1.9 ms delay.

Fig. 5.12 shows what happens to the pressure spectrum when the delays are changed for a fixed gain of 6.6×10^{-4}. The waterbed effect is apparent: a decrease of one peak implicates an exacerbation at other frequencies. Here, more delay implies *increasing* values of L_{ps} between 150 and 230 Hz, but *decreasing* noise at frequencies lower than 140 Hz and higher than 250 Hz. The colors correspond to the gradient taken in the direction of increasing delays.

Fig. 5.13 shows the pressure spectrum for various Gain-Delay controllers. If the first peak at 150 Hz is being pushed down, a secondary peak at 200–220 Hz rises. The Gain-Delay controller does not offer enough design freedom to choose the increase of noise in the spectrum, one has to resort to $\mathcal{H}_\infty$ controllers for this feature.

Fig. 5.14 shows the measured and modeled decrease of the spectrum with the Gain-Delay controllers. The measured pressure spectrum corresponds to the modeled sensitivity $S(j\omega) = 1/(1-CP)$. The model has been obtained with the technique outlined in Section 4.3.1—it accurately predicts the behavior of the controlled combustor.

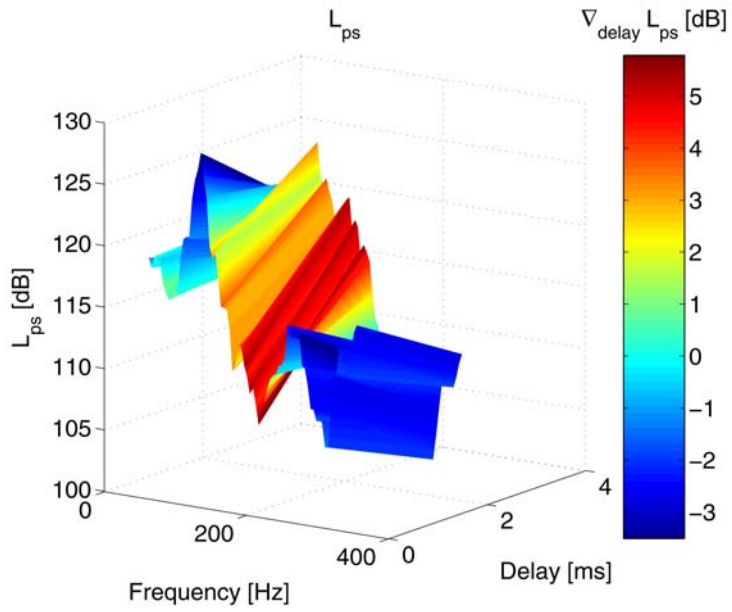

Figure 5.12: *The Gain-Delay-controlled pressure spectrum of 36/650/2.1 for a fixed gain of 6.6×10^{-4} and changing delays from 0–2 ms. If one peak decreases, others increase—a consequence of the waterbed effect. The colors indicate the value of the gradient in the direction of increasing values of the delay.*

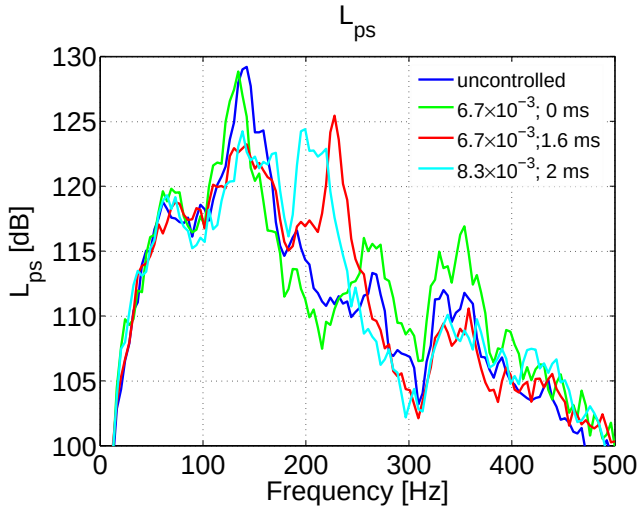

Figure 5.13: *The pressure spectrum read at 303 mm for various Gain-Delay controllers for the case 36/650/2.1 with a loudspeaker as actuator. The waterbed effect is recognized.*

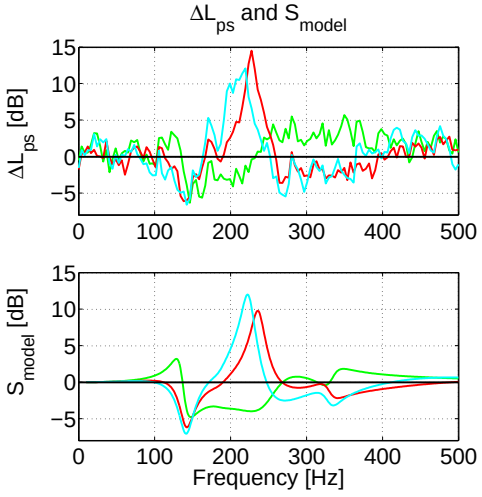

Figure 5.14: *The measured and modeled pressure spectrum reduction for various Gain-Delay controllers for the case 36/650/2.1.*

5.3.2 Loudspeaker and $\mathcal{H}_\infty$ Control

Section 5.3.1 showed the shortcomings of the simple Gain-Delay controller, and that the model is indeed accurate. This knowledge can now be used to build a model-based robust $\mathcal{H}_\infty$ controller. This process is shown in Fig. 5.15. The key weighting function is W_e^{-1} for the sensitivity (red), featuring a dip around 150 Hz. This is where the peak is in the pressure spectrum, and where noise reduction is desired. Moreover, control signal authority (blue) is restricted, otherwise saturation problems would become worse. The complementary sensitivity function (not shown) is simply a low pass filter. The resulting controller is depicted in red in Fig. 5.16; the controller in green is the original controller multiplied by 0.5. The controller has been implemented on the test rig with various gains to study the effects of actuator saturation.

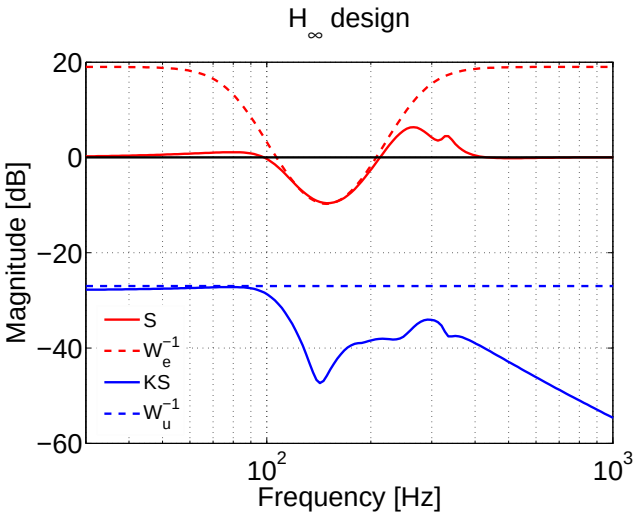

Figure 5.15: *The $\mathcal{H}_\infty$ design process for the case 36/650/2.1. Pressure spectrum reduction is desired around 150 Hz.*

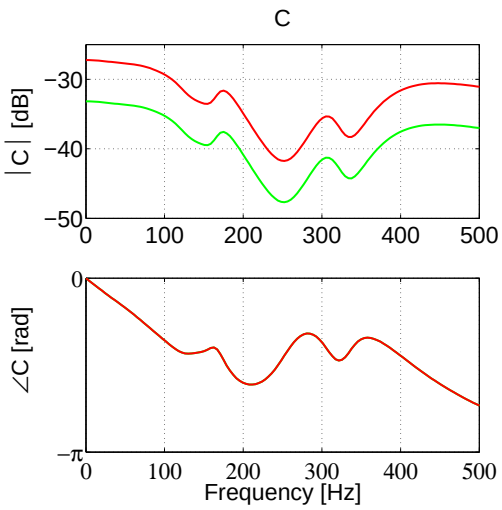

Figure 5.16: *The $\mathcal{H}_\infty$ controllers. They are implemented with gains 1 and 0.5, respectively. Case 36/650/2.1.*

The uncontrolled and $\mathcal{H}_\infty$-controlled spectrum is shown in Fig. 5.17, where a peak reduction of about 8 dB occurs. A closer look at the achieved and modeled pressure spectrum reduction is taken in Fig. 5.18. The reduction with the controller implemented with gain 1 is not better than with the controller multiplied by 0.5, although it should according to the model. The culprit is of course saturation.

Fig. 5.19 compares the Gain-Delay to the $\mathcal{H}_\infty$ controller for the case 36/650/2.1. It makes the point that the model-based $\mathcal{H}_\infty$ controller performs better because the designer can choose the locations of the inevitable pressure increase. In particular, the increase obtained at 200 Hz with the Gain-Delay controller is avoided.

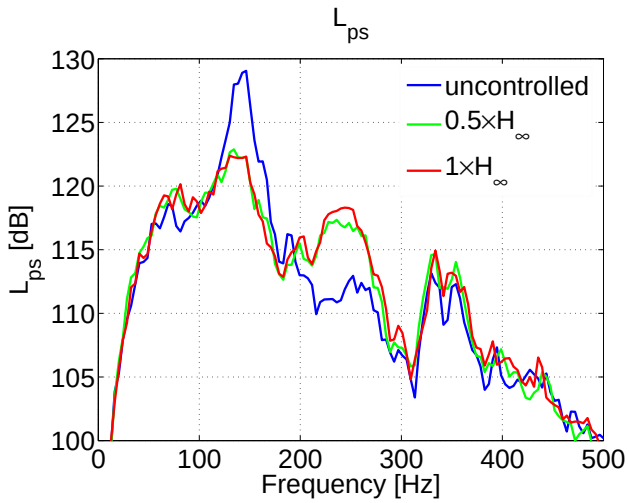

Figure 5.17: *The pressure spectrum at 123 mm of the uncontrolled and $\mathcal{H}_\infty$-controlled case. Saturation prevents further pressure reduction expected from the controller implemented with gain 1. Flame case 36/650/2.1.*

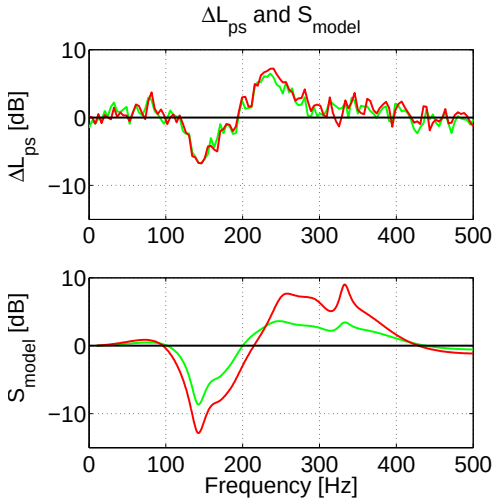

Figure 5.18: *The modeled sensitivity for two $\mathcal{H}_\infty$ controllers, multiplied by 1 and 0.5. Nearly no improvement occurs if the gain is set to 1, because of actuator saturation. Flame case 36/650/2.1.*

A direct comparison is also carried out for the operating condition 40/550/1.9, see Fig. 5.20. It also shows the pressure spectrum of the duct without the loudspeakers. Their Helmholtz effect is recognized as the difference between the blue and the green plot. Again, the $\mathcal{H}_\infty$ controller outperforms the Gain-Delay controller.

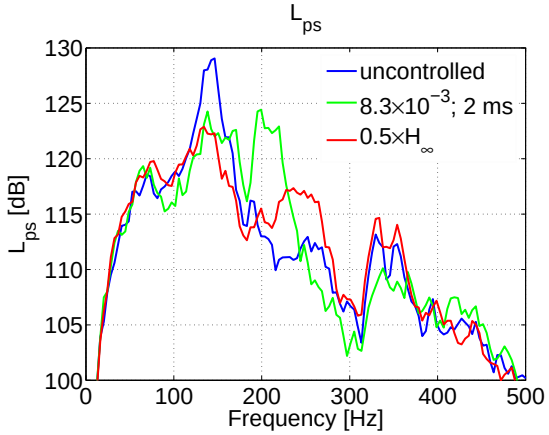

Figure 5.19: *Direct comparison of the Gain-Delay and $\mathcal{H}_\infty$ controller for the case 36/650/2.1. Pressure read at 303 mm. The $\mathcal{H}_\infty$ controller performs better.*

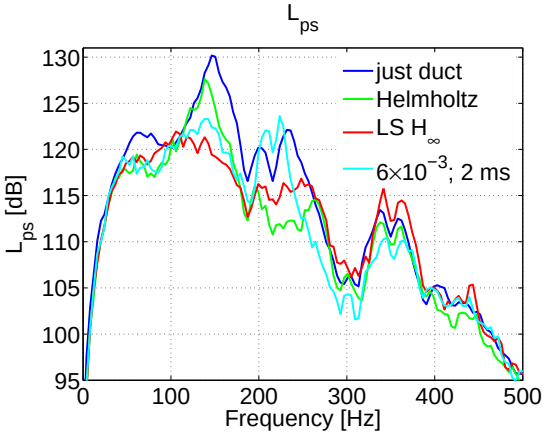

Figure 5.20: *Direct comparison of the pressure spectra at 123 mm with the Gain-Delay and $\mathcal{H}_\infty$ controller; and without a controller. Case 40/550/1.9.*

5.4 Control Experiments: Fuel Injector as Actuator

The previous section has shown that a loudspeaker can control the combustor, but it suffers from actuator saturation. A fuel injector has a much higher control authority, but may negatively affect the flame anchoring and therefore introduce instability and higher emissions.

5.4.1 Effect of Fuel Injector Offsets on Pressure Spectrum

Since the fuel injector is operated around some mean position, the effect of the necessary control signal offset and the ensuing mean flow through the valve are investigated. The additionally injected fuel is not as well mixed as the bulk of the air/fuel mixture, and more emissions occur subsequently. The offset should therefore be kept as small as possible, without trading off too much control authority. Fig. 5.21 shows the effect of various offsets on the pressure spectrum for the operating condition 36/700/2.1. Significant changes in flame anchoring and pressure spectrum occur beyond 0.35 V, so the mean position for further experiments is fixed at 0.25 V. Emissions only increase slightly for this value, see [101]. The picture is similar for 36/700/1.875, see Fig. 5.22, and the offset is also fixed at 0.25 V. The spectra are only affected in the frequency range shown.

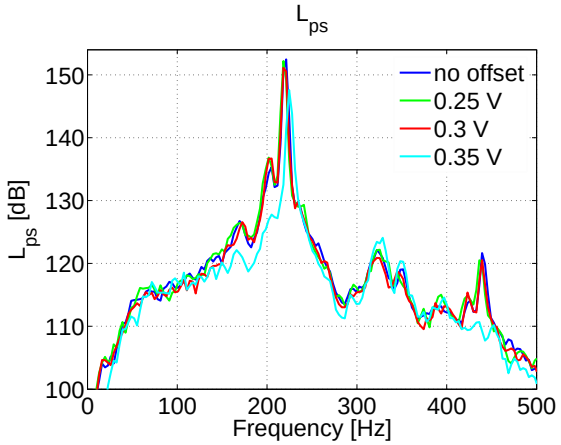

Figure 5.21: *The effect of the fuel injector control signal offset on the pressure spectrum for 36/700/2.1.*

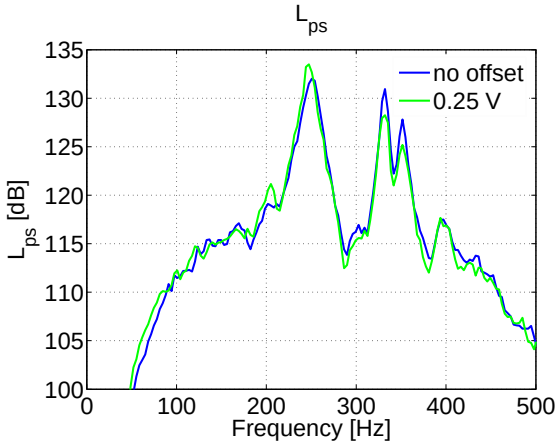

Figure 5.22: *The effect of the fuel injector control signal offset on the pressure spectrum for 36/700/1.875.*

5.4.2 Effect of Fuel Injector Control on Flame Structure

The case 40/550/1.9 is well controlled with a loudspeaker as actuator (apart from the saturation), but with a fuel injector the story looks different. The pressure signal as a function of time is plotted in Fig. 5.23, where a Gain-Delay controller with gain 3×10^{-4} and delay 0.3 ms is used.

Although this is a fuel rich regime, 550 K is a relatively low preheat temperature. The additionally injected fuel disrupts the flame anchoring mechanism and causes the flame to change its flame type. Periodic pressure bursts occur, which are accompanied by a visible change in flame structure. The flame is flapping back and forth between the inner and outer recirculation zones. This shows that it is not possible to control *any* type of flame with the fuel injector.

The spectrum during a thermal transient is nevertheless shown in Fig. 5.24. The Gain-Delay controller is able to reduce the first two peaks, at the cost of a higher peak at 240 Hz. This case is not investigated further, as the flame structure should not be altered to make correct statements about the performance of the controller.

In contrast, the operating condition 36/700/1.875 has a higher preheat temperature—additional fuel injection does not interfere strongly with the flame position. This is why further control experiments are carried out with this operating condition.

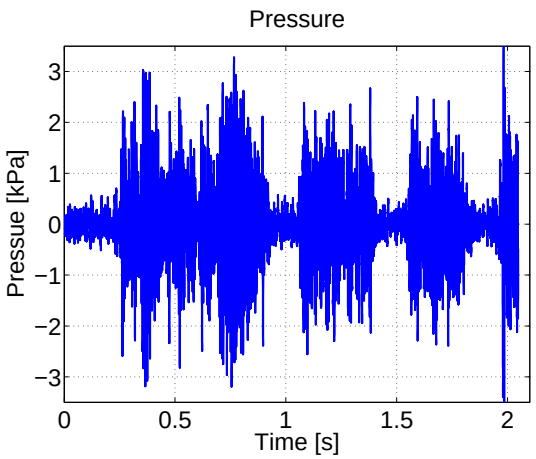

Figure 5.23: *The time trace of the pressure with a Gain-Delay controller for 40/550/1.9. Periodic bursts occur, a consequence of the changing flame structure caused by the secondary injection of fuel.*

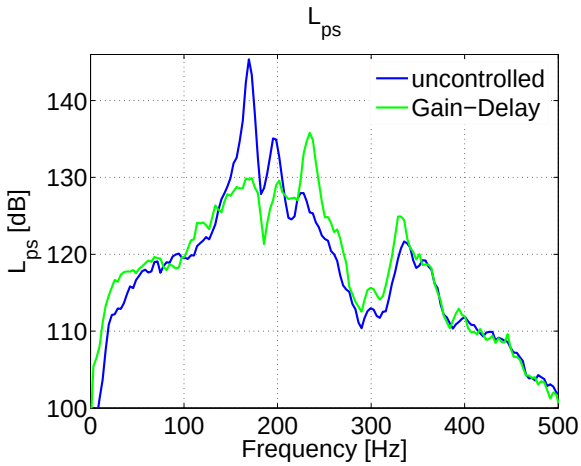

Figure 5.24: *The pressure spectrum obtained with a Gain-Delay controller for 40/550/1.9.*

5.4.3 Fuel Injector and Gain-Delay Control

The fuel injector is first operated under Gain-Delay control. Two cases are examined: flame type IIb 36/700/2.1 and flame type IIIa 36/700/1.875.

Case 36/700/2.1

The Gain-Delay controller is implemented with overall *positive* feedback, and various gains for a set delay of 0.7 ms are investigated. Fig. 5.25 shows the achieved pressure spectrum, and Fig. 5.26 the measured and modeled pressure spectrum reduction. The model of this operating condition has been obtained with the technique presented in Section 4.3.2.

The main peak at 218 Hz is strongly decreased, and its harmonic at 436 Hz disappears. Amplification of a secondary peak around 120 Hz becomes more pronounced as the gain is increased. This is an inevitable consequence of the waterbed effect, since sensitivity cannot be destroyed but merely shifted to other frequencies. Control signal saturation becomes more severe for gains higher than 2×10^{-4}.

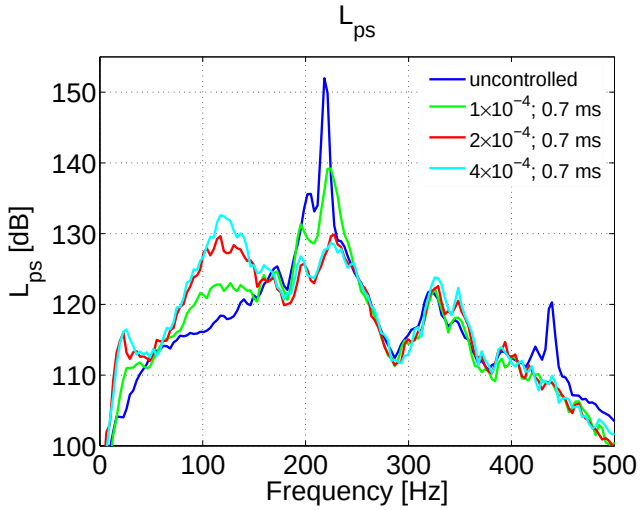

Figure 5.25: *The pressure spectrum for various positive gains using a Gain-Delay controller and the fuel injector. Flame case 36/700/2.1.*

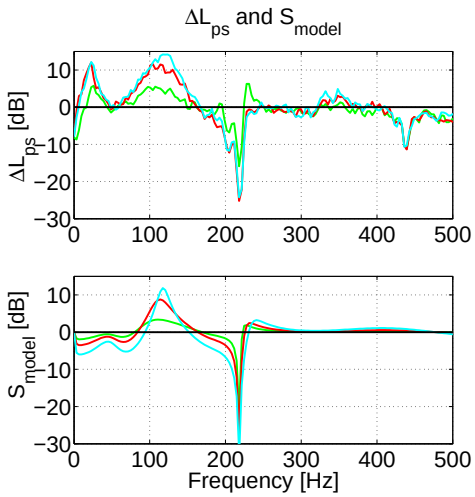

Figure 5.26: *The achieved and modeled pressure spectrum reduction for 36/700/2.1. The agreement between measurement and model is very good.*

The effect of changing the delay for a given gain of 1.4×10^{-4} is presented in Fig. 5.27 for the spectrum and in Fig. 5.28 for the measured and modeled spectrum reduction. The peak at 218 Hz is shifted to higher frequencies as the delay is increased, because the controller provides more phase loss.

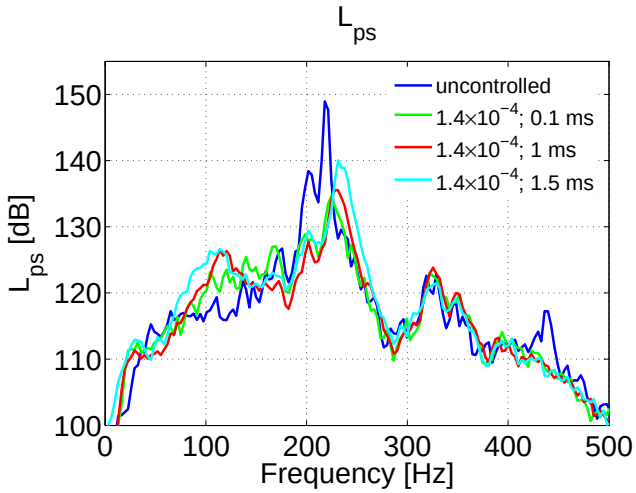

Figure 5.27: *The pressure spectrum for a positive gain and various delays for 36/700/2.1. Increasing delays move the resonant peak to higher frequencies.*

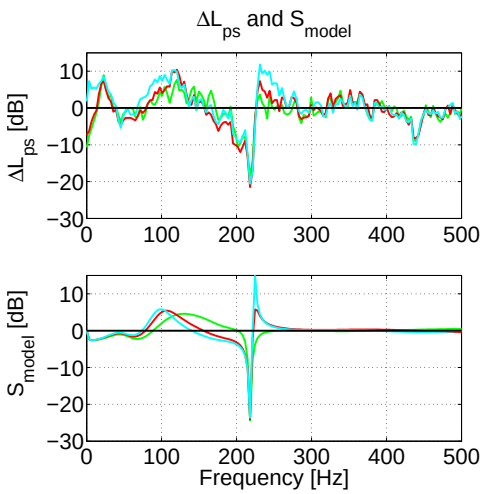

Figure 5.28: *The achieved and modeled pressure spectrum reduction for 36/700/2.1.*

The next controller presented is a Gain-Delay controller with overall *negative* feedback. Various values for the gain and the delay are tried, the resulting spectra are shown in Fig. 5.29, and the measured and modeled pressure spectrum reduction in Fig. 5.30. The main instability at 218 Hz is strongly decreased, and the secondary peak at 436 Hz due to saturation also vanishes. A low-frequency secondary peak at around 40 Hz appears, which is associated with flame anchoring problems. In that case, the flame has a tendency to flap back and forth between the two recirculation zones, a phenomenon similar to the one described in Section 5.4.2.

In order to investigate the behavior of the Gain-Delay controller, the averaged sound-pressure level L_{eq} as a function of the gain and delay is depicted in Fig. 5.31. Two minima can be discerned: -2×10^{-4} with a delay of -2.4 ms; and 2.5×10^{-4} with a delay of 0 ms. The difference between the two optimal delays corresponds to about 180° for 218 Hz. If the absolute value of the gain is increased more, the main peaks are suppressed more, but the growing secondary peaks cause the L_{eq} to rise.

The waterbed effect is observed in Fig. 5.32, where the pressure spectrum is shown for increasing gains and a set delay of 0.1 ms. The peak at 218 Hz decreases significantly, but a secondary peak in the 100 Hz range starts to grow.

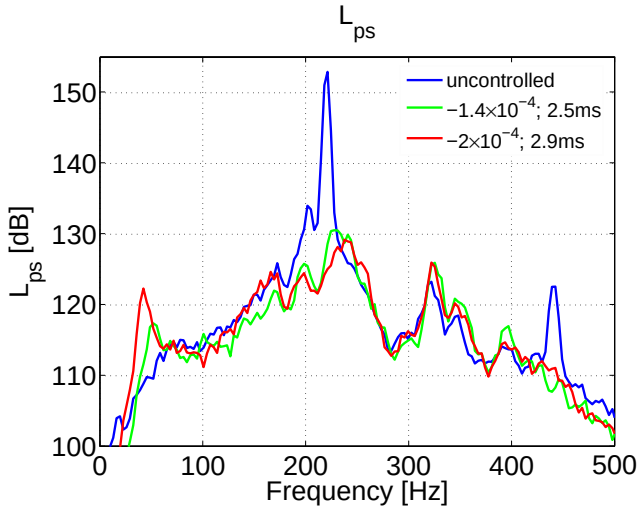

Figure 5.29: *The pressure spectrum for various negative gains for 36/700/2.1. A low-frequency mode around 40 Hz appears, which is associated with flame anchoring problems.*

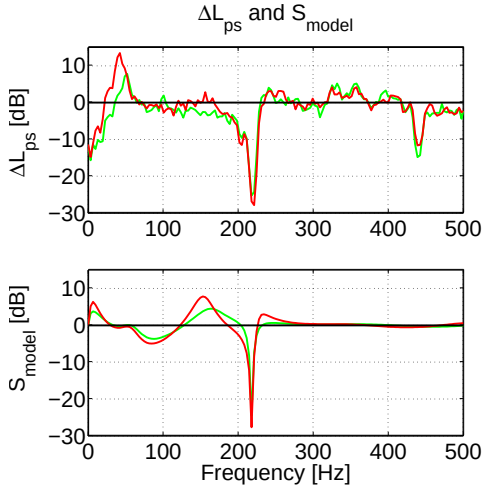

Figure 5.30: *The achieved and modeled pressure spectrum reduction for 36/700/2.1.*

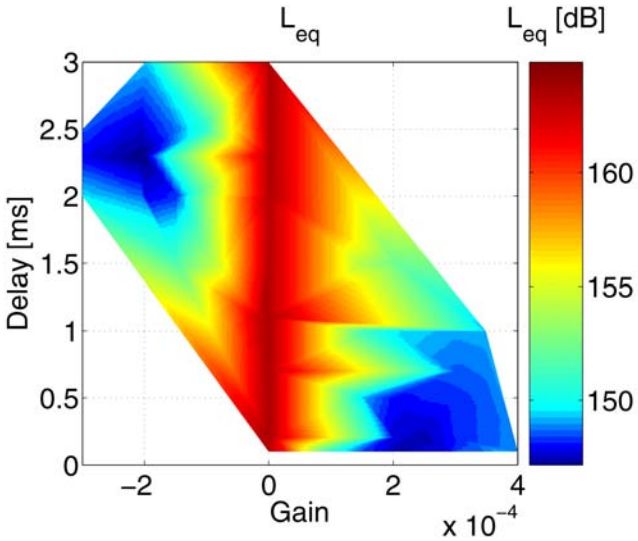

Figure 5.31: *The sound-pressure level L_{eq} as a function of various Gain-Delay parameters for 36/700/2.1. Two minima exist: one at -2×10^{-4} with a delay of -2.4 ms; and one at 2.5×10^{-4} with a delay of 0 ms.*

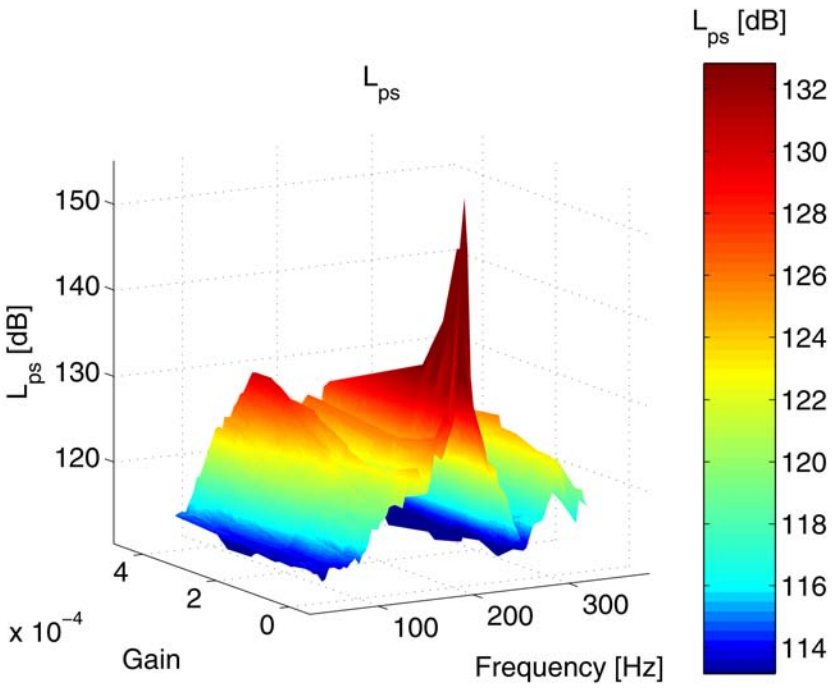

Figure 5.32: *The pressure spectrum for changing gains for 36/700/2.1. With increasing gains, the main instability at 218 Hz decreases, but a low-frequency mode around 100 Hz starts to grow. This is a consequence of the waterbed effect.*

Case 36/700/1.875

The previous section showed that the flame type IIb 36/700/2.1 can be satisfactorily controlled with a Gain-Delay controller, because one strong single peak instability is present. The flame type IIIa 36/700/1.875 on the other hand exhibits three peaks of roughly equal amplitude. Gain-Delay controllers can only provide optimal gain and phase at one single frequency, and are thus not expected to perform well in this case. Fig. 5.33 shows the achieved pressure spectrum with *positive* feedback configuration. Fig. 5.34 depicts the modeled and achieved pressure spectrum reduction. The reduction is rather poor.

The picture looks similar for overall *negative* feedback, see Fig. 5.35 and 5.36 for the spectrum and its reduction. The model predicts the behavior of the combustor accurately. Neither positive nor negative feedback can substantially decrease all three peaks at the same time.

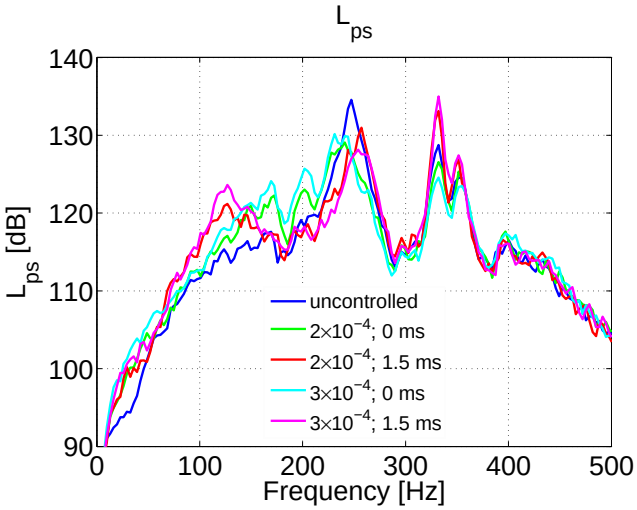

Figure 5.33: *The pressure spectrum for various positive gains for 36/700/1.875. A Gain-Delay controller with the fuel injector is used.*

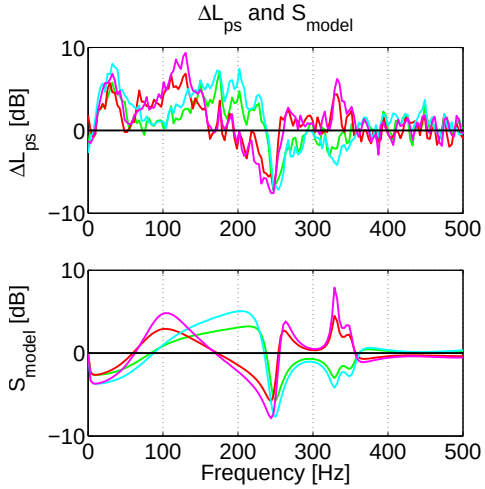

Figure 5.34: *The achieved and modeled pressure spectrum reduction for 36/700/1.875. The model works very well, but the pressure reduction is mediocre.*

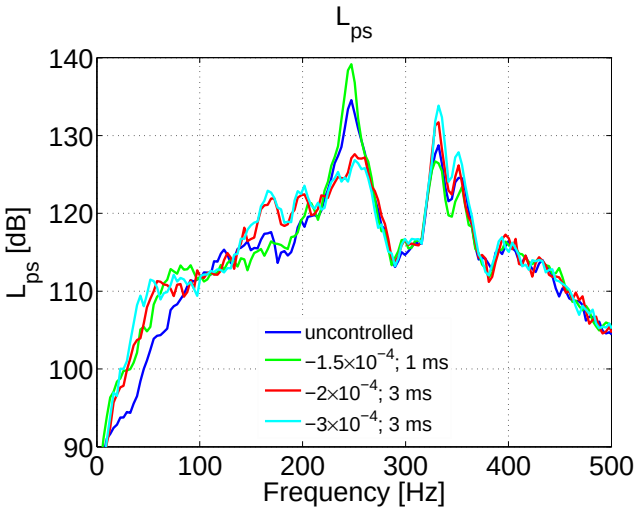

Figure 5.35: *The pressure spectrum for various negative gains for 36/700/1.875.*

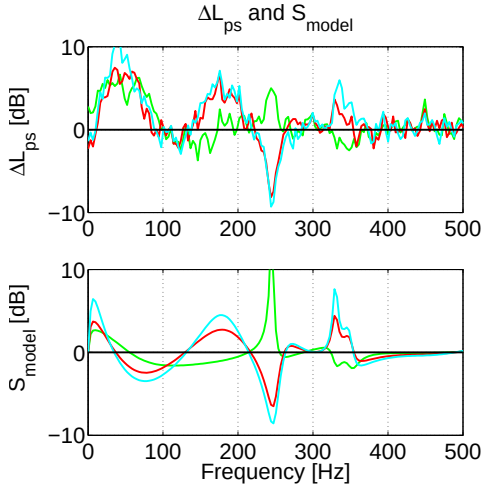

Figure 5.36: *The achieved and modeled pressure spectrum reduction for 36/700/1.875.*

5.4.4 Fuel Injector and $\mathcal{H}_\infty$ Control

The $\mathcal{H}_\infty$ design procedure outlined in Section 5.2.4 is now used on the models derived as explained in Section 4.3.2. Two cases are considered, 36/700/2.1 and 36/700/1.875.

Case 36/700/2.1

The main objective is to have a low sensitivity around 218 Hz. After the first iteration, it was found that the control signal has to be restricted in the low-frequency range. The bound W_u^{-1} is therefore set up as a high-pass filter. The bound on the complementary sensitivity W_y^{-1} is not used as shaping filter. Fig. 5.37 shows the weighting functions, the realized sensitivity S and KS. One of the problems with $\mathcal{H}_\infty$ control is the high

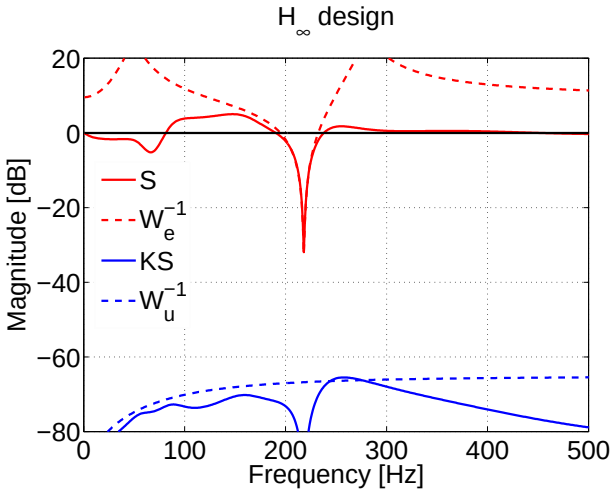

Figure 5.37: *The design process for $\mathcal{H}_\infty$ for the case 36/700/2.1. Low values of the sensitivity are desired around 218 Hz, and the control signal has to be restricted in the lower frequencies.*

order of the resulting controller, so that order reduction has to be performed. Hankel singular values of the balanced system are convenient to that end. Fig. 5.38 shows the Hankel values of the $\mathcal{H}_\infty$ controller plotted in Fig. 5.39, the order can be reduced from 27 to 6 without noticeably deteriorating the controller shape. Enhanced numerical stability is also achieved. The controller's simple shape explains why the simple Gain-Delay controller is also successful for the case 36/700/2.1. When the $\mathcal{H}_\infty$ controllers are implemented on the test rig, they are multiplied by a variable gain such that the human operator can intervene in case of developing harm. Here, they are multiplied by two gains, namely 0.5 and 1. The achieved pressure spectrum is shown in Fig. 5.40. The main instability at 218 Hz and its harmonic at 436 Hz are reduced. If the controller is

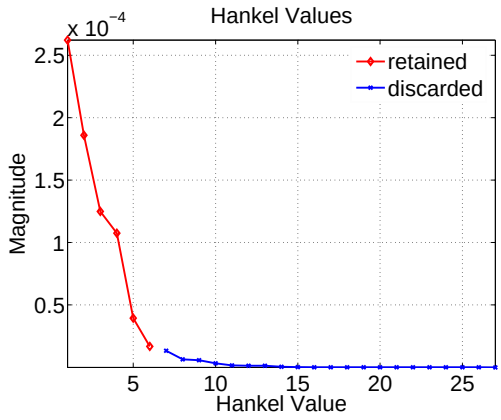

Figure 5.38: *The Hankel values of the $\mathcal{H}_\infty$ controller. An order reduction from 27 down to 6 is carried out.*

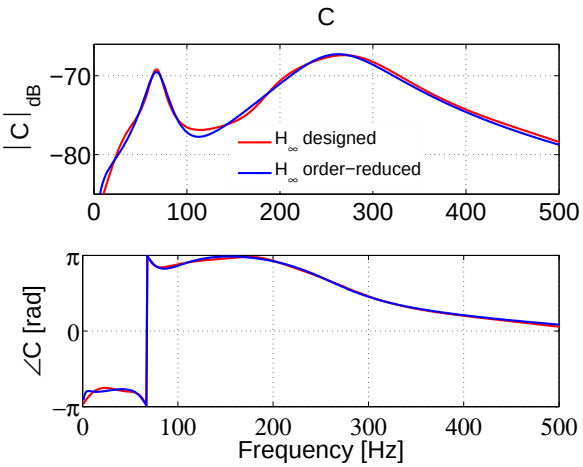

Figure 5.39: *The designed and order-reduced $\mathcal{H}_\infty$ controllers. The order reduction does not deteriorate the simple shape.*

implemented with a gain of 1, the performance is better than with 0.5. The measured and modeled spectrum reduction are plotted in Fig. 5.41. Their agreement is very good, except for frequencies below 50 Hz. This range is difficult to model because of alterations in the flame anchoring mechanism.

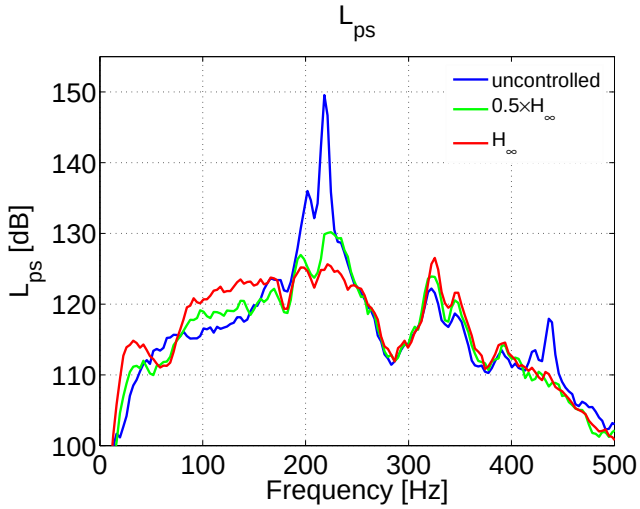

Figure 5.40: *The pressure spectrum with the $\mathcal{H}_\infty$ controllers implemented with gains 0.5 and 1. The main instability at 218 Hz is eliminated.*

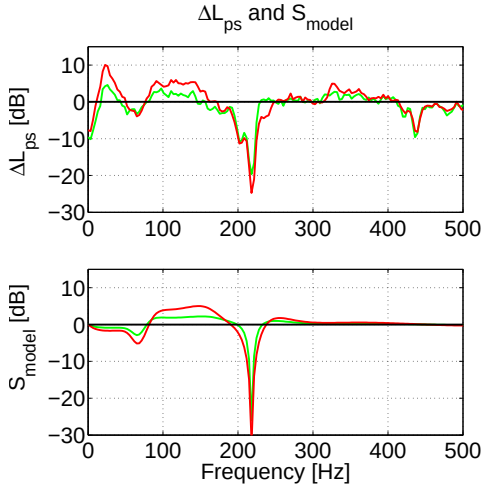

Figure 5.41: *The modeled and achieved pressure spectrum reduction with the $\mathcal{H}_\infty$ controllers for 36/700/2.1.*

Case 36/700/1.875, Three-Peak Reduction

This operating condition features three peaks in the pressure spectrum, one at 250 Hz and two others close to each other at 330 Hz and 350 Hz. Suppression is desired for these frequency ranges, so the sensitivity weighting function W_e is introduced, as seen in Fig. 5.42. The achieved sensitivity S is plotted as solid graph, and lies below the given bound W_e^{-1}. The control authority is also restricted in the low-frequency regime, to prevent flame anchoring problems and control signal saturation, see Fig. 5.42. Therefore, KS is bounded by a high-pass filter W_u^{-1}.

The designed $\mathcal{H}_\infty$ controller is state-reduced from order 27 down to 12, by using Hankel values, see Figs. 5.43 and 5.44. This controller is now noticeably more complex than a Gain-Delay controller.

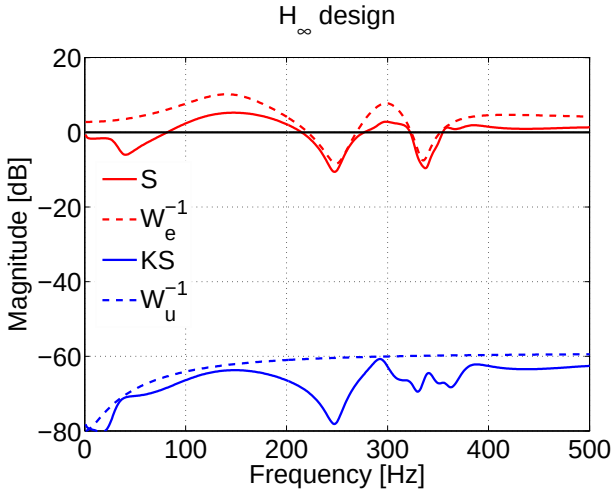

Figure 5.42: *The design process for $\mathcal{H}_\infty$ for the case 36/700/1.875. Pressure reduction is desired in two frequency bands, the control signal is limited in the low-frequency range.*

The controller is again implemented with various gains, namely 0.25, 0.75, and 1. The measured pressure spectra with and without controller are displayed in Fig. 5.45. To give a better appreciation of the pressure spectrum *reduction*, they are shown in the top plot of Fig. 5.46. The bottom plot depicts the expected sensitivity with the identified model. When the gain is set to 0.25, only a slight pressure spectrum suppression is observed. A higher gain of 1 pushes down the pressure in the designed regions around 250 Hz and 330 Hz. But this is at the expense of more noise in the 150 Hz range, a consequence of the waterbed effect. Saturation hampers the improvements expected by a higher gain of 1 compared to 0.75. A comparison of the two plots proves the very good accuracy of the identified model. For frequencies below 50 Hz, the model is less satisfactory, because flame anchoring issues dominate.

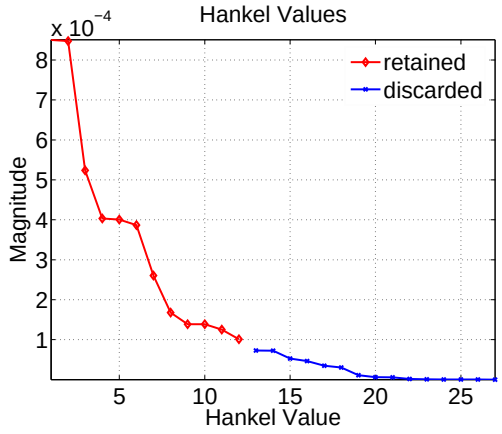

Figure 5.43: *The Hankel values of the $\mathcal{H}_\infty$ controller. An order reduction from 27 to 12 is performed.*

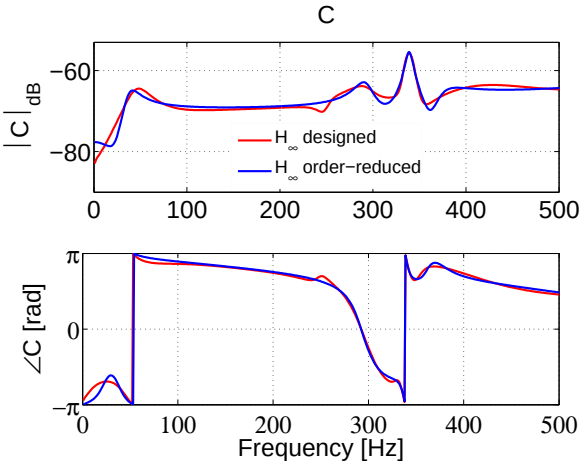

Figure 5.44: *The designed and order-reduced $\mathcal{H}_\infty$ controllers for 36/700/1.875. The controller shape is not affected much by the order reduction.*

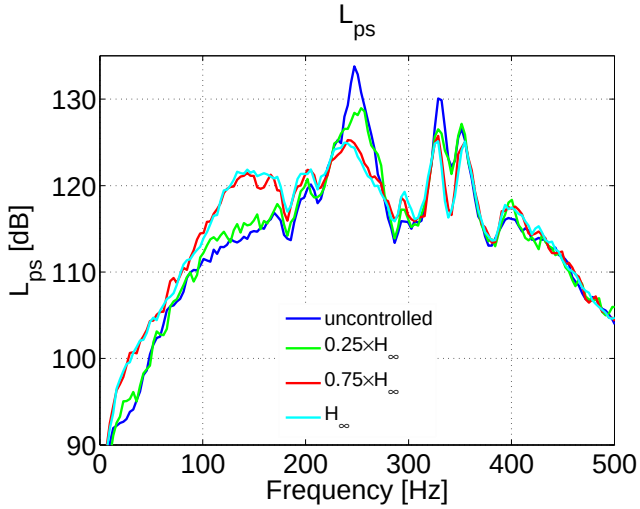

Figure 5.45: *The pressure spectrum obtained with the $\mathcal{H}_\infty$ controllers with gains 0.25, 0.75, and 1 for 36/700/1.875. Saturation hinders the improvements expected from the higher gain of 1 compared to 0.75.*

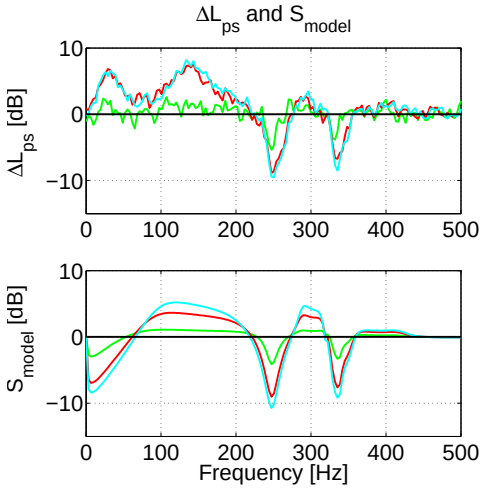

Figure 5.46: *The modeled and achieved spectrum reduction with the $\mathcal{H}_\infty$ controllers. The model is accurate.*

Case 36/700/1.875, One-Peak Reduction

This experiment shows the flexibility of the $\mathcal{H}_\infty$ approach. The main objective is now to decrease the peak at 250 Hz, taking into account that the 330 Hz range cannot be dealt with effectively, due to controller saturation. To that end, the bound on the sensitivity is designed such that the resulting sensitivity has a large dip around 250 Hz. The resulting controller is again implemented on the test rig with two gains, namely 0.5 and 1. The design figure is omitted, but the resulting controllers are shown in Fig. 5.47, with gains 0.5 and 1. The measured pressure spectrum with and without

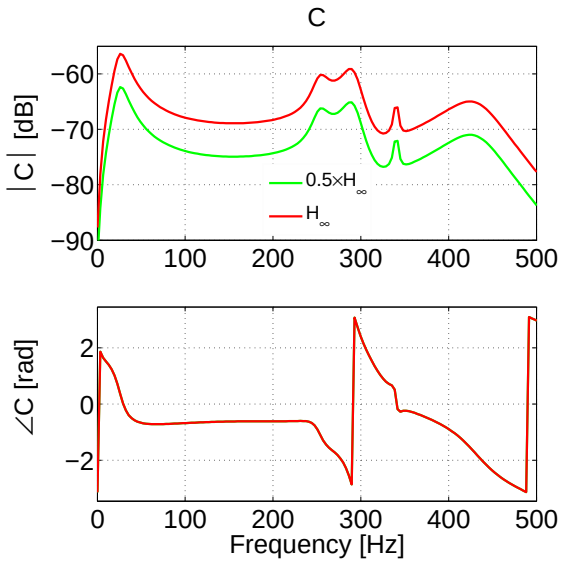

Figure 5.47: *The designed $\mathcal{H}_\infty$ controllers for 36/700/1.875, targeting the first resonance.*

controller is shown in Fig. 5.48. The suppression of the first peak is clearly visible, but also a rise in pressure spectrum around 150 Hz. To make things clearer, the measured pressure spectrum *reduction* is depicted in the top plot of Fig. 5.49, and the bottom plot shows the designed sensitivity. The model works well for frequencies higher than 50 Hz. The performance increase between gains 0.5 and 1 is not as marked as can be expected from the design process. This is because actuator saturation starts to limit the effectiveness. But the first peak is reduced by 14 dB, and the pressure spectrum around 340 Hz is still pushed down by 4 dB. This experiment shows the flexibility of the $\mathcal{H}_\infty$ controller design methodology. Only the sensitivity weighting function has to be adapted to the new objective, and a new $\mathcal{H}_\infty$ controller is readily available.

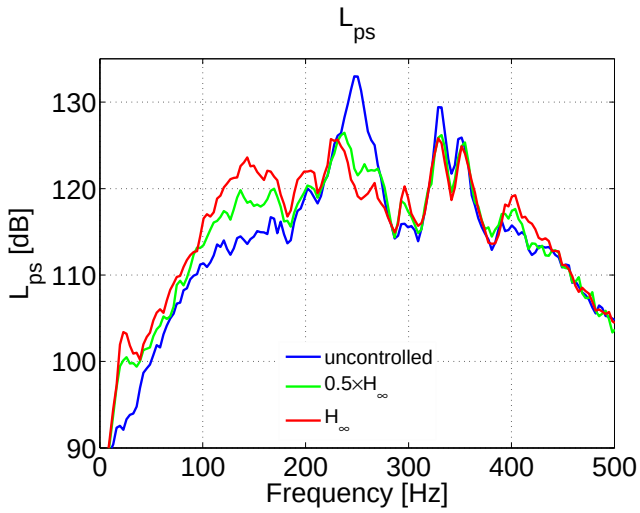

Figure 5.48: *The pressure spectrum achieved with the $\mathcal{H}_\infty$ controllers, implemented with gains 0.5 and 1.*

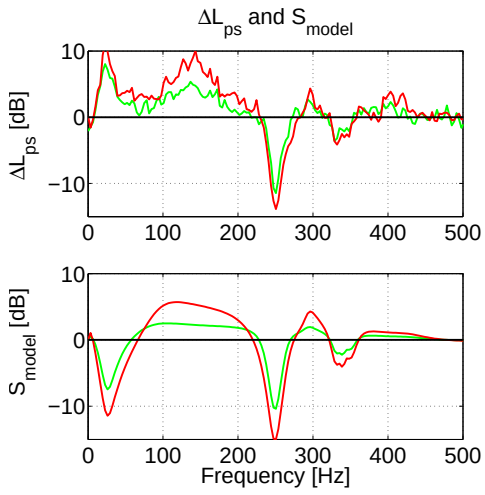

Figure 5.49: *The modeled and achieved spectrum reduction with the $\mathcal{H}_\infty$ controllers for 36/700/1.875, targeting the first resonance.*

5.4.5 Fuel Injector: Controller Comparison and Robustness Study

In order to assess the performance of the various controllers under changing conditions, the $\mathcal{H}_\infty$, peak, and phase-shift controllers are competing against each other directly. This is done for two operating conditions.

Case 36/700/2.1

This operating condition is quite sensitive to changes of the combustor cooling fluid. As the combustor is fired up, the instability at around 230 Hz grows and its frequency decreases, until it settles at about 218 Hz, see Fig. 5.50. This supports the point that in order to compare the controllers reliably for this case, they have to be run one after the other for short instants of time. The controllers are selected based on previous good performances. Note that they all have the same phase at 218 Hz, where the peak in the spectrum occurs, see Fig. 5.51. They are run in series during a start-up transient for the case 36/700/2.1—each controller provides the control signal for 10 s, and then the uncontrolled spectrum is recorded, too.

The control effort is measured as the averaged control signal level $L_{eq,u}$ of the control signal u: $L_{eq,u} = 10\log_{10}\frac{(u^2)_{av}}{u^2_{ref}}$, $(u^2)_{av}$ being the mean squared control signal and u^2_{ref}=1 V. Its evolution over time is plotted in Fig. 5.52. The peak filter requires

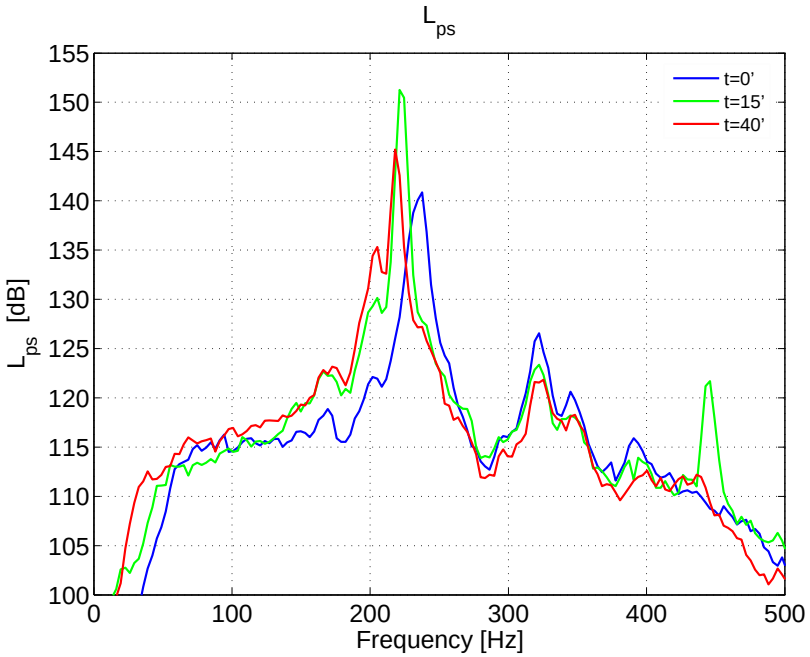

Figure 5.50: *Evolution of the pressure spectrum L_{ps} as the combustor heats up. It peaks at about 15 minutes after the start. Case 36/700/2.1.*

the highest control efforts, the $\mathcal{H}_\infty$ #2 and the positive Gain-Delay controllers are less demanding. They all generally increase slightly over time, consistent with the observation made in Fig. 5.50.

The uncontrolled averaged sound-pressure level L_{eq} measured at 123 mm peaks at 15 minutes and then decreases, see Fig. 5.54(a). The controllers have been laid out to decrease the instability around 218 Hz, which is initially quite sharp and contains most of the acoustic energy. As the combustor heats up, the acoustic energy is spread out over a wider frequency range and low-frequency components become more pronounced. The controllers thus become less effective at reducing L_{eq}.

Similarly, Fig. 5.55(a) shows the value of the peak in the pressure spectrum. It follows a similar pattern as the averaged sound-pressure level L_{eq}. The controlled peaks of the pressure spectrum stay around the same values. Fig. 5.54(b) shows the reduction in L_{eq} achieved by the various controllers. It indicates that $\mathcal{H}_\infty$ #1 performs best for all times, and the Gain-Delay controllers worst.

The superiority of the model-based controllers is also evidenced in the reduction of the pressure peak reduction, see Fig. 5.55(b). Here, $\mathcal{H}_\infty$ #2 performs best, followed by $\mathcal{H}_\infty$ #1. However, $\mathcal{H}_\infty$ #2 has a higher gain than $\mathcal{H}_\infty$ #1, and thus requires higher control inputs, see Fig. 5.52.

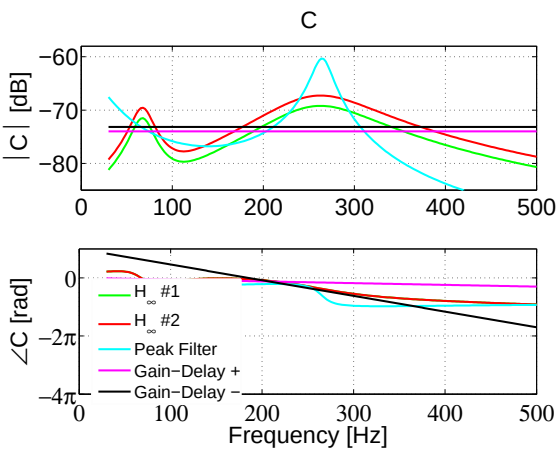

Figure 5.51: *The controllers used for the direct comparison for 36/700/2.1. They all have the same phase at the resonant frequency 218 Hz.*

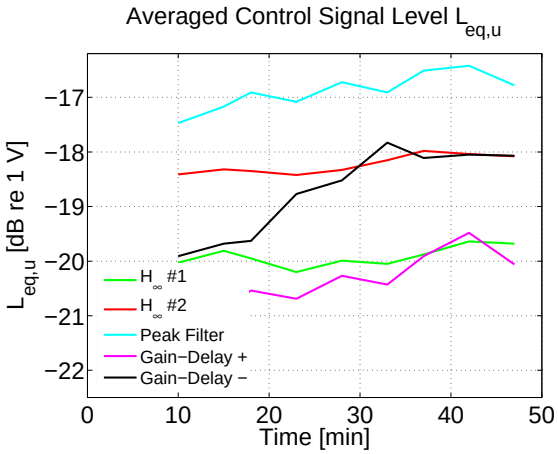

Figure 5.52: *The averaged control signal level $L_{eq,u}$ as a function of time. It generally rises, because the acoustic energy also increases over time.*

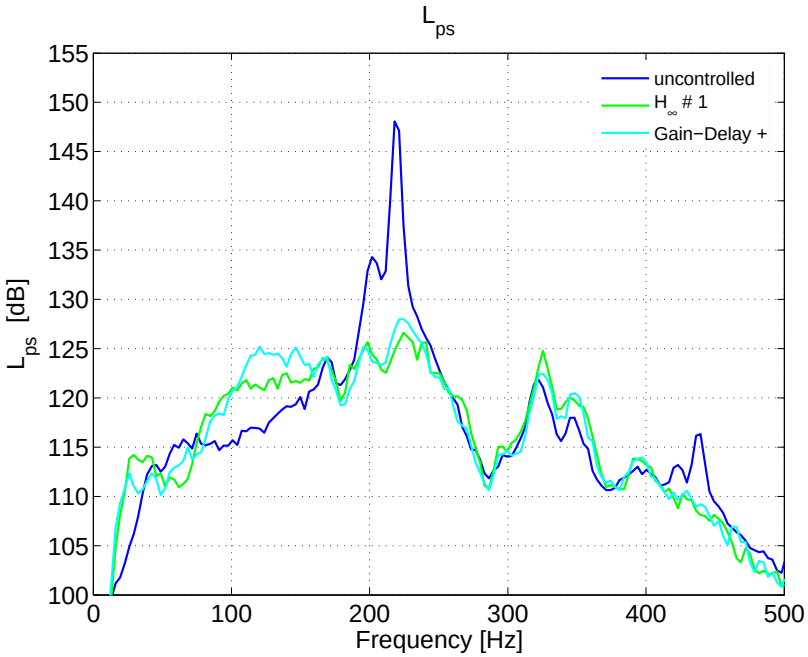

Figure 5.53: *The sound-pressure spectrum $L_{ps}(f)$ for 36/700/2.1. An $\mathcal{H}_\infty$ controller is compared with a Gain-Delay controller. The $\mathcal{H}_\infty$ #1 controller outperforms the Gain-Delay controller.*

Since the combustor spectrum exhibits the highest peak $L_{ps,max}(f)$ after about 15 minutes, the reduction of L_{eq} is also highest then, as is the peak reduction $L_{ps,max}(f)$.

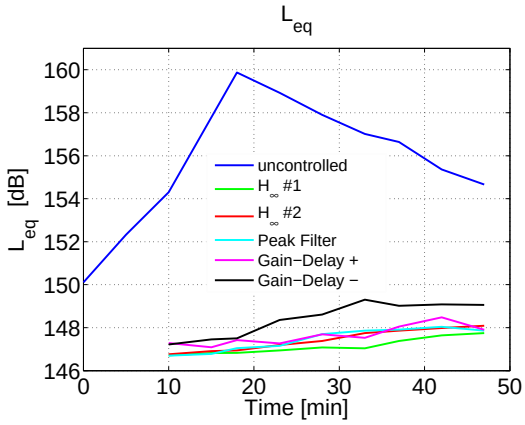

(a) L_{eq}

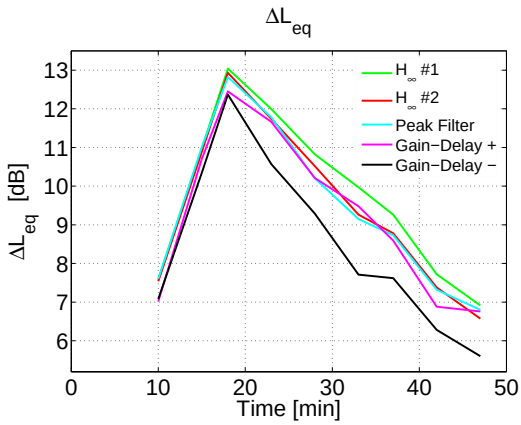

(b) L_{eq} *reduction*

Figure 5.54: *The averaged sound-pressure level L_{eq} for various controllers as a function of time. It peaks at about 15 minutes. The bottom plot shows the reduction achieved by the controllers. The $\mathcal{H}_\infty$ #1 controller performs best, the Gain-Delay controllers worst.*

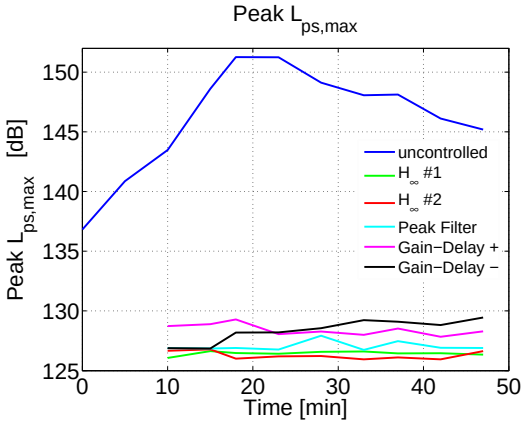

(a) $L_{ps,max}(f)$

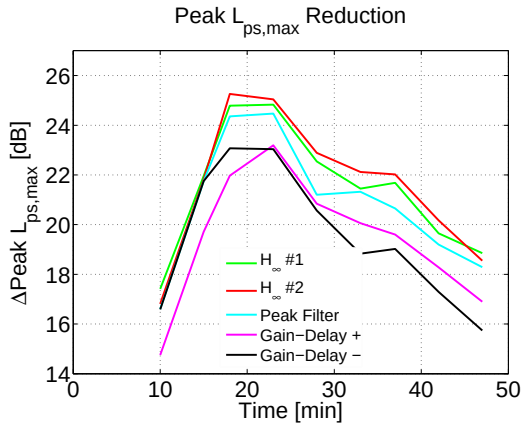

(b) $L_{ps,max}(f)$ *reduction*

Figure 5.55: *The peak value of the spectrum $L_{ps,max}(f)$ for various controllers as a function of time. The bottom plot shows the reduction achieved by the controllers. The $\mathcal{H}_\infty$ #2 controller performs best, the Gain-Delay controllers worst.*

The Peak Filter offers acceptable L_{eq} and good $L_{ps,max}(f)$ reduction, but also demands the highest control input. The Gain-Delay controllers perform worst in both L_{eq} and $L_{ps,max}(f)$ reduction.

Finally, Fig. 5.53 compares the pressure spectrum achieved by the $\mathcal{H}_\infty$ #1 and the positive Gain-Delay controller. The superiority of the model-based approach is evident.

Case 36/700/1.875

The case 36/700/1.875 is thermally much more stable than the previous case, so the pressure spectrum does not drift. Fig. 5.56 shows the employed controllers: again three $\mathcal{H}_\infty$, one peak, and two Gain-Delay controllers. The phase for the controllers is similar at the first peak, for the second it is different. The individual spectrum reductions for the various controllers are shown in Fig. 5.57, along with the predictions from the model. The model accurately predicts the observed behavior. It also shows that the $\mathcal{H}_\infty$ controllers have a clear edge over their simpler counterparts—they can achieve significant reductions in both frequency ranges.

A comparison between the achieved spectrum for $\mathcal{H}_\infty$ #1, $\mathcal{H}_\infty$ #3, and the positive Gain-Delay controllers is shown in Fig. 5.58.

In summary, the controllers performed as shown in Fig. 5.59. The red bars shows the reduction in averaged sound-pressure level ΔL_{eq}, the yellow bars the reduction of the first peak around 350 Hz and finally the green bar the reduction in the second peak region around 330 Hz. It becomes clear that the model-based $\mathcal{H}_\infty$ controllers perform best in all three areas, demonstrating the superiority of this approach over ad-hoc controllers.

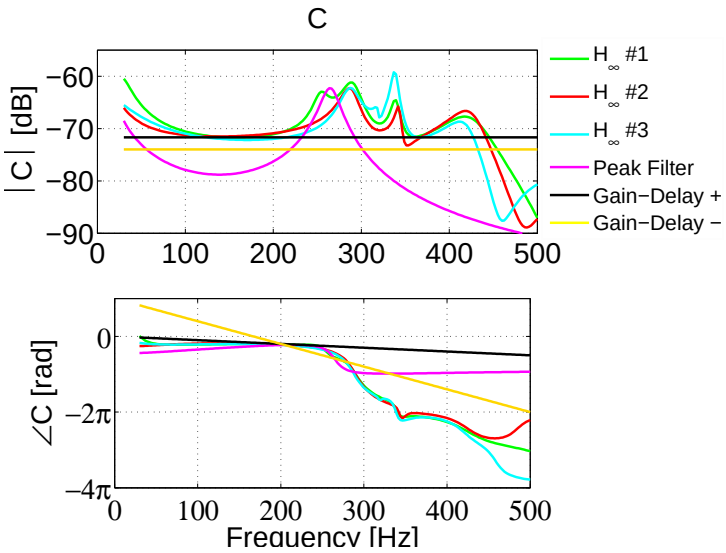

Figure 5.56: *The controllers used for the direct comparison for 36/700/1.875. They have a similar phase around 250 Hz, but differ at 330 Hz.*

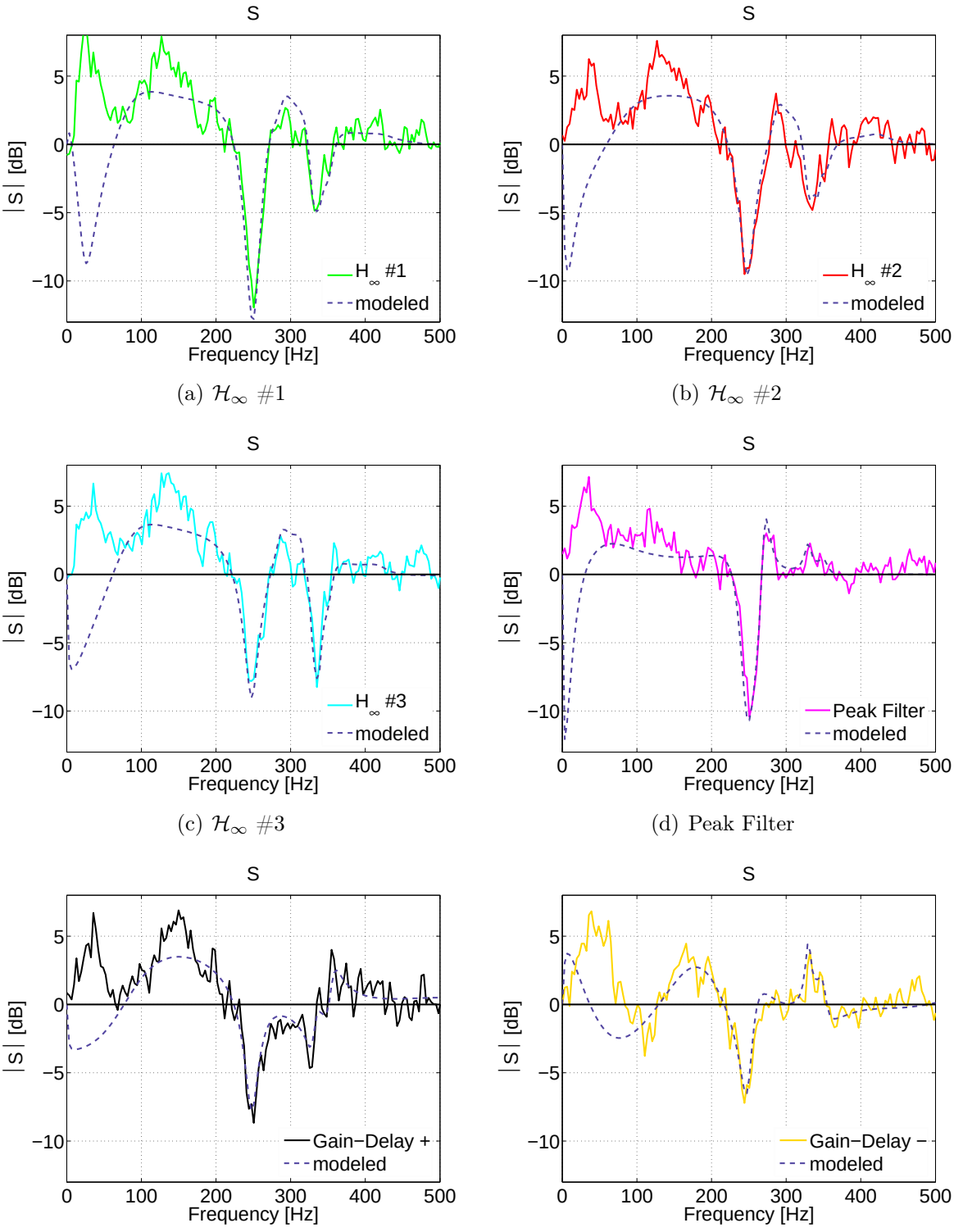

(a) $\mathcal{H}_\infty$ #1

(b) $\mathcal{H}_\infty$ #2

(c) $\mathcal{H}_\infty$ #3

(d) Peak Filter

(e) Gain-Delay +

(f) Gain-Delay -

Figure 5.57: *The measured and modeled pressure spectrum reductions for six controller types. Case 36/700/1.875.*

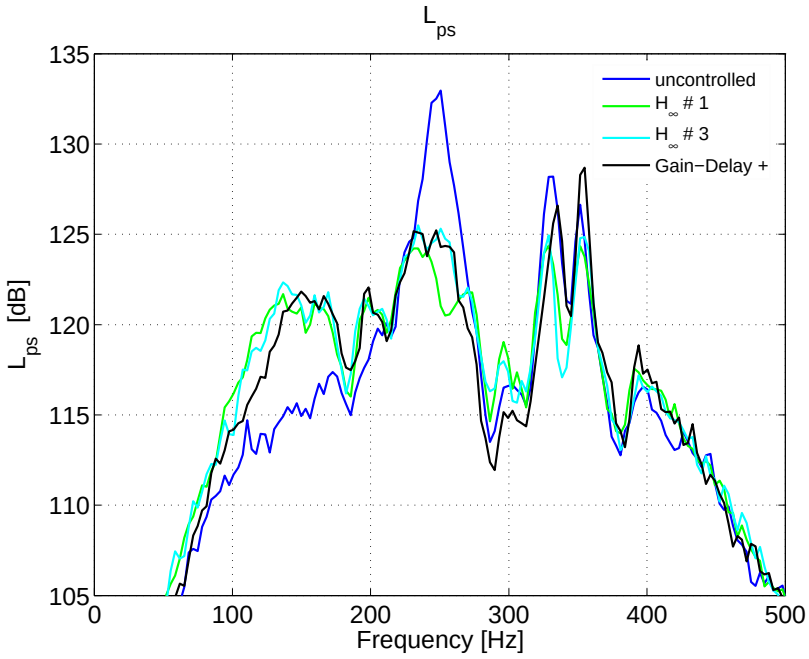

Figure 5.58: *The averaged sound-pressure level $L_{ps}(f)$ for 36/700/1.875. It compares the $\mathcal{H}_\infty$ #1, $\mathcal{H}_\infty$ #3, and the positive Gain-Delay controllers. $\mathcal{H}_\infty$ #1 is able to push down the first peak at 250 Hz and the second at 330 Hz at the same time. The Gain-Delay controller in contrast* increases *the second peaks.*

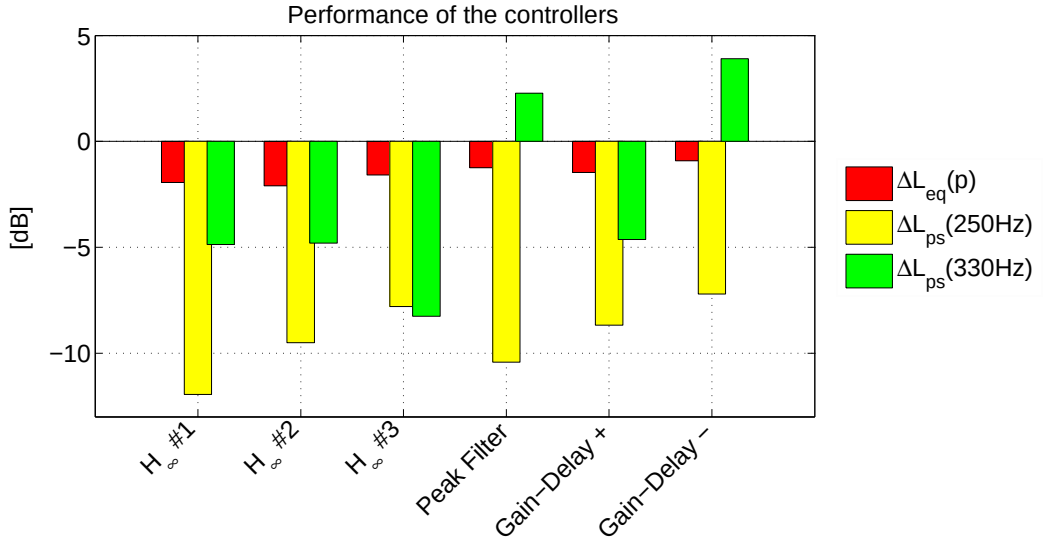

Figure 5.59: *The performance of the various controllers for 36/700/1.875. The first column displays the equivalent sound-pressure level reduction, the second the pressure spectrum peak reduction at 250 Hz, and the third the reduction at the second peak at 330 Hz. The model-based $\mathcal{H}_\infty$ controllers have a clear edge over their simpler counterparts.*

5.4.6 Fuel Injector and CMA-ES Optimization

The goal of this study is to improve controllers online while the combustor is running. A suitable cost function is defined which an optimization algorithm aims to minimize.

The Covariance Matrix Adaptation Evolution Strategy CMA-ES has been developed by Niko Hansen [116]. It is a population based evolutionary algorithm able to cope with noisy objective functions. The algorithm is described in more detail in the first journal publication in Section E. Two control structures are subjected to this optimization: Gain-Delay and $\mathcal{H}_\infty$ controllers.

Gain-Delay control is convenient because there are only two parameters to adjust, which is often done in a trial-and-error way. Its performance is often satisfactory if the spectrum of the instability only features one dominant peak. Model-based $\mathcal{H}_\infty$ controllers on the other hand offer more design freedom and generally better performance. However, their often complex nature with 10-20 parameters makes online optimization difficult. Thermal transients during start-up change the location and height of the pressure peaks, and the (steady-state) model of the process is not always accurate. Therefore, the combination of a model-based controller and an online optimization using robust evolutionary algorithms is well suited. More specifically, a previously designed $\mathcal{H}_\infty$ controller [212] is shifted in the frequency domain by multiplication of the controller's A and B matrix by a frequency shift parameter. The gain and optionally an additional delay are also adjusted, giving two (three) parameters to be optimized by the evolutionary algorithm. This is compared with a Gain-Delay controller, where only the gain and the delay are optimized by the algorithm. The cost function to be minimized is selected as the equivalent continuous level of the sound pressure

$$L_{eq} = 10 \log_{10} \frac{(p_s^2)_{av}}{p_{ref}^2} \tag{5.3}$$

where $(p_s^2)_{av}$ is the mean squared pressure and p_{ref}=20 μPa the reference pressure.

The sound-pressure level L_{eq} is acquired from a measurement of a few seconds with a given parameter setting, where the outcome is subject to a considerable uncertainty. A tradeoff between accuracy and speed can be identified. The accuracy of L_{eq} is improved with longer evaluation times. On the other hand, longer evaluation times decrease the number of completed measurements in a given time span and therefore slow down the adaptation of the controller parameters. This problem will be approached by an adaptive evaluation time to acquire L_{eq}.

Implementation of the Algorithm on the Test Rig

The CMA-ES delivers a set of controller parameters to be evaluated together with a requested function evaluation time. The controller parameters undergo an affine transformation from the interval $[0, 1]$ onto respective intervals as given below. The controller is assembled and written to the real-time board. In order to avoid any risks with potentially bad parameter settings delivered by the CMA-ES algorithm, the gain of the new controller is ramped up over the course of two seconds, such that the human operator can intervene in case of developing harm. After the data acquisition has been completed, the controller gain is ramped down, and an intermediate controller keeps the combustor in a stable regime. Meanwhile, pressure data is logged, a new controller is developed and transferred to the real-time board.

The total cycle time thus consists of ramping the controller gain up and down (about 2 s each), pressure data acquisition (determined by the algorithm, $1 - 10$ s), data logging (1 s) and CMA-ES computation time (negligible). The maximum time that pressure can be logged is currently limited to 10 s, due to real-time board memory constraints. The controller is sampled at 10 kHz, the frequency content of the pressure signal warrants no aliasing effects during sampling. For the following experiments, the preheat temperature and the mass flow are kept constant at 700 K and 36 g/s, respectively. Two values for λ are investigated, namely $\lambda = 2.1$ and $\lambda = 1.875$.

Experiment: Gain-Delay Controller, Cold Start, $\lambda = 2.1$ and Switch to $\lambda = 1.875$.

The combustor is fired up from ambient temperature, an operating condition is set with a mass flow of 36 g/s, a preheat temperature of 700 K, and an air/fuel ratio of $\lambda = 2.1$, and the Gain-Delay controller is turned on. As the system heats up, the sound-pressure level L_{eq} rises. Previous studies have shown that the admissible maximum absolute value of the gain for a Gain-Delay controller decreases as the combustor heats up for this operating condition. This is attributed to the fact that the low-frequency content of the pressure signal rises, and the resulting low-frequency components of the fuel injection tend to alter the flame stabilization. The flame then flaps back and forth and increases the noise floor.

The heat-up phase is also evident in the pressure spectra of the controlled combustor taken at 1000 s and 4700 s, shown in Fig. 5.60. The plant is uncontrolled and Gain-Delay controlled (gain -1.8×10^{-4}, delay 0.3 ms), the resulting L_{eq} are 159.87 dB, 146.90 dB, and 147.48 dB, respectively.

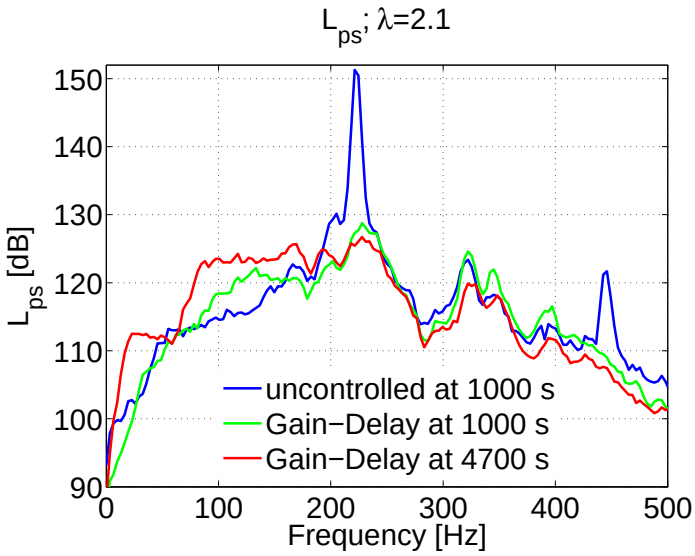

Figure 5.60: *A comparison of the uncontrolled and controlled spectra of the pressure signal at* 1000 *s and* 4700 *s for the same Gain-Delay controller and* $\lambda = 2.1$.

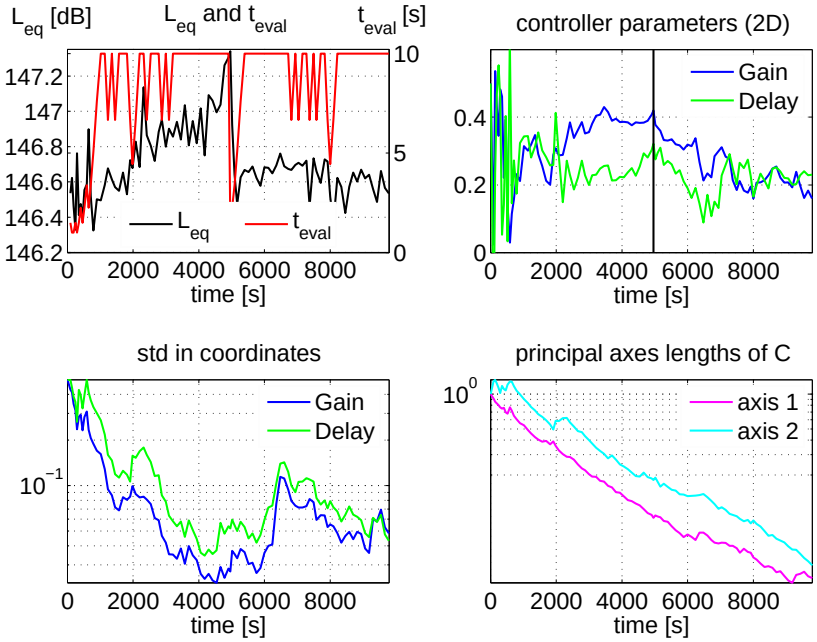

Figure 5.61: *Parameter evolution for the CMA-ES optimization of a Gain-Delay-controller. At* 4800 *s, the operating condition is changed from* $\lambda = 2.1$ *to* $\lambda = 1.875$.

The CMA-ES optimizes the gain and the delay of the Gain-Delay controller. The evolution of the parameters is shown in Fig. 5.61, where the gain interval $[-3\times10^{-4}, 0]$ and the delays from $\{0.1, 0.2, \ldots, 1.15\}$ ms are mapped onto $[0, 1]$. Previous experiments with manual tuning have shown that actuator saturation and flame stabilization problems occur if the gain is chosen lower than -3×10^{-4}, or the delay is higher than 1.5 ms. The initial gain and delay passed to the CMA-ES algorithm are -1×10^{-7} and 1.5 ms, respectively. During the first 4800 seconds L_{eq} rises as the combustor heats up, and the optimal value of the gain increases from about -2.5×10^{-4} at 1000 s to -1.8×10^{-4} at 4800 s. The rise of L_{eq} is related to the persistent change of the system conditions during heat-up and seems to have no adverse effect on the optimization. During the first 1000 s the evaluation time increases and reaches 10 s, the maximum allowed. That means noise is becoming an issue. The standard deviations decrease during the first 4000 seconds and rise again as the operating condition is changed.

At 4800 s, the operating condition is changed from $\lambda = 2.1$ to $\lambda = 1.875$, and the evaluation time is manually set to 1 s.

Four cost function landscapes for different time intervals are shown in Fig. 5.62. They are obtained by Delauney triangulation of a second-order polynomial fit to the L_{eq} results for the individual delay slices. The noise levels are on the order of 2 dB for evaluation times of 1 s, and gradient-based search algorithms would fail in this problem. Pentagrams show the best parameter set for each generation; the larger they are, the later they have been acquired for each plot. A black circle marks the last of the pentagrams. The topmost plot shows the L_{eq} for the first 150 function evaluations (up to 1300 s). It shows that the gain can be chosen quite negative; and the overall landscape features low L_{eq} values. For the function evaluations from 150 to 250 ($1300-2700$ s), the evaluation time increases and yields results with less noise. A trend to less negative values for the gain becomes apparent (the pentagrams indicating the best of the generations are moving to the right), and the general background noise level rises (indicated by areas getting darker).

The black polygon is the convex hull of *all* controller parameter values tried in the given time range. The function evaluations $250-325$ ($2700-3800$ s), shown in the third plot, indicate that the optimal value for the gain lies around -1.8×10^{-4} and for the delay around $0.4-0.5$ ms. The parameters evaluated are now narrowed down to the smaller black polygon. If this result is compared to the last plot showing function evaluations $325-390$ ($3800-4800$ s), the optimal values for the gain and the delay are confirmed, but the cost function evaluated L_{eq} rises. This is in accord with the observation that the combustor exhibits slowly rising sound-pressure levels for $\lambda = 2.1$.

At run 395 (4800 s), the lambda value is changed to $\lambda = 1.875$. This operating conditions exhibits less thermal drift than the previous one. The changing operating

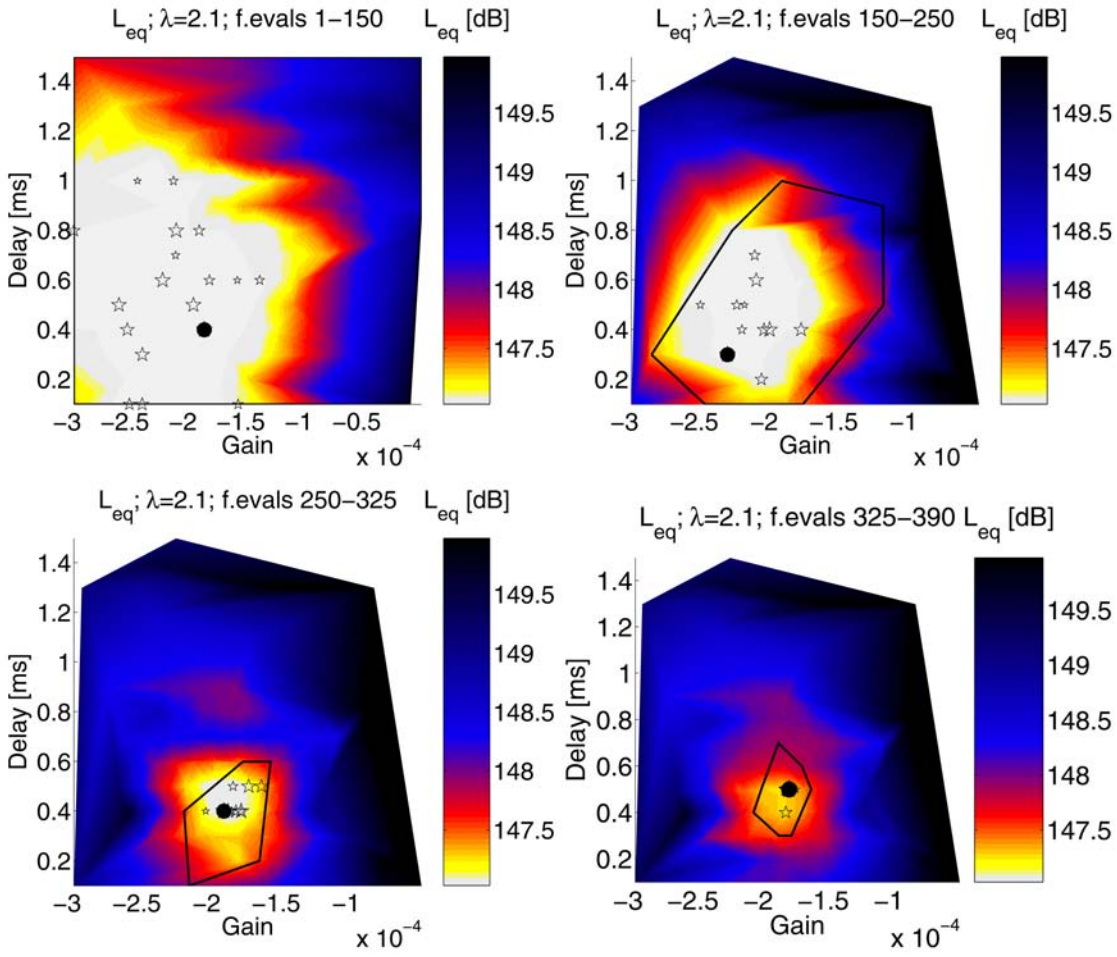

Figure 5.62: *CMA-ES optimization of a Gain-Delay controller for $\lambda = 2.1$, heating up. Function evaluations, from top plot down:* 1−150*;* 150−250*;* 250−325*;* 325−390*. Pentagrams show the best parameter set for each generation, the larger they are, the later they have been acquired for each plot. The black polygon is the convex hull of all controller parameter values tried in the given time range.*

conditions can clearly be discerned in the cost function L_{eq} shown in Fig. 5.63. The algorithm finds a new minimum, now the gain can be chosen more negative.

The evaluation time increases immediately again, indicating no big improvement of the signal-to-noise ratio, even though the controller is less close to its optimal regime. This suggests that σ should be increased together with t_{eval}. The course of σ supports this conjecture. It increases by a factor of three and shows the adaptive capability of the algorithm. In this experiment, it takes 8 generations until the increase of σ appears. The CMA-ES successfully adjusts the controller parameters to new optimal values, see Fig. 5.61, upper right.

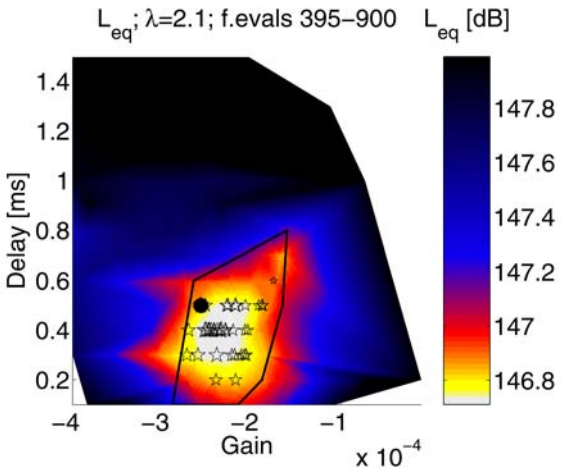

Figure 5.63: *CMA-ES optimization of a Gain-Delay controller for* $\lambda = 1.875$*. Function evaluations* $395 - 740$ *(*$4900 - 9800$ *s).*

Experiment: $\mathcal{H}_\infty$ Controller, Two Parameters Optimized, $\lambda = 1.875$.

An $\mathcal{H}_\infty$ controller has been designed for the operating condition with $\lambda = 1.875$, where the goal was to simultaneously decrease the three peaks at 250 Hz and around 330 Hz. In order to keep the number of parameters small and to speed up convergence, only the gain and the frequency shift are optimized.

The intervals for the frequency shift, $[0.95, 1.05]$, and gains $[0.4, 1.1]$, are mapped onto $[0, 1]$, see Fig. 5.64. The cost function landscape is shown in Fig. 5.65. It is obtained by DACE, a Matlab toolbox for working with kriging approximations to computer models, which has been kindly provided by Hans Bruun Nielsen from the Technical University of Denmark[1]. A second-order polynomial has been used as regression model and a Gaussian correlation. For this experiment with an $\mathcal{H}_\infty$ controller, the cost function is flatter than with the Gain-Delay controller, because the controller is model-based, and thus already performs well. However, the optimization shows that in order to decrease L_{eq}, the gain has to be reduced to about 0.7. This is explained by the fact that the $\mathcal{H}_\infty$ design process has been laid out primarily to decrease the three peaks in the spectrum, without special concern given to the reduction of L_{eq}.

[1] http://www2.imm.dtu.dk/~hbn/dace/

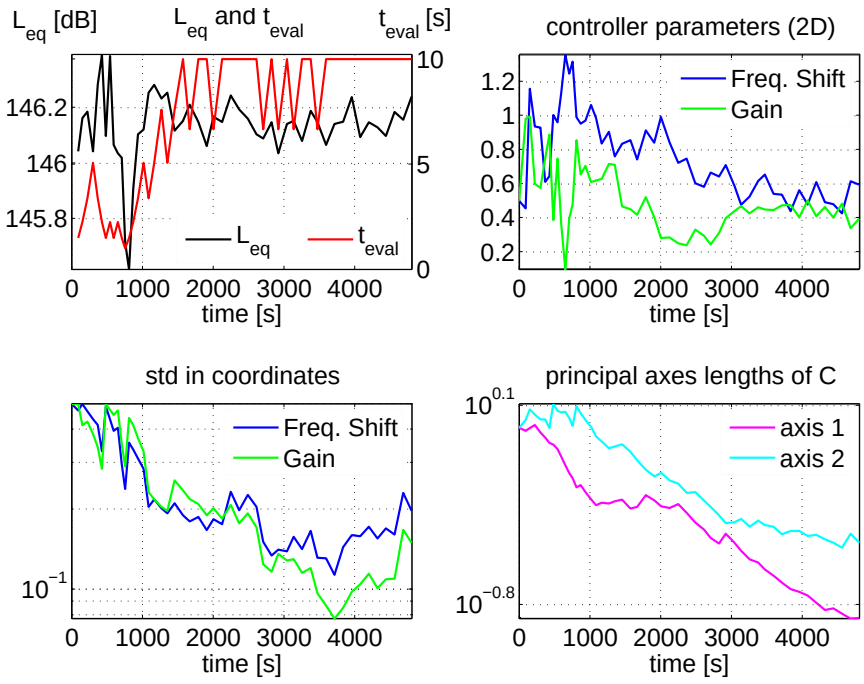

Figure 5.64: *Parameter evolution for the CMA-ES optimization of an $\mathcal{H}_\infty$ controller for $\lambda = 1.875$.*

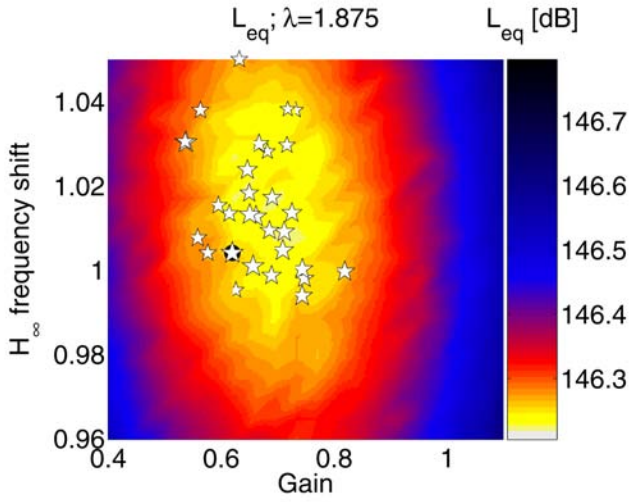

Figure 5.65: *The resulting cost function landscape for the CMA-ES optimization of an $\mathcal{H}_\infty$ controller for $\lambda = 1.875$. Pentagrams show the best parameter set for each generation.*

Experiment: $\mathcal{H}_\infty$ Controller, Three Parameters Optimized, $\lambda = 1.875$.

For the following experiment, three parameters are optimized by the CMA-ES: the gain and frequency shift of the $\mathcal{H}_\infty$ controller, and an additional time delay.

The evolution of the parameters is shown in Fig. 5.66 (frequency shift interval $[0.95, 1.05]$, gains $[0.4, 1.1]$, delays $[1, 10]$). The initial values are all set to 1.

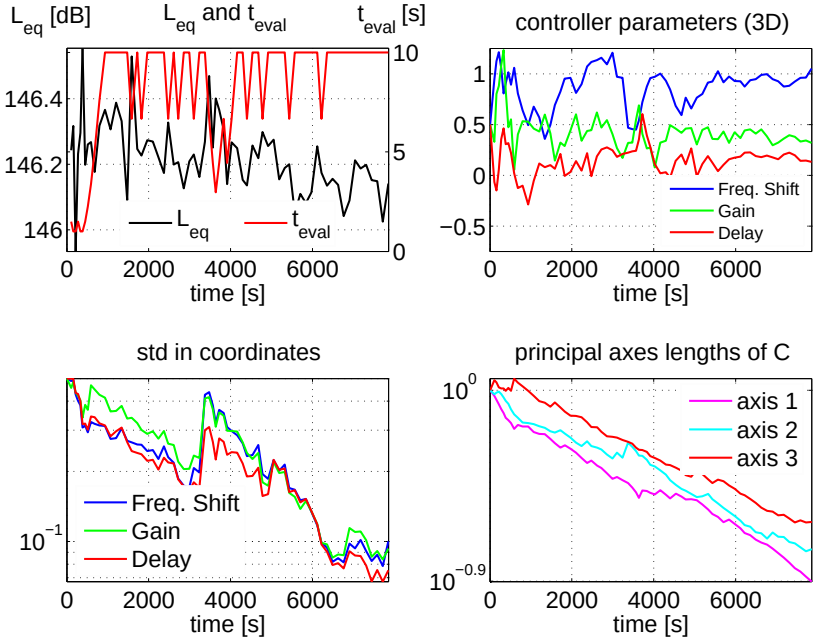

Figure 5.66: *Parameter evolution for the CMA-ES optimization of an $\mathcal{H}_\infty$ controller for $\lambda = 1.875$. Three parameters are being optimized.*

The cost function now takes three arguments. In order to make the graphical interpretation of the results more accessible, four cost function landscapes with fixed delays of 0.1 ms to 0.4 ms are shown in Fig. 5.67. The topmost plot corresponds to the bottom plot of Fig. 5.64, where only the frequency shift and gain are adjusted, but the delay is kept at 0.1 ms for all experiments. Gain and frequency shift have similar values but exhibit a larger variation. The minimum L_{eq} is lower for a delay of 0.2 ms, and even lower for a delay of 0.3 ms, while it increases again for 0.4 ms (bottom plot).

The Bode plots of the designed and optimized $\mathcal{H}_\infty$ controllers are shown in Fig. 5.68. The superior performance of the $\mathcal{H}_\infty$ controller goes hand in hand with a more complex shape. The optimized controller has nearly the same phase as the designed one, but the gain is lower. Since the delay is adjusted additionally, it is possible to move the controller in the frequency domain while keeping the phase similar.

As a result for the operating condition characterized by $\lambda = 1.875$, the spectra achieved with the optimized Gain-Delay and $\mathcal{H}_\infty$ controllers are compared to the

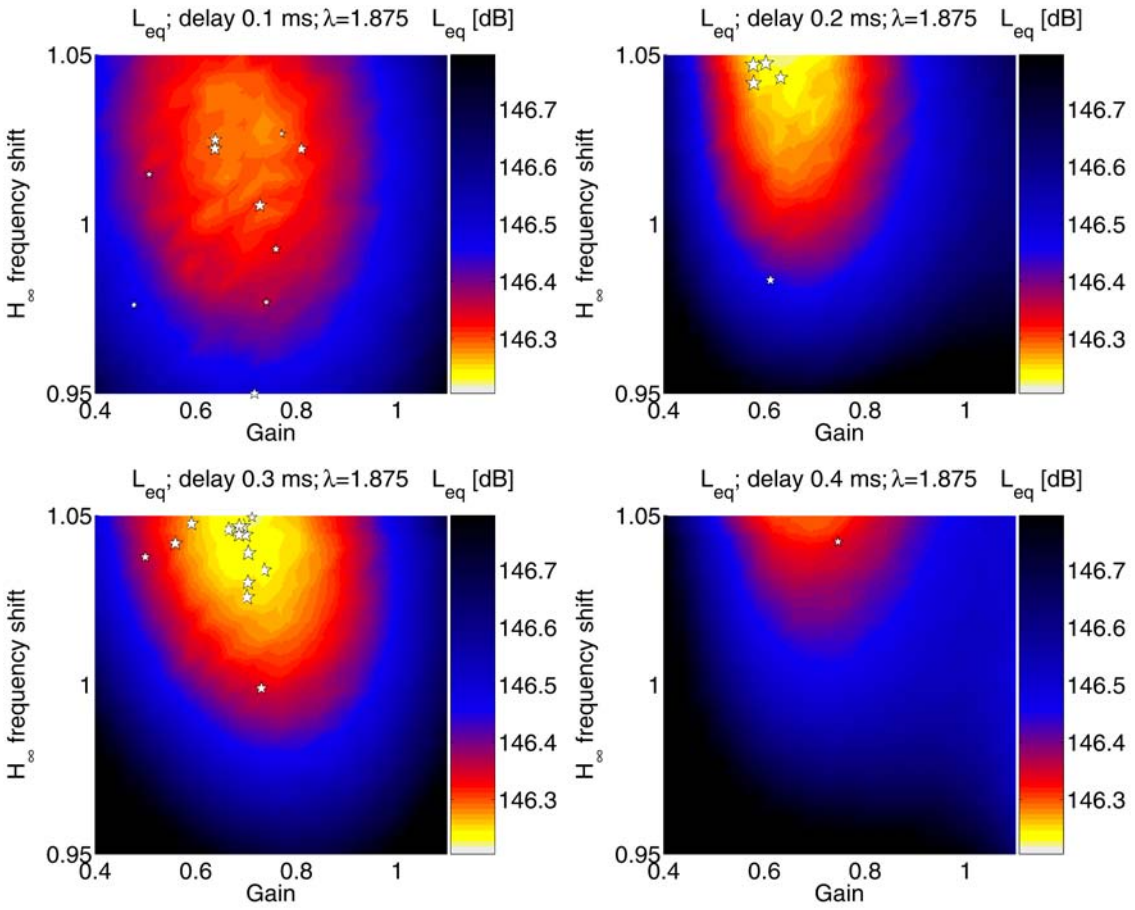

Figure 5.67: *CMA-ES optimization of an $\mathcal{H}_\infty$ controller for $\lambda = 1.875$. Delays from top plot down:* 0.1 *ms*-0.4 *ms. Pentagrams show the best parameter set for each generation.*

uncontrolled plant in Fig. 5.69. The L_{eq} of the uncontrolled plant is 148.72 dB, the Gain-Delay controller reduces it to 146.67 dB, and finally the $\mathcal{H}_\infty$ controller reaches 146.16 dB, which is about 15% lower again. Moreover, the $\mathcal{H}_\infty$ controller is able to simultaneously push down all three peaks and to attain the flattest spectrum. This is achieved thanks to the model-based approach, conferring the most design freedom to the engineer.

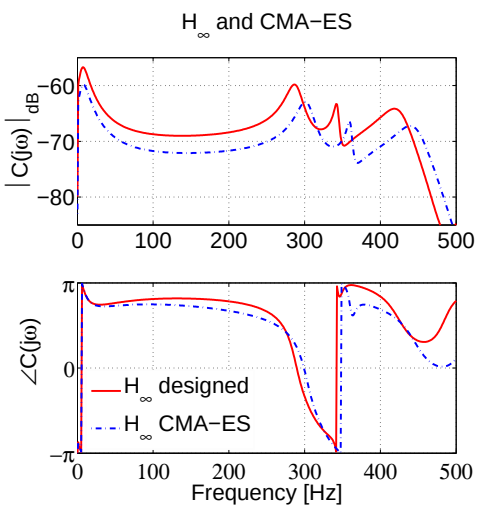

Figure 5.68: *The designed and the CMA-ES-optimized $\mathcal{H}_\infty$ controllers for $\lambda = 1.875$.*

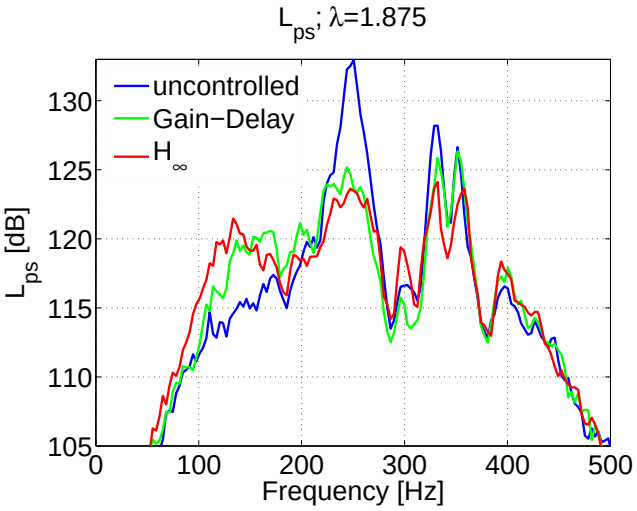

Figure 5.69: *Comparison of the pressure spectra when the plant is uncontrolled, Gain-Delay, and $\mathcal{H}_\infty$ controlled. Both controllers are CMA-ES optimized, $\lambda = 1.875$.*

Experiment: $\mathcal{H}_\infty$ Controller, Two Parameters Optimized, $\lambda = 2.1$.

Finally, the CMA-ES is used to improve an $\mathcal{H}_\infty$ controller designed for $\lambda = 2.1$. The parameter evolution is shown in Fig. 5.70 (frequency shift interval $[0.95, 1.05]$, gain interval $[0.4, 1.1]$), and the cost function landscape in Fig. 5.71. It becomes clear that a lower gain can decrease the L_{eq} compared with the designed controller, but the frequency shift does not have a decisive effect. The final standard deviations for gain and frequency shift differ by a factor of about three (lower left of the top plot of Fig. 5.70) reflecting the different sensitivities of the parameters.

The Bode plots of the designed and the optimized controllers are shown in Fig. 5.72. The controller phase is quite flat and therefore tolerant against frequency shifts. The combustor pressure spectrum exhibits only one very distinct peak, and it suffices to provide the right amount of gain and phase at this frequency.

To compare the spectra attained by the CMA-ES optimized Gain-Delay and $\mathcal{H}_\infty$ controllers against the one from the uncontrolled plant, they are plotted together in Fig. 5.73. The values of L_{eq} are 159.87 dB, 147.48 dB, and 147.35 dB, respectively. They are shown for the plant which has been running for several hours and is therefore heated up. In this case, the $\mathcal{H}_\infty$ controller performs only slightly better than the Gain-Delay controller, but the control signal contains about 10% less energy.

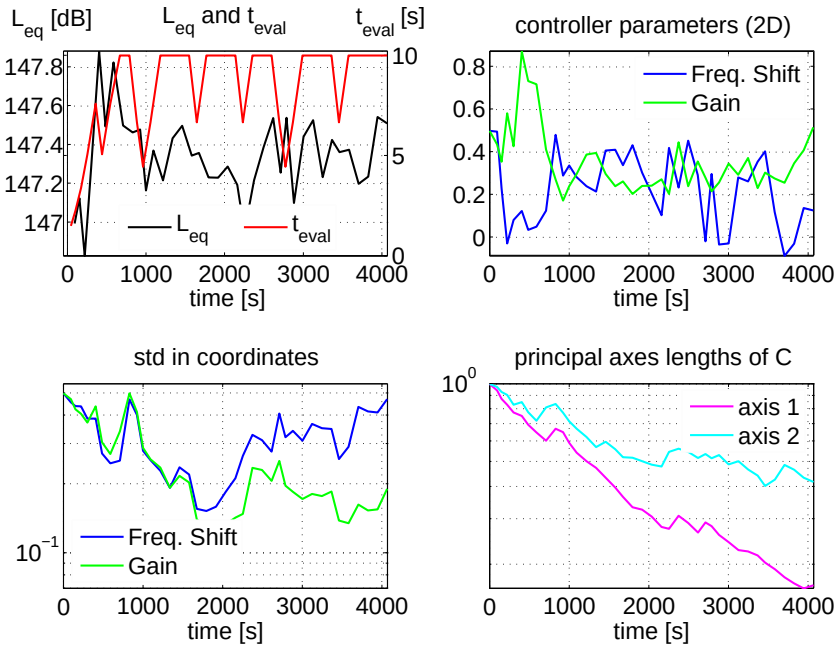

Figure 5.70: *Parameter evolution for the CMA-ES optimization of an $\mathcal{H}_\infty$ controller for $\lambda = 2.1$.*

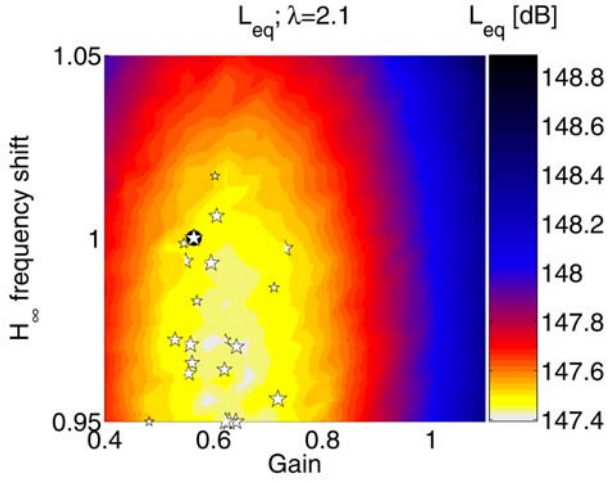

Figure 5.71: *The resulting cost function landscape for the CMA-ES optimization of an $\mathcal{H}_\infty$ controller for $\lambda = 2.1$. Pentagrams show the best parameter set for each generation.*

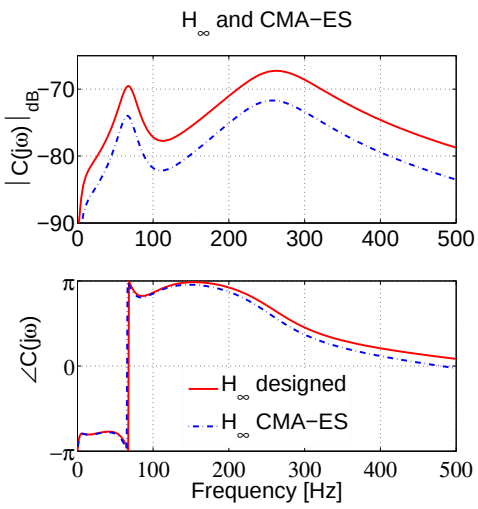

Figure 5.72: *The designed and the CMA-ES-optimized $\mathcal{H}_\infty$ controller for $\lambda = 2.1$.*

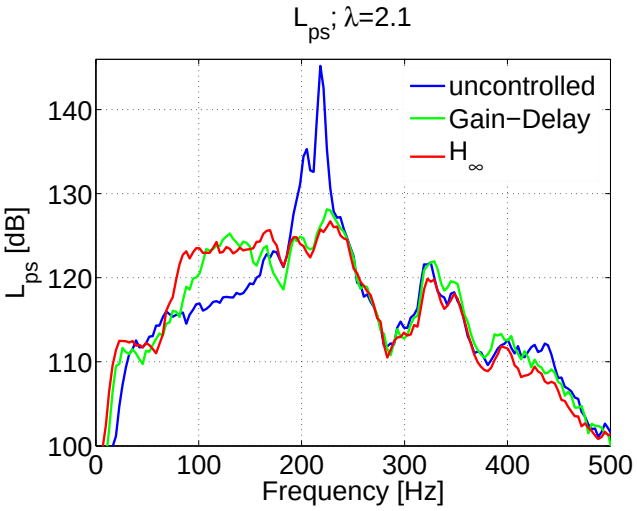

Figure 5.73: *Comparison of the uncontrolled with the Gain-Delay and $\mathcal{H}_\infty$ controlled plant for $\lambda = 2.1$. Both controllers are CMA-ES optimized.*

Summary

This chapter presented the control experiments carried out. First, passive approaches have been investigated. Helmholtz resonators work only in a limited frequency range, and are preferably mounted downstream. Secondly, active control has been implemented with two actuators: loudspeakers and a secondary fuel injector mounted close to the flame. The former also acts as Helmholtz resonator, but actuator saturation is a serious constraint. The latter offers more control authority, but must be installed close to the flame. The offset of the control signal has to be chosen correctly.

Gain-Delay control works reasonably well for operating conditions with a single large peak in the pressure spectrum. But model-based $\mathcal{H}_\infty$ controllers perform better, especially when applied to more challenging cases. Such a case features three peaks in the pressure spectrum, and $\mathcal{H}_\infty$ control gives the control engineer the freedom to decrease either all three peaks, or to focus on a single peak.

A novel way to improve controllers is presented. The CMA-ES algorithm evaluates the performance of various controllers online while the combustor is running. It then manipulates them so as to decrease a given cost function. This algorithm is noise-resistant and able to cope with changing operating conditions. A drawback of evolutionary algorithms is their rather slow convergence time, and the potential to propose bad controller parameters to be evaluated.

6

Summary and Conclusions

Da steh' ich nun...

JWvG

This thesis has presented the results of an investigation on thermoacoustic oscillations in premixed gas turbine combustors.

A discussion of the problem and an extensive literature survey explained the mechanisms involved.

A test rig has been built at ETH Zürich to study combustion instabilities. It is built around ALSTOM's EV burner; the premixed flame is swirl-stabilized in two recirculation zones and burns natural gas. The acoustic pressure fluctuations in the combustor are sensed with microphones; loudspeakers are mounted to identify and control the test rig. To achieve more control authority, a secondary fuel injector is installed close to the flame. This magnetostrictive injector is manufactured by MOOG Japan and offers a high bandwidth.

The model of the combustor is derived based on the network idea. The constituent blocks represent elements such as the ducts, burner, flame, and end conditions. For each of them, a physical model is derived and validated with measurements. In particular, the $L-\zeta$ burner model and the $n-\tau$ flame model work remarkably well. They have been investigated over a wide range of operating conditions, and linked to the results from optical investigations. The different flame types identified in a companion thesis [101] are reproduced as different parameters in the $n-\tau$ flame model.

The blocks are finally assembled to the network model. The transfer functions obtained in this way correspond well to experimentally measured ones. Here, the input is the loudspeaker voltage and the output the sensed pressure.

A new and easy-to-implement strategy to obtain the transfer function from the voltage to the fuel injector to a pressure reading is introduced. This method is robust, works in a closed-loop manner and can be implemented quickly. It yields excellent results.

In order to control combustion oscillations, passive strategies based on Helmholtz resonators are studied. They work well over a limited frequency range, and are more efficient downstream than upstream. To have more design freedom and control authority, active feedback control is introduced.

The problem is treated from a control engineer's point of view, hence fundamental limits of feedback control are elaborated. Two actuators are implemented on the test rig: loudspeakers and a secondary fuel injector. The loudspeaker housing by itself acts as a passive Helmholtz resonator. When active control methods are added on top, high pressure reductions are obtained. However, actuator saturation is identified as a serious constraint. Therefore, only the fuel injector is an industry-relevant actuator.

The effect of additionally injected fuel on the flame and pressure spectrum is studied. It is shown that it is not possible to control any type of flame, because problems with the flame anchoring process occur. Moreover, the control signal offset which determines the mean flow through the valve has to be carefully negotiated as a function of available control authority and increasing emissions. A number of controller structures are subsequently evaluated—their respective merits and disadvantages are highlighted.

For operating conditions where a distinct peak in the pressure spectrum is present, simple Gain-Delay controllers perform satisfactorily. More advanced designs such as the robust model-based $\mathcal{H}_\infty$ controller still yield better results. The superiority of this approach is clearly manifested in a more complex case, where three peaks are present in the pressure spectrum. It allows the control engineer to design a controller such that all three peaks are pushed down at the same time. The focus can also be concentrated on one peak only, which is then reduced more. Actuator saturation, mainly of the electrical amplifier driving the injector, becomes also a problem but to a lesser degree.

A novel idea to improve controllers online is presented, namely the CMA-ES optimization routine. It is shown how this algorithm can make Gain-Delay and $\mathcal{H}_\infty$ controllers better by minimizing a cost function, in this case the averaged sound-pressure level. This algorithm is noise-resistant and able to cope with changing operating conditions.

The author hopes that some of the ideas and findings presented in this thesis may find their way to industrial application and contribute to the improvement of gas turbines.

A

Additional Fuel Injector Controllers

Success is the ability to go from one failure
to another with no loss of enthusiasm.

Sir Winston Churchill

The following section presents three other control structures which have been evaluated: a manual controller design carried out directly in the Nyquist diagram; an online tuned complex lead-lag controllers; and a peak filter controller. These controllers are either wearisome to design, or did not perform as well as the ones presented in the main section. However, they have been useful in identifying the plant, see Section 4.3.2.

A.1 Fuel Injector and Manual Loop Shaping Control

Manual loop shaping in the Nyquist diagram is tried as a design procedure. A controller has been assembled in a trial-and-error fashion with basic elements such as peak filters, complex lead-lag elements and the like.

The design process is guided by desired bounds on the sensitivity, see Fig. A.1. It is also monitored in the Nyquist diagram, see Fig. A.2. For the case 36/700/1.875, noise suppression in two frequency bands is desired. The resulting controllers are again implemented with various gains. The measured pressure spectra are shown in Fig. A.3, the measured and modeled sensitivity in Fig. A.4. For higher gains, saturation of the control signal occurs, and the modeled sensitivity cannot be realized. The modeled pressure spectrum reduction has been achieved, but it is difficult and cumbersome to find good controllers this way.

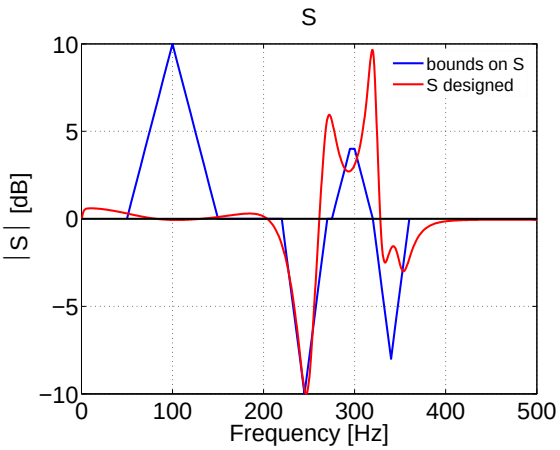

Figure A.1: *The design process for manual loop shaping controllers. To guide the design, desired bounds on the sensitivity are displayed. Case 36/700/1.875.*

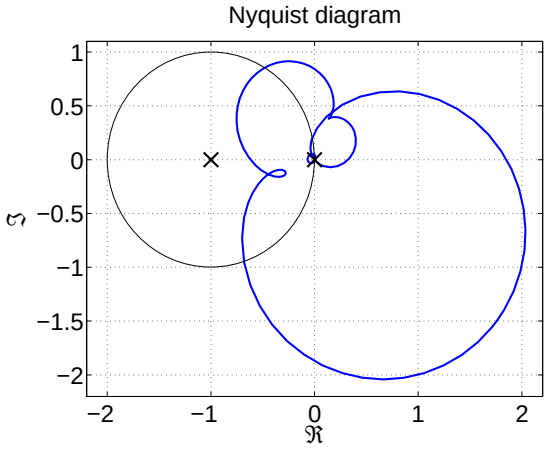

Figure A.2: *The Nyquist diagram for manual loop shaping. Case 36/700/1.875.*

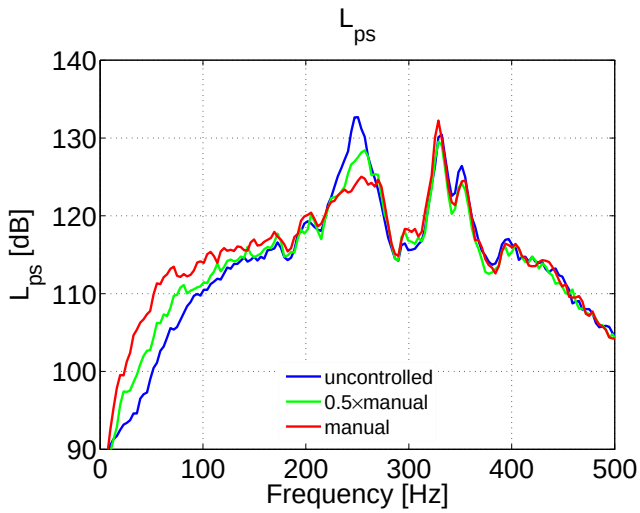

Figure A.3: *The pressure spectra achieved with the manual loop shaping controllers for 36/700/1.875.*

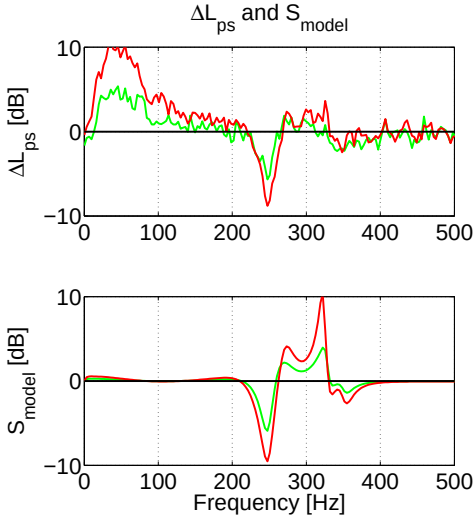

Figure A.4: *The modeled and achieved pressure spectrum reduction for 36/700/1.875.*

A.2 Fuel Injector and Complex Lead-Lag Control

The complex lead-lag controller is an extension to the classic lead-lag controller [203, 202]. It features additional parameters that determine the under- and overshoot and the slope of the gain curve.

The implemented controllers for the case 36/700/1.875 are shown in Fig. A.5.

The measured pressure reduction is shown in Fig. A.6. The results are not satisfactory, because online tuning is not straightforward. It is not possible to decrease all three peaks. However, the model proves to be very accurate. This controller does not perform significantly better than the Gain-Delay type. Nevertheless, it has its justification in the sense that it helps to find a model of the combustor, see Section 4.3.2.

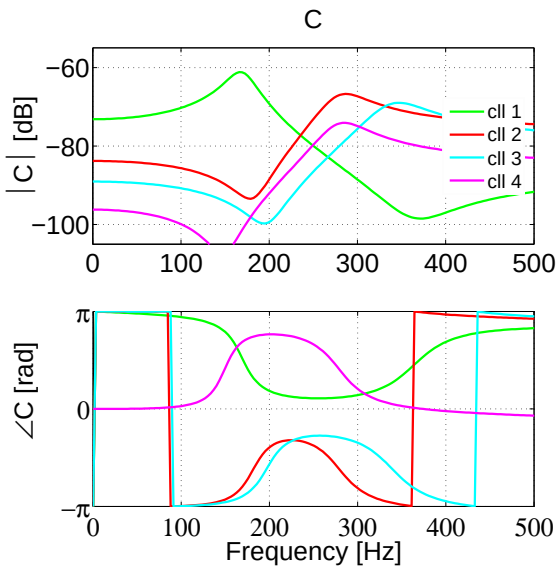

Figure A.5: *The complex lead-lag controllers used to control 36/700/1.875.*

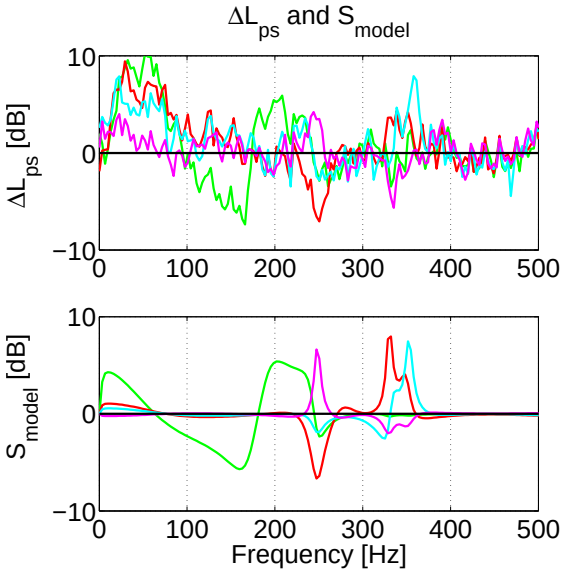

Figure A.6: *The modeled and achieved pressure spectrum reduction with the complex lead-lag controllers for 36/700/1.875.*

A.3 Fuel Injector and Peak Filter Control

In order to concentrate the actuation power in a certain frequency band, a peak filter is proposed for the case 36/700/1.875, see Fig. A.7. The measured pressure spectrum reduction is presented in Fig. A.8. The peak at 250 Hz is reduced by around 13 dB, but the band of reduction is not very wide. The peak filter controller cannot cope with three peaks either, like the Gain-Delay controller. However, the peak at 250 Hz can be reduced by about 12 dB. The results could be improved by augmenting the peak filter with an adjustable delay, to get the right phase at the desired location.

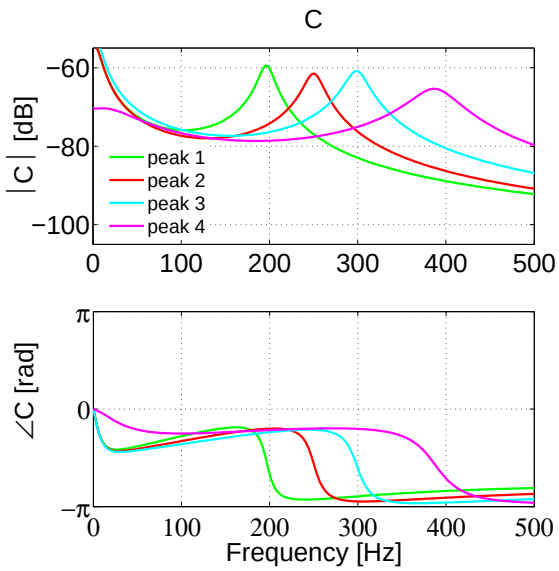

Figure A.7: *The peak controllers used to control 36/700/1.875.*

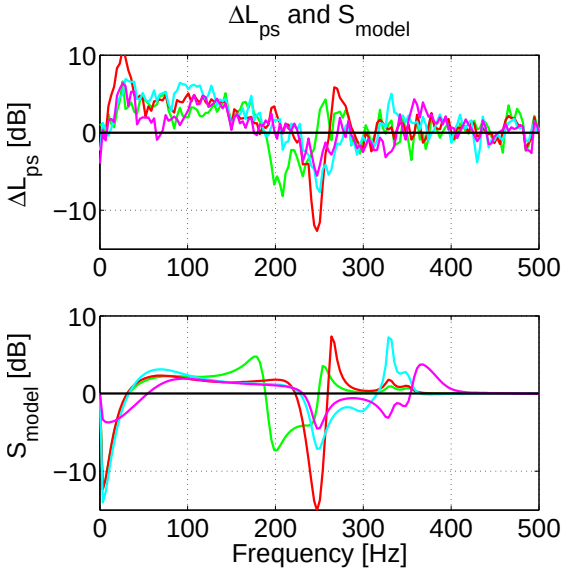

Figure A.8: *The modeled and achieved pressure spectrum reduction with the peak controllers for 36/700/1.875.*

B

Historical Notes on Gas Turbines

I am not young enough to know everything.

Oscar Wilde

B.1 From Early Developments to the Steam Turbine

Since the Romans built the first water turbines around 70 B.C. to grind grain, a lot of engineers have applied themselves to improving them. Hero of Alexandria reported the first steam-powered engine around AD 62 [303] (or 120 B.C. [151], the exact dates are unknown), the aeolipile "windball", which was later analyzed by Leonhard Euler (1707–1783), who found the equation named after him. In 1822, Claude Burdin coined the term "turbine", from the Latin "turbo": "that which spins" or in German "Wirbel, Zauberrad" [200]. James B. Francis had developed his high-efficiency radial-inflow turbines by 1875, and the first useful steam turbine was built in 1831 by William Avery. However, the steam turbine that really had an impact was Charles Parsons (1854–1931) multistage axial-flow reaction turbine rated at 10 horsepower. Brown-Boveri from Baden, founded in 1892, built turbines taking licenses from Parsons designs starting from 1900. Between 1901 and 1906, they delivered 500 steam turbines and installed a total of 12 GW worth of steam turbines by 1929, which was unmatched by any other European Company. In 1928, the world's most powerful steam turbine rated at 160 MW was installed in New York, the "Hellgate". Nowadays, steam turbines are used in combined-cycle plants with gas turbines, having outputs exceeding 500 MW.

Aurel Stodola (1859–1942) as a very influential researcher and teacher added an appendix on gas turbines to the second edition of his textbook "Steam and Gas Turbines" in 1905. He became professor for Mechanical Engineering at ETH in 1892, where he served until 1929. He wrote in 1903: "Die Wissenschaft beansprucht als ihr Sonderrecht, auf den Höhen des reinen Gedankens zu weilen; den Kampf mit der widerstrebenden Materie überlässt sie den Ingenieuren. Wohlan, wir nehmen diesen

Kampf auf und wollen wie bisher, mit unverdrossener Ausdauer an dem grossen Problem, das eine Daseinsfrage der Menschheit ist, arbeiten: an der Vervollkommnung der Energieumwandlung in den Wärmekraftmaschinen." [151].

B.2 The Gas Turbine

Steam Turbines are relatively easy to build compared to gas turbines, but they require large steam producers. In contrast to internal combustion engines, the maximum working fluid temperatures must be lower, so that compression and expansion losses have to be kept as small as possible. Hans Holzwarth proposed a 200 horsepower gas turbine in 1906–1908, which was constructed by Brown Boveri. This design was based on a constant volume cycle (or explosion type, similar to a Diesel engine). Theoretically, the efficiency is higher, but mechanical complexities (valves etc.) make the design difficult and the operation is not smooth. Moreover, a constant pressure system can handle higher mass flows. Brown Boveri Company BBC also designed the Velox steam generator. The first industrial gas turbine was presented to the public in 1939 at the national exposition "Landesausstellung" in Zürich by BBC. It served then in Neuchâtel producing electricity, and was recognized as a Historic Landmark by the ASME in 1988.

BBC merged with the Swedish company ASEA in 1988 to become ABB (Asea Brown Boveri). ABB formed a joint venture with ALSTOM (Als-thom was created in 1928 as a merger between "Société Alsacienne de Constructions Mécaniques, Belfort" and "Compagnie Française Thomson-Houston", changing its name to ALSTOM in 1989) and sold more of its power division in 2000.

Escher-Wyss (founded in 1805) designed the closed-cycle gas turbine in 1939, which is mostly fitted with helium as the working fluid, to be used with coal and nuclear heat input. Heinrich Zoelly (1862–1937) of Escher-Wyss also designed successful steam turbines, which competed with BBC's products on the European Continent.

Today, land-based gas turbines are used in naval vessels (GE's two-shaft marine aeroderivative LM2500 gas turbine is rated at 25 MW, used by 27 international navies, and powering more than 360 ships. The more recent LM6000 delivers 40 MW at a thermal efficiency of 42%, featuring dry low emission technology), tanks (the Abrams M1 tank with a weight of 60 tons has a top speed of 75 km/h, thanks to its 1500 horsepower Lycoming gas turbine engine), on oil platforms, as emergency backup power units and, last but not least, in power plants. Gas turbines can be started quickly, and have a high power-to-weight ratio. A very good overview of the history of gas turbines is given in [303], where also current developments are addressed.

C

Thermodynamic Analysis of Gas Turbines

In this house, we obey the laws of thermodynamics!

Homer Simpson (after Lisa constructs a perpetual motion machine whose energy increases with time)

C.1 Definitions and Characterization

The following definition is found in [303]: "A turbomachine produces a change in enthalpy in a stream of fluid passing through it and transfers work through a rotating shaft: the interaction between the fluid and the machine is primarily fluid-dynamic lift." Another is in [72]: "We classify as turbomachines all those devices in which energy is transferred either to, or from, a continuously flowing fluid by the dynamic action of one or more moving blade rows."

A gas turbine is a heat engine that accepts and rejects heat—and produces work. It consists of a compressor, a heater, and an expander. The environment then cools down the exiting fluid for open-cycle gas turbines.

Compared to internal combustion engines, gas turbines perform the tasks of compression, heating, expansion, and discharge at various locations and continuously, whereas the former accomplish them as batch processes in the same cylinder at different times. This means that the components can be designed, tested, and developed individually, and then linked together. Moreover, combustion in gas turbines occurs at nearly constant pressure, whereas in internal combustion engines this occurs in a nearly constant volume. These facts allow for high volume flows and a high power to weight ratio. However, a higher peak cycle temperature can be allowed in internal combustion engines because this peak only occurs temporarily. Turbine blades have to be cooled in sophisticated ways to deal with higher (constant) turbine inlet temperatures, approaching 1800 K in modern turbines. Steam turbines work with a fluid

that changes phase, which requires big steam generators and a large heat input. In gas turbines, the compressor needs a lot of work input, and the combustion chamber can be designed smaller.

C.2 Working Principles of Gas Turbines

Brayton Cycle

Gas turbines run a Joule (or Brayton) cycle, and the fundamental principle upon which they rest is the following fact: in a temperature vs. entropy T–s diagram, lines of constant pressure have an increasing slope with temperature and are displaced parallel to each other, see Fig. C.1. The derivation is as follows:

Differentiating the definition of enthalpy and using the Gibbs equation

$$h = u + pv \tag{C.1}$$
$$Tds = du + pdv \tag{C.2}$$

yields

$$dh - vdp = Tds = du + pdv \tag{C.3}$$

The perfect gas law states that

$$dh = c_p dT \tag{C.4}$$
$$du = c_v dT \tag{C.5}$$

Inserting Eq. C.4 and C.5 into Eq. C.3 gives

$$c_p dT - vdp = Tds = c_v dT + pdv \tag{C.6}$$

Two cases are distinguished: constant pressure and constant volume

$$\left.\frac{\partial T}{\partial s}\right|_p = \frac{T}{c_p} \tag{C.7}$$
$$\left.\frac{\partial T}{\partial s}\right|_v = \frac{T}{c_v} \tag{C.8}$$

The differential equations are solved

$$T|_p = T_1\, e^{\frac{T}{c_p}s} \tag{C.9}$$
$$T|_v = T_2\, e^{\frac{T}{c_v}s} \tag{C.10}$$

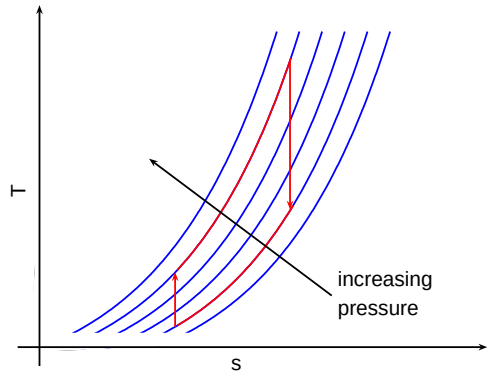

Figure C.1: *Temperature versus entropy T–s diagram for a perfect gas. Lines of constant pressure are plotted in blue. The connected red lines show the ideal Brayton cycle. The work input required for compression is smaller than the turbine work output gained.*

Lines of constant pressure, Eq. C.9, are plotted in Fig. C.1. Their shape makes the ideal Brayton cycle possible, shown as red lines. The work required for compression is lower than the turbine work output obtained [303]. In reality, the processes involved are not isentropic but one has to account for various losses. For a given maximum turbine inlet temperature, there exists an optimum pressure ratio to be delivered by the compressor. If a heat exchanger is to be incorporated, yet another pressure ratio is optimal.

Other Cycles

Closed-cycle gas turbines use helium as a working fluid, because the heat capacity at constant pressure c_p at 1.013 bar and 21 °C is 0.02 kJ/(mol.K) compared to 0.029 kJ/(mol.K) for air. This yields steeper slopes in Fig. C.1. But more importantly, higher fluid velocities can be used and optimum cycle pressure ratios are lower, and corrosion is not a problem anymore. This cycle is often used in nuclear power plants, as heat must be transferred to the working fluid, which could also be done through external combustion.

The hot gas leaving the gas turbines can be used in a heat-recovery steam generator HRSG to generate process steam (for paper plants, breweries or heating buildings), or the steam is used in a subsequent steam turbine. In this configuration, efficiencies go as high as 60%. The steam may also be injected back into the gas turbine, either into the combustor or in the turbine stages. This increases the power and, if injected into the combustor, also lowers emission levels. The downside is that the water used must be very pure, or else corrosion and potential blockages become a problem.

D

Combustion Systems

"Would you tell me, please, which way I ought to go from here?"
"That depends a good deal on where you want to get to," said the Cat.
"I don't much care where–" said Alice.
"Then it doesn't matter which way you go," said the Cat.

Lewis Carroll, in "Alice's Adventures in Wonderland"

D.1 Combustor Technology

The earliest aircraft engines were fitted with can (or tubular) combustors, which were followed by cannular (or tubo-annular), and finally annular combustors. They make optimal use of space due to their reverse flow arrangement and have a clean aerodynamic layout, leading to a low pressure loss. A larger combustor volume makes it easier to achieve a low pressure drop, high efficiency, good outlet temperature distribution and satisfactory stability characteristics.

Aircraft gas turbines usually run on kerosene, but for land-based gas turbines there is a move from oil to gas. It is believed that the supply of natural gas will last longer than oil, and most importantly, gas turbines fueled on natural gas achieve lower emission (NO_x, CO_2) levels.

Turbulent flame speeds are on the order of 10 m/s, but axial-flow compressors deliver air at 100–200 m/s. Thus, the need of a flame holder arises, which makes the combustion system responsible for the largest pressure loss in the engine (this also calls for a diffuser, since pressure loss is proportional to the square of the air velocity). The standard or aircraft type combustion system splits the compressed air stream into two, into the first is injected the fuel which then burns at approximately stoichiometric conditions. This primary zone anchors the flame and provides sufficient time, temperature, and turbulence to complete the combustion of the air-fuel mixture. A toroidal flow reversal recirculates a portion of the hot combustion gases to provide continuous ignition. This is accomplished by fitting a swirler in the dome around the

injector, giving rise to coherent large-scale structures. Vortex breakdown then assures better mixing than with bluff bodies, because of strong shear regions, high turbulence, and rapid mixing rates. The second stream is used for wall cooling and dilution so as the keep the turbine inlet temperature below critical levels and assure a desired radial distribution (higher at the turbine tips where centripetal stresses are lower than closer to the hub, or the inverse if they are cooled from the hub), know as pattern factor.

J.R. Joyce is cited in [165], who wrote in 1950: "The atomizer in an aircraft engine cannot be regarded as heavily taxed; indeed, one may say that it leads a privileged and sheltered existence. In the first place, its rations are of the highest quality. It is fed with high grade fuel, which is thoroughly cleansed before reaching it. Next, it is located in a position where it does no more than look at the blazing inferno it has created from a front row stall. It is shrouded in a loose-fitting jacket through which cool air is continuously passing, primarily for the purpose of serving its protection and comfort. Its lot is a happy one."

Catalytic combustors and pressurized circulating fluidized bed combustion for coal burning gas turbines may become important in the future. Other considerations for combustor design are re-ignition at high altitudes in aircraft engines, flame holding during compressor surges and transients, thermal stresses, and temperature gradients.

D.2 Laminar and Turbulent Flames

The burning velocity of laminar flames is the velocity with which a plane flame front moves in a direction normal to its surface through the adjacent unburnt gas [166]. It is influenced by the equivalence ratio, initial temperature, and pressure. Flame speed can be increased through introduction of turbulence, which increases the surface by wrinkling the flame front. Higher pressures favor auto-ignition and spontaneous ignition—this must be avoided in lean-premix combustors. Flashbacks occur when the flame speed exceeds the approach flow velocity, and the flame subsequently travels upstream of the combustion zone into the premixing section, causing dangerous situations.

The equivalence ratio ϕ is the actual fuel/air ratio divided by the stoichiometric fuel/air ratio [166], so that $\phi < 1$ indicates a lean regime and $\phi > 1$ a rich one. In this thesis, also the air/fuel ratio $\lambda = \phi^{-1}$ is used. The adiabatic flame temperature is the (calculated) temperature that the flame would attain if the net energy liberated by the chemical reaction that converts the fresh mixture into combustion products were fully utilized in heating those products [166]. By radiation and convection, a significant part of the energy is lost and the flame therefore does not attain this theoretical temperature.

D.3 Emissions

In a gas turbine burning natural gas, the overall chemical reaction is the following:

$$CH_4+2O_2 \rightarrow CO_2+2H_2O$$

The "true" reaction scheme is of course much more complex [103]. Small amounts of carbon monoxide CO, unburned hydrocarbons UHC, particulate matter PM, oxides of sulfur, and oxides of nitrogen NO_x will also be present. Sunlight and NO_x combined give rise to smog, acid rain, and contribute to ozone depletion at higher altitudes.

The rate of formation of NO_x depends exponentially on flame temperature (Zeldovich mechanism [166, 41]), and roughly linearly on residence time in the combustor. But there is a tradeoff, namely it is generally the case that if NO_x is reduced, CO and UHC are increased. A flame temperature decrease from 1900 K to 1800 K can halve NO_x emissions, but below 1700 K, carbon monoxide becomes an issue. The combustion temperature should therefore be held as uniform as possible, as local hot spots will generate high levels of NO_x. For low emission combustors, the temperature should be kept between 1680 K to 1900 K. By injecting water, emissions were found to be reduced to 75 ppmvd (parts per million by volume of dry exhaust gas corrected to standard pressure and temperature) and lower. Water or steam injection increases power but decreases the thermal efficiency. Of course, since large amounts of pure water (comparable to the fuel flow [291]) to prevent fouling are needed, this technique can not be applied all over the world, and it also increases capital cost.

Another way of controlling emissions is selective catalytic reduction (SCR), but this only works in a limited temperature range of 285–400 °C.

On the other hand, the dry low NO_x technique is based on premixing the air and fuel prior to combustion [2]. The ABB-ALSTOM EV burner is composed of two offset half cones which are shifted to form two diametrically-opposed air inlet slots of constant width. Gaseous fuel is injected along the lips or with a lance. Flame stabilization is achieved in free space due to the sudden breakdown of a swirling flow at the burner exit plane.

In lean-premixed combustors, the heat release is concentrated at the flame front, whereas in conventional combustors it is smeared across a much wider region. Combustion efficiencies are around 99%, defined as the heat released in combustion divided by the heat available in the fuel.

An "advanced zero emissions power plant" project is described in [113], where 100% capture of CO_2 and 0% NO_x is the target. This is accomplished by N_2 removal from the air and burning of natural gas in this nitrogen-free atmosphere with subsequent storage of compressed CO_2. A "rich-catalytic lean-burn" combustion concept is presented in [53], where NO_x levels lower than 2 ppm are achieved.

E

A Note on Newton's Exclamation

Ex nihilo nihil fit.

Lukrez, "De rerum natura" I,155f

"If I have seen further, it is by standing on the shoulders of giants." Newton wrote this quote in a letter dated February 5th 1675 or 1676 to Robert Hooke (1635–1702), with whom he fought a lifelong bitter rivalry. Hooke claimed that Newton stole his hypothesis on light from his "Micrographia". But Newton on his part argued that Hooke built upon Descartes who in turn was inspired by Marcantonia de Dominis and Ariotto. Newton's comment was very likely intended to be sarcastic as Hooke was a very short man. However, Newton also stands on the shoulders of giants: In 1621, Robert Burton writes in his "Anatomy Of Melancholy": "Pygmies placed on the shoulders of giants see more than the giants themselves." Burton himself takes a seat on the shoulders of the 12th century scholastic Bernard de Chartres who is quoted as saying "In comparison with the ancients we stand like dwarves on the shoulders of giants". The thought goes back to Priscian, a 6th century grammarian who wrote: "The younger the scholars, the more sharp-sighted" and so on.

Variations on this quote are the following:[1]

- "If I have seen farther than others, it is because I was standing on a really big heap of midgets." *K. Eric Drexler*
- "If I have seen further than others, it is because I am surrounded by dwarves." *attributed to Murray Gell-Mann, Prof. emerit. at CalTech*
- "If I have not seen as far as others, it is because giants were standing on my shoulders." *Harold Abelson, Professor at MIT*

[1] Among others, the following web sites provide interesting information:
http://www.aerospaceweb.org/question/history/q0162b.shtml
http://c2.com/cgi/wiki?ShouldersOfGiants

Bibliography

Gutta cavat lapidem non vi, sed saepe cadendo;
Sic homo fit sapiens bis non, sed saepe legendo.

Ovid, "Epistulae ex Ponto" IV 10,5;
Giordano Bruno, "Il candelaio" III, 7

[1] Al-Masoud, N. and T. Singh: *Optimal actuator/sensor placement for control of combustion instabilities.* Journal of Propulsion and Power, 19(1):148–151, 2003.

[2] Alkabie, H.: *Design methods of the ABB ALSTOM POWER gas turbine dry low emission combustion system.* Proceedings of the Institution of Mechanical Engineers Part A-Journal of Power and Energy, 214(A4):293–315, 2000.

[3] Ananthkrishnan, N., S. Deo and F. E. C. Culick: *Reduced-order modeling and dynamics of nonlinear acoustic waves in a combustion chamber.* Combustion Science And Technology, 177(2):221–247, 2005.

[4] Annaswamy, A. M., O. M. El Rifai, M. Fleifil, J. P. Hathout and A. F. Ghoniem: *A model-based self-tuning controller for thermoacoustic instability.* Combustion Science and Technology, 135(1-6):213–240, 1998.

[5] Annaswamy, A. M., O.M. El Rifai, M. Fleifil and A. F. Ghoniem: *A model-based active-adaptive controller for thermoacoustic instability.* In *Proceedings of the 1997 IEEE conference on control applications*, Hartford, USA, 1997.

[6] Annaswamy, A. M., M. Fleifil, J. P. Hathout and A. F. Ghoniem: *Impact of linear coupling on the design of active controllers for the thermoacoustic instability.* Combustion Science and Technology, 128(1-6):131–180, 1997.

[7] Annaswamy, A. M., M. Fleifil, J. W. Rumsey, R. Prasanth, J. P. Hathout and A. F. Ghoniem: *Thermoacoustic instability: Model-based optimal control designs and experimental validation.* IEEE Transactions on Control Systems Technology, 8(6):905–918, 2000.

[8] Annaswamy, A. M. and A. F. Ghoniem: *Active Control in Combustion Systems.* IEEE Control Systems Magazine, 15(6):49–63, 1995.

[9] Annaswamy, A. M. and A. F. Ghoniem: *Active control of combustion instability: Theory and practice.* IEEE Control Systems Magazine, 22(6):37–54, 2002.

[10] Anonymus: *A New Frigorifick Experiment Shewing, How a Considerable Degree of Cold May be Suddenly Produced without the Help of Snow, Ice, Haile, Wind, or Niter, and That at Any Time of the Year.* Philosophical Transactions (1665-1678), 1(15):255–261, 1666.

[11] Anthoine, J., M. Mettenleiter, O. Repellin, J. M. Buchlin and S. Candel: *Influence of adaptive control on vortex-driven instabilities in a scaled model of solid propellant motors.* Journal of Sound and Vibration, 262(5):1009–1046, 2003.

[12] Arana, C. A., B. Sekar, M. A. Mawid and C. B. Graves: *Determination of thermoacoustic response in a demonstrator gas turbine engine.* Journal of Engineering for Gas Turbines and Power-Transactions of the ASME, 124(1):46–57, 2002.

[13] Ariyur, K. B., A. Banaszuk and M. Krstić: *Identification of averaged dynamics of a controlled combustion instability.* In *39th IEEE Conference on Decision and Control*, volume 3, pages 2017–2022, Sydney, Australia, 2000.

[14] Armitage, C. A., A. J. Riley, R. S. Cant, A. P. Dowling and S. R. Stow: *Flame transfer function for swirled LPP combustion from experiments and CFD.* In *2004 ASME Turbo Expo*, volume 1, pages 527–537, Vienna, Austria, 2004.

[15] Auer, M. P., C. Gebauer, K. G. Mosl, C. Hirsch and T. Sattelmayer: *Active instability control: Feedback of combustion instabilities on the injection of gaseous fuel.* In *2004 ASME Turbo Expo*, volume 1, pages 11–19, Vienna, Austria, 2004.

[16] Backhaus, S. and G. W. Swift: *A thermoacoustic Stirling heat engine.* Nature, 399(6734):335–338, 1999.

[17] Baillot, F. and D. Demare: *Physical mechanisms of a lifted nonpremixed flame stabilized in an acoustic field.* Combustion Science and Technology, 174(8):73–98, 2002.

[18] Balachandran, R., B. O. Ayoola, C. F. Kaminski, A. P. Dowling and E. Mastorakos: *Experimental investigation of the nonlinear response of turbulent premixed flames to imposed inlet velocity oscillations.* Combustion And Flame, 143(1-2):37–55, 2005.

[19] Banaszuk, A., K. B. Ariyur, M. Krstić and C. A. Jacobson: *An adaptive algorithm for control of combustion instability.* Automatica, 40(11):1965–1972, 2004.

[20] Banaszuk, A., C. A. Jacobson, A. I. Khibnik and P. G. Mehta: *Linear and Nonlinear Analysis of controlled combustion processes. Part I: Linear Analysis.* In *International Conference on Control Applications*, Hawaii, USA, 1999.

[21] Banaszuk, A., C. A. Jacobson, A. I. Khibnik and P. G. Mehta: *Linear and Nonlinear Analysis of controlled combustion processes. Part II: Nonlinear Analysis.* In *International Conference on Control Applications*, Hawaii, USA, 1999.

[22] Banaszuk, A., Y. Zhang and C. Jacobson: *Adaptive Control of Combustion Instability Using Extremum-Seeking.* In *American Control Conference*, Chicago, USA, 2000.

[23] Barooah, P. and T. Anderson: *Active combustion instability control with spinning valve actuator.* In *2002 ASME Turbo Expo*, Amsterdam, The Netherlands, 2002.

[24] Bellows, B. D., A. Hreiz and T. Lieuwen: *Nonlinear Dynamics of an Unstable Swirl Combustor: Frequency Locking and Open Loop Control.* In *20th International Colloquium on the Dynamics of Explosions and Reactive Systems*, Montreal, Canada, 2005.

[25] Bellows, B. D. and T. Lieuwen: *Nonlinear Response of a Premixed Combustor to Forced Acoustic Oscillations.* In *42nd AIAA Aerospace Sciences Meeting and Exhibit*, Reno, USA, 2004.

[26] Bellucci, V., P. Flohr and C. O. Paschereit: *Numerical and experimental study of acoustic damping generated by perforated screens.* AIAA Journal, 42(8):1543–1549, 2004.

[27] Bellucci, V., P. Flohr, C. O. Paschereit and F. Magni: *On the use of Helmholtz resonators for damping acoustic pulsations in industrial gas turbines.* Journal Of Engineering For Gas Turbines And Power-Transactions Of The ASME, 126(2):271–275, 2004.

[28] Bellucci, V., B. B. H. Schuermans, D. Nowak, P. Flohr and C. O. Paschereit: *Thermoacoustic modeling of a gas turbine combustor equipped with acoustic dampers.* Journal Of Turbomachinery-Transactions Of The ASME, 127(2):372–379, 2005.

[29] Bellucci, V., B. B. H. Schuermans, C. O. Paschereit and P. Flohr: *Thermoacoustic Simulation of Lean Premixed Flames using an enhanced time-lag model.* In *31st AIAA Fluid Dynamics Conference and Exhibit*, Anaheim, USA, 2001.

[30] Bernier, D., S. Ducruix, F. Lacas, S. Candel, N. Robart and T. Poinsot: *Transfer function measurements in a model combustor: Application to adaptive instability control.* Combustion Science and Technology, 175(5):993–1013, 2003.

[31] Bernier, D., F. Lacas and S. Candel: *Instability mechanisms in a premixed prevaporized combustor.* Journal Of Propulsion And Power, 20(4):648–656, 2004.

[32] Bigge, R.: *The Thermoacoustic Freezer*, The New York Times, Dec. 12, 2004.

[33] Billoud, G., M. A. Galland, C. H. Huu and S. Candel: *Adaptive Active Control of Combustion Instabilities.* Combustion Science and Technology, 81(4-6):257–283, 1992.

[34] Bisio, G.: *Thermodynamic analysis of Sondhauss and Rijke oscillations - analogies and possible applications.* In *Proceedings of the 31st Intersociety Energy Conversion Engineering Conference, IECEC 96*, volume 2, pages 1434–1440, Washington DC, USA, 1996.

[35] Bittanti, S., A. De Marco, G. Poncia and W. Prandoni: *Identification of a model for thermoacoustic instabilities in a Rijke tube.* IEEE Transactions on Control Systems Technology, 10(4):490–502, 2002.

[36] Blonbou, R., A. Laverdant, S. Zaleski and P. Kuentzmann: *Active adaptive combustion control using neural networks.* Combustion Science and Technology, 156:25–47, 2000.

[37] Blonbou, R., A. Laverdant, S. Zaleski and P. Kuentzmann: *Active control of combustion instabilities on a Rijke tube using neural networks.* Proceedings of the Combustion Institute, 28:747–755, 2000.

[38] Bloxsidge, G. J., A. P. Dowling, N. Hooper and P. J. Langhorne: *Active Control of Reheat Buzz.* AIAA Journal, 26(7):783–790, 1988.

[39] Bloxsidge, G. J., A. P. Dowling and P. J. Langhorne: *Reheat Buzz - an Acoustically Coupled Combustion Instability. 2.Theory.* Journal of Fluid Mechanics, 193:445–473, 1988.

[40] Boaghe, O. M., S. A. Billings, L. M. Li, P. J. Fleming and J. Liu: *Time and frequency domain identification and analysis of a gas turbine engine.* Control Engineering Practice, 10(12):1347–1356, 2002.

[41] Brand, D.: *Control-oriented modeling of NO emissions of SI engines. Diss. ETH No. 16037.* PhD thesis, ETH Zürich, 2005.

[42] Brookes, S. J., R. S. Cant, I. D. J. Dupère and A. P. Dowling: *Computational modeling of self-excited combustion instabilities.* Journal of Engineering for Gas Turbines and Power-Transactions of the ASME, 123(2):322–326, 2001.

[43] Brüel & Kjaer, Ltd.: *Microphone Handbook; Vol. 1: Theory.* Nærum, Denmark, 1996.

[44] Burnley, V. S. and F. E. C. Culick: *Influence of random excitations on acoustic instabilities in combustion chambers.* AIAA Journal, 38(8):1403–1410, 2000.

[45] Cammarata, L., A. Fichera and A. Pagano: *Neural prediction of combustion instability.* Applied Energy, 72(2):513–528, 2002.

[46] Campos-Delgado, D. U., D. Allgood, K. Zhou and S. Acharya: *Identification and active control of thermoacoustic instabilities.* In *IEEE conference on control applications*, Mexico City, Mexico, 2001.

[47] Campos-Delgado, D. U., B. B. H. Schuermans, K. M. Zhou, C. O. Paschereit, E. A. Gallestey and A. Poncet: *Thermoacoustic instabilities: Modeling and control.* IEEE Transactions on Control Systems Technology, 11(4):429–447, 2003.

[48] Campos-Delgado, D. U., K. Zhou, D. Allgood and S. Acharya: *Active control of combustion instabilities using model-based controllers.* Combustion Science and Technology, 175(1):27–53, 2003.

[49] Candel, S.: *Combustion dynamics and control: Progress and challenges.* Proceedings of the Combustion Institute, 29:1–28, 2002.

[50] Candel, S., S. Ducruix, D. Durox and D. Veynante: *Combustion Dynamics: Analysis and control-modeling.* In *Von Karman Institute Lecture Series: Active Control of Engine Dynamics*, Brussels, Belgium, 2001.

[51] Candel, S., S. Ducruix, T. Schuller, D. Durox and F. Lacas: *Dynamical Processes in Active Control of Combustion Instabilities.* In *5th Symposium on Smart Control of Turbulence*, Tokyo, Japan, 2004.

[52] Carson, J. M.: *Subharmonic and Non-Subharmonic Pulsed Control of Thermoacoustic Instabilities: Analysis and Experiment.* PhD thesis, Virginia Polytechnic and State University, 2001.

[53] Castaldi, M. J., S. Etemad, W. C. Pfefferle, V. Khanna and K. O. Smith: *Rich-catalytic lean-burn combustion for low-single-digit NO_x gas turbines.* Journal Of Engineering For Gas Turbines And Power-Transactions Of The ASME, 127(1):27–35, 2005.

[54] Cho, J. H. and T. Lieuwen: *Modeling the response of premixed flames to mixture ratio perturbations.* In *2001 ASME Turbo Expo*, volume 2, pages 67–76, Atlanta, USA, 2003.

[55] Cho, J. H. and T. Lieuwen: *Laminar premixed flame response to equivalence ratio oscillations.* Combustion And Flame, 140(1-2):116–129, 2005.

[56] Chu, Y. C., A. P. Dowling and K Glover: *Robust Control of combustion oscillations.* In *IEEE conference on control applications*, Trieste, Italy, 1998.

[57] Chu, Y. C., K. Glover and A. P. Dowling: *Control of combustion oscillations via $\mathscr{H}_\infty$ loop-shaping, μ-analysis and Integral Quadratic Constraints.* Automatica, 39(2):219–231, 2003.

[58] Clanet, C. and G. Searby: *First experimental study of the Darrieus-Landau instability.* Physical Review Letters, 80(17):3867–3870, 1998.

[59] Cohen, J. M. and A. Banaszuk: *Factors affecting the control of unstable combustors.* Journal of Propulsion and Power, 19(5):811–821, 2003.

[60] Cohen, J. M., j. r. hibshman, W. Proscia, T. J. rosfjord, B. E. Wake, J. B. McVey, j lovett, m ondas, J. C. DeLaat and k breisacher: *Longitudinal-Mode Combustion Instabilities: Modeling and Experiments.* In *Symposium on Active Control Technology for Enhanced Performance Operational Capabilities of Military Aircraft, Land Vehicles and Sea Vehicles*, Braunschweig, Germany, 2000. NATO, Research and Technology Organization.

[61] Cohen, J. M., N. M. Rey, C. A. Jacobson and T. J. Anderson: *Active control of combustion instability in a liquid-fueled low-NO_x combustor.* Journal of Engineering for Gas Turbines and Power-Transactions of the ASME, 121(2):281–284, 1999.

[62] Cohen, J. M., J. H. Stufflebeam and W. Proscia: *The effect of fuel/air mixing on actuation authority in an active combustion instability control system.* Journal of Engineering for Gas Turbines and Power-Transactions of the ASME, 123(3):537–542, 2001.

[63] Cohen, J. M., B. E. Wake and D. Choi: *Investigation of instabilities in a lean, premixed step combustor.* Journal of Propulsion and Power, 19(1):81–88, 2003.

[64] Coker, A., Y. Neumeier, T. Lieuwen, B. T. Zinn and S. Menon: *Studies of active instability control effectiveness in a high pressure, liquid fueled combustor.* In *41st AIAA Aerospace Sciences Meeting and Exhibit*, Reno, USA, 2003.

[65] Crocco, L.: *Aspects of Combustion Stability in Liquid Propellant Rocket Motors.1. Fundamentals - Low Frequency Instability with Monopropellants.* Journal of the American Rocket Society, 21(6):163–178, 1951.

[66] Culick, F. E. C.: *Some Recent Results for Nonlinear Acoustics in Combustion- Chambers.* AIAA Journal, 32(1):146–169, 1994.

[67] Dawson, Virginia P.: *Ideas into hardware: a history of NASA's Rocket Engine Test Facility.* History Enterprises Inc. in cooperation with NASA History, Cleveland, USA, 2004.

[68] De Zilwa, S. R. N., S. Sivasegaram and J. H. Whitelaw: *Control of combustion oscillations close to stoichiometry.* Flow Turbulence and Combustion, 63(1-4):395–414, 2000.

[69] DeLaat, J. C. and C. T. Chang: *Active Control of High Frequency Combustion Instability in Aircraft Gas-Turbine Engines.* In *16th International Symposium on Airbreathing Engines*, Cleveland, USA, 2003.

[70] Dequand, S., S. Hulshoff, H. van Kuijk, J. Willems and A. Hirschberg: *Helmholtz-like resonator self-sustained oscillations, part 2: Detailed flow measurements and numerical simulations.* AIAA Journal, 41(3):416–423, 2003.

[71] Dequand, S., X. Luo, J. Willems and A. Hirschberg: *Helmholtz-like resonator self-sustained oscillations, part 1: Acoustical measurements and analytical models.* AIAA Journal, 41(3):408–415, 2003.

[72] Dixon, S. L.: *Fluid mechanics and thermodynamics of turbomachinery.* Butterworth-Heinemann, Boston, 4th edition, 1998.

[73] Docquier, N. and S. Candel: *Combustion control and sensors: a review.* Progress in Energy and Combustion Science, 28(2):107–150, 2002.

[74] Dowling, A. P.: *The Calculation of Thermoacoustic Oscillations.* Journal of Sound and Vibration, 180(4):557–581, 1995.

[75] Dowling, A. P.: *Nonlinear self-excited oscillations of a ducted flame.* Journal of Fluid Mechanics, 346:271–290, 1997.

[76] Dowling, A. P.: *A kinematic model of a ducted flame.* Journal of Fluid Mechanics, 394:51–72, 1999.

[77] Dowling, A. P.: *The 1999 Lanchester lecture: Vortices, sound and flames—a damaging combination.* Aeronautical Journal, 104(1033):105–116, 2000.

[78] Dowling, A. P. and S. Hubbard: *Instability in lean premixed combustors.* Proceedings of the Institution of Mechanical Engineers Part A-Journal of Power and Energy, 214(A4):317–332, 2000.

[79] Dowling, A. P. and A. S. Morgans: *Feedback control of combustion oscillations.* Annual Review Of Fluid Mechanics, 37:151–182, 2005.

[80] Dowling, A. P. and S. R. Stow: *Acoustic analysis of gas turbine combustors.* Journal of Propulsion and Power, 19(5):751–764, 2003.

[81] Ducruix, S., D. Durox and S. Candel: *Theoretical, and experimental determinations of the transfer function of a laminar premixed flame.* Proceedings of the Combustion Institute, 28:765–773, 2000.

[82] Ducruix, S., T. Schuller, D. Durox and S. Candel: *Combustion dynamics and instabilities: Elementary coupling and driving mechanisms.* Journal of Propulsion and Power, 19(5):722–734, 2003.

[83] Dunstan, W. J., R. R. Bitmead and S. M. Savaresi: *Fitting nonlinear low-order models for combustion instability control.* Control Engineering Practice, 9(12):1301–1317, 2001.

[84] Dupère, I. D. J. and A. P. Dowling: *The use of Helmholtz resonators in a practical combustor.* Journal Of Engineering For Gas Turbines And Power-Transactions Of The ASME, 127(2):268–275, 2005.

[85] Eisinger, F. L. and R. E. Sullivan: *Avoiding thermoacoustic vibration in burner/furnace systems.* Journal of Pressure Vessel Technology-Transactions of the ASME, 124(4):418–424, 2002.

[86] Eldredge, J. D. and A. P. Dowling: *The absorption of axial acoustic waves by a perforated liner with bias flow.* Journal of Fluid Mechanics, 485:307–335, 2003.

[87] Emiris, I. and J. H. Whitelaw: *Control of combustion oscillations.* Combustion Science and Technology, 175(1):157–184, 2003.

[88] Eroglu, A., K. Döbbeling, F. Joos and P. Brunner: *Vortex generators in lean-premix combustion.* Journal of Engineering for Gas Turbines and Power-Transactions of the ASME, 123(1):41–49, 2001.

[89] Estève, S. J. and M. E. Johnson: *Reduction of sound transmission into a circular cylindrical shell using distributed vibration absorbers and Helmholtz resonators.* Journal of the Acoustical Society of America, 112(6):2840–2848, 2002.

[90] Evesque, S.: *Adaptive Control of Combustion Oscillations.* PhD thesis, University of Cambridge, 2000.

[91] Evesque, S., A. M. Annaswamy, S. Niculescu and A. P. Dowling: *Adaptive control of a class of time-delay systems.* Journal of Dynamic Systems Measurement and Control-Transactions of the ASME, 125(2):186–193, 2003.

[92] Evesque, S. and A. P. Dowling: *LMS algorithm for adaptive control of combustion oscillations.* Combustion Science and Technology, 164:65–93, 2001.

[93] Evesque, S., A. P. Dowling and A. M. Annaswamy: *Self-tuning regulators for combustion oscillations.* Proceedings of the Royal Society of London Series A- Mathematical Physical and Engineering Sciences, 459(2035):1709–1749, 2003.

[94] Evesque, S., S. Park, A. J. Riley, A. M. Annaswamy and A. P. Dowling: *Adaptive combustion instability control with saturation; theory and validation.* Journal Of Propulsion And Power, 20(6):1086–1095, 2004.

[95] Fannin, C. A.: *Linear modeling and analysis of thermoacoustic instabilities in a gas turbine combustor.* PhD thesis, Virginia Polytechnic Institute and State University, 2000.

[96] Fichera, A. and A. Pagano: *Application of neural dynamic optimization to combustion-instability control.* 83(3):253, 2006.

[97] Fischer, A.: *Hybride, thermoakustische Charakterisierung von Drallbrennern.* PhD thesis, Technische Universität München, 2004.

[98] Fleifil, M., A. M. Annaswamy, Z. A. Ghoniem and A. F. Ghoniem: *Response of a laminar premixed flame to flow oscillations: A kinematic model and thermoacoustic instability results.* Combustion and Flame, 106(4):487–510, 1996.

[99] Fleifil, M., A. M. Annaswamy, J. W. Rumsey, A. Kojic and A. F. Ghoniem: *A Physically based nonlinear model of combustion instability and active control.* In *Proceedings of the 1998 IEEE conference on control applications*, Trieste, Italy, 1998.

[100] Freudenberg, J. S. and D. P. Looze: *Right Half Plane Poles and Zeros and Design Tradeoffs in Feedback-Systems.* IEEE Transactions on Automatic Control, 30(6):555–565, 1985.

[101] Fritsche, D.: *Origin and Control of Thermoacoustic Instabilities in Lean Premixed Gas Turbine Combustion. Diss. ETH No. 16360.* PhD thesis, ETH Zürich, 2005.

[102] Fritz, J., M. Kroner and T. Sattelmayer: *Flashback in a swirl burner with cylindrical premixing zone.* Journal Of Engineering For Gas Turbines And Power-Transactions Of The ASME, 126(2):276–283, 2004.

[103] Frouzakis, G. E. and K. Boulouchos: *Analysis and reduction of the CH4-air mechanism at lean conditions.* Combustion Science And Technology, 159:281–303, 2000.

[104] Fung, Y. T. and V. Yang: *Active Control of Nonlinear Pressure Oscillations in Combustion-Chambers.* Journal of Propulsion and Power, 8(6):1282–1289, 1992.

[105] Fung, Y. T., V. Yang and A. Sinha: *Active Control of Combustion Instabilities with Distributed Actuators.* Combustion Science and Technology, 78(4-6):217–245, 1991.

[106] Gallagher, J. C. and S. Vigraham: *Active Control of Thermoacoustic Instability in a Model Combustor with Neruomorphic Evolvable Hardware.* In *Lecture Notes in Computer Science*, volume 2723, pages 431–441. Springer Verlag, Berlin, Heidelberg, 2003.

[107] Geering, H. P.: *Robuste Regelung.* IMRT Press, Institut für Mess- und Regeltechnik, 8092 Zürich, 1999.

[108] Gentemann, A., A. Fischer, S. Evesque and W. Polifke: *Acoustic Transfer Matrix Reconstruction and Analysis for Ducts with Sudden Change of Area.* In *9th AIAA/CEAS Aeroacoustics Conference and Exhibit*, Hilton Head, USA, 2003.

[109] Gentemann, A., C. Hirsch, K. Kunze, F. Kiesewetter, T. Sattelmayer and W. Polifke: *Validation of flame transfer function reconstruction for perfectly premixed swirl flames.* In *2004 ASME Turbo Expo*, volume 1, pages 501–510, Vienna, Austria, 2004.

[110] Ghoniem, A. and A. M. Annaswamy: *Model-Based Active Control of Combustion, Recent Developments and Implementations.* In *4th Symposium on Smart Control of Turbulence*, Tokyo, Japan, 2003.

[111] Giezendanner, R., O. Keck, P. Weigand, W. Meier, U. Meier, W. Stricker and A. Aigner: *Periodic combustion instabilities in a swirl burner studied by phase-locked planar laser-induced fluorescence.* Combustion Science and Technology, 175(4):721–741, 2003.

[112] Göransson, A.: *Active Control of Combustion Instabilities.* Technical Report, Lund Institute of Technology, 2001.

[113] Griffin, T., S. G. Sundkvist, K. Asen and T. Bruun: *Advanced zero emissions gas turbine power plant.* Journal Of Engineering For Gas Turbines And Power-Transactions Of The ASME, 127(1):81–85, 2005.

[114] Gulati, A. and R. Mani: *Active Control of Unsteady Combustion-Induced Oscillations.* Journal of Propulsion and Power, 8(5):1109–1115, 1992.

[115] Gysling, D. L., G. S. Copeland, D. C. McCormick and W. M. Proscia: *Combustion system damping augmentation with Helmholtz resonators.* Journal of Engineering for Gas Turbines and Power-Transactions of the ASME, 122(2):269–274, 2000.

[116] Hansen, N., S. D. Müller and P. Koumoutsakos: *Reducing the time complexity of the derandomized evolution strategy with covariance matrix adaptation (CMA-ES).* Evolutionary Computation, 11(1):1–18, 2003.

[117] Hardalupas, Y. and A. Selbach: *Imposed oscillations and non-premixed flames.* Progress in Energy and Combustion Science, 28(1):75–104, 2002.

[118] Hathout, J. P., A. M. Annaswamy and A. Ghoniem: *Modeling and control of combustion instability using fuel injection.* In *AVT Nato Symposium*, Braunschweig, Germany, 2000.

[119] Hathout, J. P., M. Fleifil, A. M. Annaswamy and A. F. Ghoniem: *Role of actuation in combustion control.* Combustion Science and Technology, 167:57–82, 2001.

[120] Hathout, J. P., M. Fleifil, A. M. Annaswamy and A. F. Ghoniem: *Combustion instability active control using periodic fuel injection.* Journal of Propulsion and Power, 18(2):390–399, 2002.

[121] Hathout, J. P., M. Fleifil, J. W. Rumsey, A. M. Annaswamy and A. F. Ghoniem: *Model-Based Analysis and Design of Active Control of Thermoacoustic Instability.* In *Proceedings of the 1997 IEEE conference on control applications*, Hartford, USA, 1997.

[122] Hayashi, A. K., Y. Yamazaki, T. Mizuno, S. Ogawa, T. Yamamoto, S. Kagiya and T. Motegi: *Active control of combustion oscillations for premixed combustion systems.* Journal De Physique IV, 12(PR7):281–289, 2002.

[123] Hersh, A. S., B. E. Walker and J. W. Celano: *Helmholtz resonator impedance model, part 1: Nonlinear behavior.* AIAA Journal, 41(5):795–808, 2003.

[124] Heutschi, K.: *Skript Akustik I.* Inst. für Signal und Informationsverarbeitung, ETH Zürich, 2004.

[125] Heutschi, K.: *Skript Akustik II.* Inst. für Signal und Informationsverarbeitung, ETH Zürich, 2004.

[126] Hong, B. S., V. Yang and A. Ray: *Robust feedback control of combustion instability with modeling uncertainty.* Combustion and Flame, 120(1-2):91–106, 2000.

[127] Huang, J. and V. Yang: *Modeling and Control of Combustion Dynamics in Lean-Premixed Swirl-Stabilized Combustors.* In *6th Symposium on Smart Control of Turbulence*, Tokyo, Japan, 2005.

[128] Huang, Y., H. G. Sung, S. Y. Hsieh and V. G. Yang: *Large-eddy simulation of combustion dynamics of lean-premixed swirl-stabilized combustor.* Journal of Propulsion and Power, 19(5):782–794, 2003.

[129] Huang, Y. and V. Yang: *Bifurcation of flame structure in a lean-premixed swirl- stabilized combustor: transition from stable to unstable flame.* Combustion and Flame, 136(3):383–389, 2004.

[130] Hubbard, S. and A. P. Dowling: *Acoustic resonances of an industrial gas turbine combustion system.* Journal of Engineering for Gas Turbines and Power-Transactions of the ASME, 123(4):766–773, 2001.

[131] Isella, G., C. Seywert, F. E. C. Culick and E. E. Zukoski: *A further note on active control of combustion instabilities based on hysteresis.* Combustion Science and Technology, 126(1-6):381–388, 1997.

[132] Jang, S. H. and J. G. Ih: *On the multiple microphone method for measuring in-duct acoustic properties in the presence of mean flow.* Journal of the Acoustical Society of America, 103(3):1520–1526, 1998.

[133] Johnson, C. E., Y. Neumeier, J. M. Cohen, J. Y. Lee, E. Lubarsky and B. T. Zinn: *Effects of time delay and system noise upon active control of unstable combustors.* In *39th Aerospace Sciences Meeting and Exhibit*, Reno, USA, 2001.

[134] Johnson, C. E., Y. Neumeier and B. T. Zinn: *Online Identification approach for adaptive control of combustion instabilities.* In *35th AIAA/ASME/SAE/ASEE Joint Propulsion Conference and Exhibit*, Los Angeles, USA, 1999.

[135] Jones, C. M., J. G. Lee and D. A. Santavicca: *Closed-loop active control of combustion instabilities using subharmonic secondary fuel injection.* Journal of Propulsion and Power, 15(4):584–590, 1999.

[136] Jones, W. P.: *Mathematical modelling of turbulent combustion for gas turbines.* Proceedings of the Institution of Mechanical Engineers Part A-Journal of Power and Energy, 214(A4):355–365, 2000.

[137] Kaufmann, A., F. Nicoud and T. Poinsot: *Flow forcing techniques for numerical simulation of combustion instabilities.* Combustion and Flame, 131(4):371–385, 2002.

[138] Kelsall, G. and C. Troger: *Prediction and control of combustion instabilities in industrial gas turbines.* Applied Thermal Engineering, 24(11-12):1571–1582, 2004.

[139] Kemal, A. and C. T. Bowman: *Real-time adaptive feedback control of combustion instability.* In *26th Symposium (International) on Combustion*, pages 2803–2809, Pittsburgh, USA, 1996. The Combustion Institute, Pittsburgh.

[140] Kim, K., C. M. Jones, J. G. Lee and D. A. Santavicca: *Active Control of Combustion Instabilties in Lean Premixed Combustors.* In *6th Symposium on Smart Control of Turbulence*, Tokyo, Japan, 2005.

[141] Knoop, P., F. E. C. Culick and E. E. Zukoski: *Extension of the stability of motions in a combustion chamber by nonlinear active control based on hysteresis.* Combustion Science and Technology, 123(1-6):363–376, 1997.

[142] Kopasakis, G.: *High Frequency Adaptive Instability Suppression Controls in a Liquid-Fueled Combustor.* In *39th AIAA/ASME/SAE/ASEE Joint Propulsion Conference and Exhibit*, Huntsville, USA, 2003.

[143] Kopasakis, G.: *Systems Characterization of Combustor Instabilities With Controls Design Emphasis.* In *42nd Aerospace Sciences Meeting and Exhibit*, Reno, USA, 2004.

[144] Kopasakis, G. and J. C. DeLaat: *Adaptive Instability Suppression Controls in a Liquid-Fueled Combustor.* In *38th AIAA/ASME/SAE/ASEE Joint Propulsion Conference and Exhibit*, Indianapolis, USA, 2002.

[145] Koshigoe, S., T. Komatsuzaki and V. Yang: *Adaptive control of combustion instability with on-line system identification.* Journal of Propulsion and Power, 15(3):383–389, 1999.

[146] Krebs, W., P. F. Bernd Prade and S. Hoffmann: *Thermoacoustic stability chart for high-intensity gas turbine combustion systems.* Combustion Science and Technology, 174(7):99–128, 2002.

[147] Krstić, M., A. Krupadanam and C. Jacobson: *Self-tuning control of a nonlinear model of combustion instabilities.* IEEE Transactions on Control Systems Technology, 7(4):424–436, 1999.

[148] Krüger, U., J. Hüren, S. Hoffmann, W. Krebs, P. Flohr and D. Bohn: *Prediction and measurement of thermoacoustic improvements in gas turbines with annular combustion systems.* Journal of Engineering for Gas Turbines and Power-Transactions of the ASME, 123(3):557–566, 2001.

[149] Külsheimer, C. and H. Büchner: *Combustion dynamics of turbulent swirling flames.* Combustion and Flame, 131(1-2):70–84, 2002.

[150] Kunze, K., C. Hirsch and T. Sattelmayer: *Transfer function measurements on a swirl stabilized premix burner in an annular combustion chamber.* In *2004 ASME Turbo Expo*, volume 1, pages 21–30, Vienna, Austria, 2004.

[151] Lang, N.: *Aurel Stodola (1859-1942): Wegbereiter der Dampf- und Gasturbine.* Schweizer Pioniere der Wirtschaft und Technik; 75. Verein für Wirtschaftshistorische Studien, Meilen, 2003.

[152] Lang, W., T. Poinsot and S. Candel: *Active Control of Combustion Instability.* Combustion and Flame, 70(3):281–289, 1987.

[153] Langhorne, P. J.: *Reheat Buzz - an Acoustically Coupled Combustion Instability. 1.Experiment.* Journal of Fluid Mechanics, 193:417–443, 1988.

[154] Langhorne, P. J., A. P. Dowling and N. Hooper: *Practical Active Control-System for Combustion Oscillations.* Journal of Propulsion and Power, 6(3):324–333, 1990.

[155] Lartigue, G., U. Meier and C. Berat: *Experimental and numerical investigation of self-excited combustion oscillations in a scaled gas turbine combustor.* Applied Thermal Engineering, 24(11-12):1583–1592, 2004.

[156] Laverdant, A. and D. Thévenin: *Interaction of a Gaussian acoustic wave with a turbulent premixed flame.* Combustion and Flame, 134(1-2):11–19, 2003.

[157] Lawn, C. J.: *The thermo-acoustic response of a premixed swirl burner.* Proceedings of the Institution of Mechanical Engineers Part A-Journal of Power and Energy, 214(A4):333–354, 2000.

[158] Lawn, C. J., S. Evesque and W. Polifke: *A model for the thermoacoustic response of a premixed swirl burner — Part I: Acoustic aspects.* Combustion Science and Technology, 176(8):1331–1358, 2004.

[159] Lawn, C. J. and W. Polifke: *A model for the thermoacoustic response of a premixed swirl burner — Part II: The flame response.* Combustion Science and Technology, 176(8):1359–1390, 2004.

[160] Le, D. K., J. C. DeLaat and C. T. Chang: *Control of Thermo-Acoustics Instabilities: The Multi-Scale Extended Kalman Approach.* In *39th AIAA/ASME/SAE/ASEE Joint Propulsion Conference and Exhibit*, Huntsville, USA, 2003.

[161] Lee, D. H. and T. Lieuwen: *Premixed flame kinematics in a longitudinal acoustic field.* In *37th AIAA/ASME/SAE/ASEE Joint Propulsion Conference*, Salt Lake City, USA, 2001.

[162] Lee, D. H. and T. Lieuwen: *Premixed flame kinematics in a longitudinal acoustic field.* Journal of Propulsion and Power, 19(5):837–846, 2003.

[163] Lee, J. G. and D. A. Santavicca: *Experimental diagnostics for the study of combustion instabilities in lean premixed combustors.* Journal of Propulsion and Power, 19(5):735–750, 2003.

[164] Lee, S. Y., S. Seo, J. C. Broda, S. Pal and R. J. Santoro: *An experimental estimation of mean reaction rate and flame structure during combustion instability in a lean premixed gas turbine combustor.* Proceedings of the Combustion Institute, 28:775–782, 2000.

[165] Lefebvre, A.: *Fifty years of gas turbine fuel injection.* Atomization and Sprays, 10(3-5):251–276, 2000.

[166] Lefebvre, A. H.: *Gas turbine combustion.* Taylor and Francis, Philadelphia, 2nd edition, 1999.

[167] Li, Y. Y., M. A. Rotea, G. T. C. Chiu, L. G. Mongeau and I. S. Paek: *Extremum seeking control of a tunable thermoacoustic cooler.* IEEE Transactions On Control Systems Technology, 13(4):527–536, 2005.

[168] Lieuwen, T.: *Analysis of acoustic wave transmission through turbulent, premixed flames.* In *18th International Colloquium on the Dynamics of Explosions and Reactive Systems*, Seattle, USA, 2001.

[169] Lieuwen, T.: *Phase drift characteristics of self-excited, combustion-driven oscillations.* Journal of Sound and Vibration, 242(5):893–905, 2001.

[170] Lieuwen, T.: *Experimental investigation of limit-cycle oscillations in an unstable gas turbine combustor.* Journal of Propulsion and Power, 18(1):61–67, 2002.

[171] Lieuwen, T.: *Analysis of acoustic wave interactions with turbulent premixed flames.* Proceedings of the Combustion Institute, 29:1817–1824, 2003.

[172] Lieuwen, T.: *Combustion driven oscillations in gas turbines.* Turbomachinery International, 44(1):16–18, 2003.

[173] Lieuwen, T.: *Modeling premixed combustion-acoustic wave interactions: A review.* Journal of Propulsion and Power, 19(5):765–781, 2003.

[174] Lieuwen, T.: *Statistical characteristics of pressure oscillations in a premixed combustor.* Journal of Sound and Vibration, 260(1):3–17, 2003.

[175] Lieuwen, T.: *Nonlinear kinematic response of premixed flames to harmonic velocity disturbances.* Proceedings Of The Combustion Institute, 30:1725–1732, 2005.

[176] Lieuwen, T.: *Online combustor stability margin assessment using dynamic pressure data.* Journal Of Engineering For Gas Turbines And Power-Transactions Of The ASME, 127(3):478–482, 2005.

[177] Lieuwen, T. and A. Banaszuk: *Background noise effects on combustor stability.* Journal of Propulsion and Power, 21(1):25–31, 2005.

[178] Lieuwen, T. and J. H. Cho: *Coherent acoustic wave amplification/damping by wrinkled flames.* Journal of Sound and Vibration, 279(3-5):669–686, 2005.

[179] Lieuwen, T., R. Rajaram, Y. Neumeier and S. Nair: *Measurements of incoherent acoustic wave scattering from turbulent premixed flames.* Proceedings Of The Combustion Institute, 29:1809–1815, 2003.

[180] Lieuwen, T., H. Torres, C. Johnson and B. T. Zinn: *A mechanism of combustion instability in lean premixed gas turbine combustors.* Journal of Engineering for Gas Turbines and Power-Transactions of the ASME, 123(1):182–189, 2001.

[181] Lieuwen, T. and V. Yang: *Combustion Instabilities in Gas Turbine Engines: Operational Experience, Fundamental Mechanisms, And Modeling.* Progress in Astronautics and Aeronautics, Vol. 210. AIAA, 2005.

[182] Lieuwen, T. and B. T. Zinn: *The role of equivalence ratio oscillations in driving combustion instabilities in Low NO_x Gas Turbines.* In *27th Symposium (international) on combustion*, pages 1809–1816, Pittsburgh, USA, 1998.

[183] Lihoreau, B., P. Lotton, M. Bruneau and V. Gusev: *Piezoelectric source exciting thermoacoustic resonator: Analytical modelling and experiment.* Acta Acustica United with Acustica, 88(6):986–997, 2002.

[184] Liljenberg, S.: *Modeling and Stability Analysis of Thermoacoustic Instabilities in Gas Turbine Combustor Sections.* Technical Report, Virginia Polytechnic Institute and State University, 2000.

[185] Liu, G. P. and S. Daley: *Output-model-based predictive control of unstable combustion systems using neural networks.* Control Engineering Practice, 7(5):591–600, 1999.

[186] Liu, G. P. and S. Daley: *Adaptive predictive control of combustor NO_x emissions.* Control Engineering Practice, 9(6):631–638, 2001.

[187] Liu, G. P., V. Kadirkamanathan and S. A. Billings: *Predictive control for non-linear systems using neural networks.* International Journal of Control, 71(6):1119–1132, 1998.

[188] Lohrmann, M. and H. Büchner: *Scaling of stability limits in lean-premixed gas turbine combustors.* In *2004 ASME Turbo Expo*, volume 1, pages 453–463, Vienna, Austria, 2004.

[189] Mare, F. di, W. P. Jones and K. R. Menzies: *Large eddy simulation of a model gas turbine combustor.* Combustion And Flame, 137(3):278–294, 2004.

[190] Marion, J.: *Controlling Power Plant CO_2 Emissions- A long range view.* In *First National Conference on Carbon Sequestration*, Washington, DC, USA, 2001. National Energy Technology Laboratory, NETL.

[191] Marrot, F., P. Gajan, S. Pauzin and F. Simon: *Experimental application of an active control loop on backward-facing step flow.* AIAA Journal, 43(6):1176–1186, 2005.

[192] Matsui, Y.: *An Experimental-Study on Pyro-Acoustic Amplification of Premixed Laminar Flames.* Combustion and Flame, 43(2):199–209, 1981.

[193] Matveev, K. I. and F. E. C. Culick: *A model for combustion instability involving vortex shedding.* Combustion Science and Technology, 175(6):1059–1083, 2003.

[194] Matveev, K. I. and F. E. C. Culick: *A study of the transition to instability in a Rijke tube with axial temperature gradient.* Journal of Sound and Vibration, 264(3):689–706, 2003.

[195] McKelvey, T., H. Akcay and L. Ljung: *Subspace-based multivariable system identification from frequency response data.* IEEE Transactions on Automatic Control, 41(7):960–979, 1996.

[196] McKelvey, T., A. Fleming and S. O. R. Moheimani: *Subspace-based system identification for an acoustic enclosure.* Journal of Vibration and Acoustics-Transactions of the ASME, 124(3):414–419, 2002.

[197] McManus, K., W. J. Dunstan, F. Han, C. Barbu and M. Shah: *Modeling and control of combustion dynamics in industrial gas turbines.* In *2004 ASME Turbo Expo*, volume 1, pages 567–575, Vienna, Austria, 2004.

[198] McManus, K. R., T. Poinsot and S. M. Candel: *A Review of Active Control of Combustion Instabilities.* Progress in Energy and Combustion Science, 19(1):1–29, 1993.

[199] Meissner, M.: *Excitation of Helmholtz resonator by grazing air flow.* Journal Of Sound And Vibration, 256(2):382–388, 2002.

[200] Menge, Hermann: *Langenscheidts Taschenwörterbuch Latein.* Langenscheidt, Berlin, 4th edition, 2001.

[201] Merz, C.: *Regelung einer totzeitbehafteten Gasturbinenbrennkammer.* Technical Report, IMRT, ETH Zürich, 2005.

[202] Messner, W.: *The Development, Properties and Applications of the Complex Phase Lead Compensator.* In *American Control Conference*, Chicago, USA, 2000.

[203] Messner, W.: *Complex Phase Lead and Phase Lag Compensators made simple.* 2005.

[204] Mettenleiter, M., E. Haile and S. Candel: *Adaptive control of aeroacoustic instabilities.* Journal of Sound and Vibration, 230(4):761–789, 2000.

[205] Muruganandam, T. M., S. Nair, D. Scarborough, Y. Neumeier, J. Jagoda, T. Lieuwen, J. Seitzman and B. Zinn: *Active control of lean blowout for turbine engine combustors.* Journal Of Propulsion And Power, 21(5):807–814, 2005.

[206] Murugappan, S., S. Acharya, D. C. Allgood, S. Park, A. M. Annaswamy and A. F. Ghoniem: *Optimal control of a swirl-stabilized spray combustor using system identification approach.* Combustion Science and Technology, 175(1):55–81, 2003.

[207] Nagaya, K., Y. Hano and A. Suda: *Silencer consisting of two-stage Helmholtz resonator with auto- tuning control.* Journal of the Acoustical Society of America, 110(1):289–295, 2001.

[208] Neumeier, Y., E. Lubarsky and B. T. Zinn: *Liquid Injector Actuator for control of combustion processes.* In *34th AIAA/ASME/SAE/ASEE Joint Propulsion Conference and Exhibit*, Cleveland, USA, 1998.

[209] Neumeier, Y., A. Nabi, A. Arbel, M. Vertzberger and B. T. Zinn: *Open-loop performance of a fast-response, actively controlled fuel injector actuator.* Journal of Propulsion and Power, 13(6):705–713, 1997.

[210] Neumeier, Y., A. Nabi, B. T. Zinn and D. S. Lewis: *Investigation of the open loop performance of an active control system utilizing a fuel injector actuator.* In *32nd AIAA/ASME/SAE/ASEE Joint Propulsion Conference and Exhibit*, Lake Buena Vista, USA, 1996.

[211] Neumeier, Y. and B. T. Zinn: *Active control of combustion instabilities using real time identification of unstable combustor modes.* IEEE Conference on Control Applications Proceedings, pages 691–698, 1995.

[212] Niederberger, A. S. P., B. B. H. Schuermans and L. Guzzella: *Modeling and Active Control of Thermoacoustic Instabilities.* In *16th IFAC World Congress*, Prague, 2005.

[213] Niederberger, D.: *Smart Damping Materials Using Shunt Control. Diss. ETH No. 16043.* PhD thesis, ETH Zürich, 2005.

[214] Oefelein, J. C. and V. Yang: *Comprehensive Review Of Liquid-Propellant Combustion Instabilities In F1 Engines.* Journal Of Propulsion And Power, 9(5):657–677, 1993.

[215] Padmanabhan, K. T., C. T. Bowman and J. D. Powell: *An Adaptive Optimal Combustion Control Strategy.* Combustion and Flame, 100(1-2):101–110, 1995.

[216] Padmanabhan, K. T., C. T. Bowman and J. D. Powell: *On-line adaptive optimal combustor control.* IEEE Transactions on Control Systems Technology, 4(3):217–229, 1996.

[217] Pankiewitz, C., A. Fischer, C Hirsch and T. Sattelmayer: *Computation Of Transfer Matrices For Gas Turbine Combustors Including Acoustics/Flame Interaction.* In *9th AIAA/CEAS Aeroacoustics Conference and Exhibit*, Hilton Head, USA, 2003.

[218] Pankiewitz, C. and T. Sattelmayer: *Time domain simulation of combustion instabilities in annular combustors.* In *2002 ASME Turbo Expo*, volume 1, pages 309–320, Amsterdam, The Netherlands, 2002.

[219] Pankiewitz, C. and T. Sattelmayer: *Hybrid Methods For Modelling Combustion Instabilities.* In *10th International Congress on Sound and Vibration, ICSV10*, Stockholm, Sweden, 2003.

[220] Park, S.: *Modeling of Combustion Instability at Different Damkohler Conditions.* Technical Report, MIT, 2001.

[221] Park, S., A. M. Annaswamy and A. Ghoniem: *Heat release dynamics modeling of kinetically controlled burning.* Combustion and Flame, 128(3):217–231, 2002.

[222] Paschereit, C. O., P. Flohr, H. Knopfel, W. Q. Geng, C. Steinbach, P. Stuber, K. Bengtsson and E. Gutmark: *Combustion control by extended EV burner fuel lance.* In *2003 ASME Turbo Expo*, volume 1, pages 721–730, Amsterdam, The Netherlands, 2002.

[223] Paschereit, C. O., P. Flohr and B. B. H. Schuermans: *Prediction of combustion oscillations in gas turbine combustors.* In *39th Aerospace Sciences Meeting and Exhibit*, Reno, USA, 2001.

[224] Paschereit, C. O. and E. Gutmark: *Proportional control of combustion instabilities in a simulated gas-turbine combustor.* Journal of Propulsion and Power, 18(6):1298–1304, 2002.

[225] Paschereit, C. O. and E. Gutmark: *Passive Combustion Control for Enhanced Stability and Reduced Emissions in a Swirl-Stabilized Burner.* In *41st AIAA Aerospace Sciences Meeting and Exhibit*, Reno, USA, 2003.

[226] Paschereit, C. O. and E. Gutmark: *The effectiveness of passive combustion control methods.* In *2004 ASME Turbo Expo*, volume 1, pages 361–374, Vienna, Austria, 2004.

[227] Paschereit, C. O. and E. Gutmark: *Combustion instability control by time delay management.* In *12th international congress on sound and vibration, ICSV12*, Lisbon, Portugal, 2005.

[228] Paschereit, C. O., E. Gutmark and W. Weisenstein: *Acoustic Control of Combustion Instabilities and Emissions in a Gas-Turbine Combustor.* In *Proceedings of the 1998 IEEE conference on control applications*, Trieste, Italy, 1998.

[229] Paschereit, C. O., E. Gutmark and W. Weisenstein: *Control of thermoacoustic instabilities and emissions in an industrial-type gas-turbine combustor.* In *27th Symposium (International) on Combustion*, pages 1817–1824, Pittsburgh, USA, 1998. The Combustion Institute.

[230] Paschereit, C. O., E. Gutmark and W. Weisenstein: *Structure and control of thermoacoustic instabilities in a gas- turbine combustor.* Combustion Science and Technology, 138(1-6):213–232, 1998.

[231] Paschereit, C. O., E. Gutmark and W. Weisenstein: *Coherent structures in swirling flows and their role in acoustic combustion control.* Physics of Fluids, 11(9):2667–2678, 1999.

[232] Paschereit, C. O., E. Gutmark and W. Weisenstein: *Control of thermoacoustic instabilities in a premixed combustor by fuel modulation.* In *37th AIAA Aerospae Sciences Meeting and Exhibit*, Reno, USA, 1999.

[233] Paschereit, C. O., E. Gutmark and W. Weisenstein: *Excitation of thermoacoustic instabilities by interaction of acoustics and unstable swirling flow.* AIAA Journal, 38(6):1025–1034, 2000.

[234] Paschereit, C. O. and E. J. Gutmark: *Control of High-Frequency Thermoacoustic Pulsations by Distributed Vortex Generators.* AIAA Journal, 44(3), 2006.

[235] Paschereit, C. O. and B. B. H. Schuermans: *Combustion instability suppression by active control of the burner mixing profile.* In *Int. Conf. on Jets, Wakes and Separated Flows, ICJWSF-2005*, Toba-Shi, Japan, 2005.

[236] Paschereit, C. O., B. B. H. Schuermans and V. Bellucci: *Modeling and control of combustion instabilities.* In *12th international congress on sound and vibration, ICSV12*, Lisbon, Portugal, 2005.

[237] Paschereit, C. O., B. B. H. Schuermans and D. Büche: *Combustion process optimization using evolutionary algorithm.* In *2003 ASME Turbo Expo*, volume 2, pages 281–291, Atlanta, USA, 2003.

[238] Paschereit, C. O., B. B. H. Schuermans and D. U. Campos Delgado: *Active Combustion Control using an evolution algorithm.* In *39th Aerospace Sciences Meeting and Exhibit*, Reno, USA, 2001.

[239] Paschereit, C. O., B. B. H. Schuermans, W. Polifke and O. Mattson: *Measurement of transfer matrices and source terms of premixed flames.* Journal of Engineering for Gas Turbines and Power-Transactions of the ASME, 124(2):239–247, 2002.

[240] Paschereit, C.O. and E. Gutmark: *Passive combustion control applied to premix burners.* In *40th AIAA Aerospace Sciences Meeting and Exhibit*, Reno, USA, 2002.

[241] Peracchio, A. A. and W. M. Proscia: *Nonlinear heat-release/acoustic model for thermoacoustic instability in lean premixed combustors.* Journal of Engineering for Gas Turbines and Power-Transactions of the ASME, 121(3):415–421, 1999.

[242] Pierce, A. D.: *Acoustics: an Introduction to its Physical Principles and Applications.* Acoustical Society of America, Woodbury, USA, 1989.

[243] Poinsot, T., C. Lechatelier, S. M. Candel and E. Esposito: *Experimental Determination of the Reflection Coefficient of a Premixed Flame in a Duct.* Journal of Sound and Vibration, 107(2):265–278, 1986.

[244] Poinsot, T. J., A. C. Trouve, D. P. Veynante, S. M. Candel and E. J. Esposito: *Vortex-Driven Acoustically Coupled Combustion Instabilities.* Journal of Fluid Mechanics, 177:265–292, 1987.

[245] Polifke, W.: *Non-reflecting boundary conditions for acoustic transfer matrix estimation with LES.* In *Center for Turbulence Research, Proceedings of the Summer Program*, Stanford, USA, 2002.

[246] Polifke, W., A. Fischer and T. Sattelmayer: *Instability of a premix burner with nonmonotonic pressure drop characteristic.* Journal of Engineering for Gas Turbines and Power-Transactions of the ASME, 125(1):20–27, 2003.

[247] Polifke, W., J. Kopitz and A. Serbanovic: *Impact of the fuel time lag distribution in elliptical premix nozzles on combustion stability.* In *7th AIAA/CEAS Aeroacoustics Conference*, Maastricht, The Netherlands, 2001.

[248] Polifke, W. and C. O. Paschereit: *Determination of thermo-acoustic transfer matrices by experiment and computational fluid dynamics.* ERCOFTAC Bulletin, (38), 1998.

[249] Polifke, W., A. Poncet, C. O. Paschereit and K. Döbbeling: *Reconstruction of acoustic transfer matrices by instationary computational fluid dynamics.* Journal of Sound and Vibration, 245(3):483–510, 2001.

[250] Poppe, C., S. Sivasegaram and J. H. Whitelaw: *Control of NO_x emissions in confined flames by oscillations.* Combustion and Flame, 113(1-2):13–26, 1998.

[251] Prasanth, R. K., A. M. Annaswamy, J. P. Hathout and A. F. Ghoniem: *When do open-loop strategies for combustion control work?* Journal of Propulsion and Power, 18(3):658–668, 2002.

[252] Qiu, L. M., D. M. Sun, W. L. Yan, P. Chen, Z. H. Gan, X. Zhang and G. B. Chen: *Investigation on a thermo acoustically driven pulse tube cooler working at 80 K.* Cryogenics, 45(5):380–385, 2005.

[253] Rajaram, R. and T. Lieuwen: *Parametric studies of acoustic radiation from premixed flames.* Combustion Science and Technology, 175(12):2269–2298, 2003.

[254] Rajaram, R and T. Lieuwen: *Effect of Approach Flow Turbulence Characteristics on Sound Generation from Premixed Flames.* In *42nd AIAA Aerospace Sciences Meeting and Exhibit*, Reno, USA, 2004.

[255] Rajaram, R. and T. Lieuwen: *Frequency Scaling of Turbulent Premixed Flame Noise.* In *11th AIAA/CEAS Aeroacoustics Conference (26th AIAA Aeroacoustics Conference)*, Monterey, USA, 2005.

[256] Rayleigh, Lord: *The explanation of certain acoustical phenomena.* Nature, 18:319:321, 1878.

[257] Richards, G. A., M. Janus and E. H. Robey: *Control of flame oscillations with equivalence ratio modulation.* Journal of Propulsion and Power, 15(2):232–240, 1999.

[258] Richards, G. A., M. M. McMillian, R. S. Gemmen, W. A. Rogers and S. R. Cully: *Issues for low-emission, fuel-flexible power systems.* Progress in Energy and Combustion Science, 27(2):141–169, 2001.

[259] Richards, G. A., D. L. Straub and E. H. Robey: *Passive control of combustion dynamics in stationary gas turbines.* Journal of Propulsion and Power, 19(5):795–810, 2003.

[260] Richards, G. A., M. J. Yip, E. Robey, L. Cowell and D. Rawlins: *Combustion oscillation control by cyclic fuel injection.* Journal of Engineering for Gas Turbines and Power-Transactions of the ASME, 119(2):340–343, 1997.

[261] Richards, S. J.: *An Exploration of Secondary Fuel Injection as Actuation for Control of Combustion Instabilities in a Laminar Premixed Tube Combustor.* Technical Report, Virginia Polytechnic Institute and State University, 2000.

[262] Riley, A. J., S. Park, A. P. Dowling, S. Evesque and A. M. Annaswamy: *Adaptive closed-loop control on an atmospheric gaseous lean-premixed combustor.* In *2003 ASME Turbo Expo*, volume 2, pages 347–358, Atlanta, USA, 2003.

[263] Riley, A. J., S. Park, A. P. Dowling, S. Evesque and A. M. Annaswamy: *Advanced closed-loop control on an atmospheric gaseous lean-premixed combustor.* Journal Of Engineering For Gas Turbines And Power-Transactions Of The ASME, 126(4):708–716, 2004.

[264] Rogers, D. E. and F. E. Marble: *A Mechanism for High-Frequency Oscillation in Ramjet Combustors and Afterburners.* Jet Propulsion, 26(6):456–464, 1956.

[265] Rollinger, B.: *Adaptive Control of Combustion Oscillations.* Technical Report, IMRT, ETH Zürich, 2005.

[266] Russell, D. A. and P. Weibull: *Tabletop thermoacoustic refrigerator for demonstrations.* American Journal of Physics, 70(12):1231–1233, 2002.

[267] Samaniego, J. M., B. Yip, T. Poinsot and S. Candel: *Low-Frequency Combustion Instability Mechanisms in a Side-Dump Combustor.* Combustion and Flame, 94(4):363–380, 1993.

[268] Sarpotdar, S. M., N. Ananthkrishnan and S. D. Sharma: *The Rijke Tube - A Thermo-acoustic Device.* Resonance, Journal of Science Education, IIT, 8(1), 2003.

[269] Sato, H., A. K. Hayashi, M. Ikame, K. Harumi, T. Kishi, K. Hiraoka and H. Oka: *Active Control of Acoustically Coupled Pressure Oscillation in Lean Premixed Combustor by Secondary Fuel Injection.* In *5th Symposium on Smart Control of Turbulence*, Tokyo, Japan, 2004.

[270] Sattelmayer, T.: *Influence of the combustor aerodynamics on combustion instabilities from equivalence ratio fluctuations.* Journal of Engineering for Gas Turbines and Power-Transactions of the ASME, 125(1):11–19, 2003.

[271] Sattelmayer, T. and W. Polifke: *Assessment of methods for the computation of the linear stability of combustors.* Combustion Science and Technology, 175(3):453–476, 2003.

[272] Sattinger, S. S., Y. Neumeier, A. Nabi, B. T. Zinn, D. J. Amos and D. D. Darling: *Sub-scale demonstration of the active feedback control of gas- turbine combustion instabilities.* Journal of Engineering for Gas Turbines and Power-Transactions of the ASME, 122(2):262–268, 2000.

[273] Schadow, K. C.: *Combustion Dynamics: Passive Combustion Control.* In *Von Karman Institute Lecture Series: Active Control of Engine Dynamics*, Brussels, Belgium, 2001.

[274] Schadow, K. C. and E. Gutmark: *Combustion Instability Related to Vortex Shedding in Dump Combustors and Their Passive Control.* Progress in Energy and Combustion Science, 18(2):117–132, 1992.

[275] Schuermans, B. B. H.: *Modeling and Control of Thermoacoustic Instabilities.* PhD thesis, Ecole Polytechnique Fédérale de Lausanne, Switzerland, 2003.

[276] Schuermans, B. B. H., V. Bellucci, F. Guethe, F. Meili, P. Flohr and C. O. Paschereit: *A detailed analysis of thermoacoustic interaction mechanisms in a turbulent premixed flame.* In *2004 ASME Turbo Expo*, volume 1, pages 539–551, Vienna, Austria, 2004.

[277] Schuermans, B. B. H., V. Bellucci, D. Nowak and C. O. Paschereit: *Modelling of complex thermoacoustic systems: a state-space approach.* In *9th international congress on sound and vibration, ICSV9*, Orlando, USA, 2002.

[278] Schuermans, B. B. H., V. Bellucci and C. O. Paschereit: *Thermoacoustic modeling and control of multi burner combustion systems.* In *2003 ASME Turbo Expo*, volume 2, pages 509–519, Atlanta, USA, 2003.

[279] Schuermans, B. B. H., C. O. Paschereit, J. H. Linden and W. Polifke: *Prediction of Acoustic Pressure Spectra in Combustion Systems Using Swirl Stabilized Gas Turbine Burners.* In *2000 ASME Turbo Expo*, München, Germany, 2000.

[280] Schuller, T., D. Durox and S. Candel: *Self-induced combustion oscillations of laminar premixed flames stabilized on annular burners.* Combustion and Flame, 135(4):525–537, 2003.

[281] Searby, G., J. M. Truffaut and G. Joulin: *Comparison of experiments and a nonlinear model equation for spatially developing flame instability.* Physics of Fluids, 13(11):3270–3276, 2001.

[282] Selle, L., F. Nicoud and T. Poinsot: *Actual impedance of nonreflecting boundary conditions: Implications for computation of resonators.* AIAA Journal, 42(5):958–964, 2004.

[283] Seume, J. R., N. Vortmeyer, W. Krause, J. Hermann, C. C. Hantschk, P. Zangl, S. Gleis, D. Vortmeyer and A. Orthmann: *Application of active combustion instability control to a heavy duty gas turbine.* Journal of Engineering for Gas Turbines and Power-Transactions of the ASME, 120(4):721–726, 1998.

[284] Sivasegaram, S., R. F. Tsai and J. H. Whitelaw: *Control of combustion oscillations by forced oscillation of part of the fuel supply.* Combustion Science and Technology, 105(1-3):67–83, 1995.

[285] Skogestad, S. and I. Postlethwaite: *Multivariable Feedback Control: Analysis and Design.* John Wiley and Sons Ltd., Chichester, USA, 1996.

[286] Spring, P.: *Modeling and Control of Pressure-wave Supercharged Engines Systems. Diss. ETH No. 16490.* PhD thesis, ETH Zürich, 2006.

[287] Sreenivasan, K. R. and S. Raghu: *The control of combustion instability: A perspective.* Current Science, 79(6):867–883, 2000.

[288] Stein, G.: *Respect the Unstable.* IEEE Control Systems Magazine, 23(4):12–25, 2003.

[289] Stow, S. R. and A. P. Dowling: *Low-order modelling of thermoacoustic limit cycles.* In *2004 ASME Turbo Expo*, volume 1, pages 775–786, Vienna, Austria, 2004.

[290] Stow, S. R., A. P. Dowling, W. S. Cheung, G. J. M. Sims, R. W. Copplestone, J. R. Tilston and C. W. Wilson: *Measurement and analysis of flame transfer function in a sector combustor under high pressure conditions.* In *2003 ASME Turbo Expo*, volume 2, pages 187–194, Atlanta, USA, 2003.

[291] Sturgess, G. J., J. Zelina, D. T. Shouse and W. M. Roquemore: *Emissions reduction technologies for military gas turbine engines.* Journal Of Propulsion And Power, 21(2):193–217, 2005.

[292] Tachibana, S., L. Zimmer, Y. Kurosawa, K. Suzuki, J. Shinjo, Y. Mizobuchi and S. Ogawa: *Active Control of Combustion Oscillations in a Lean Premixed Combustor by Secondary Fuel Injection.* In *6th Symposium on Smart Control of Turbulence*, Tokyo, Japan, 2005.

[293] Tachibana, S., L. Zimmer, T. Yamamoto, Y. Kurosawa, S. Yoshida and K. Suzuki: *Toward Active Control of Turbulent Combustion - Development of the Demonstration Combustor System.* In *5th Symposium on Smart Control of Turbulence*, Tokyo, Japan, 2004.

[294] Tanahashi, M., S. Murakami and T. Miyauchi: *Control of Oscillating Combustion and Measurements of Turbulent Flames.* In *4th Symposium on Smart Control of Turbulence*, Tokyo, Japan, 2003.

[295] Thibaut, D. and S. Candel: *Numerical study of unsteady turbulent premixed combustion: Application to flashback simulation.* Combustion and Flame, 113(1-2):53–65, 1998.

[296] Tijani, M. E. H., J. C. H. Zeegers and Atam de Waele: *Construction and performance of a thermoacoustic refrigerator.* Cryogenics, 42(1):59–66, 2002.

[297] Tijani, M. E. H., J. C. H. Zeegers and Atam de Waele: *Design of thermoacoustic refrigerators.* Cryogenics, 42(1):49–57, 2002.

[298] Truffin, K. and T. Poinsot: *Comparison and extension of methods for acoustic identification of burners.* Combustion and Flame, 142(4):388–400, 2005.

[299] Vaudrey, M. A., W. T. Baumann and W. R. Saunders: *Stability and operating constraints of adaptive LMS-based feedback control.* Automatica, 39(4):595–605, 2003.

[300] Vaudrey, M. A., W. T. Baumann and W. R. Saunders: *Time-averaged gradient control of thermoacoustic instabilities.* Journal of Propulsion and Power, 19(5):830–836, 2003.

[301] Venkataraman, K. K., L. H. Preston, D. W. Simons, B. J. Lee, J. G. Lee and D. A. Santavicca: *Mechanism of combustion instability in a lean premixed dump combustor.* Journal of Propulsion and Power, 15(6):909–918, 1999.

[302] Weigand, P., W. Meier, X. R. Duan, W. Stricker and M. Aigner: *Investigations of swirl flames in a gas turbine model combustor: I. Flow field, structures, temperature, and species distributions.* In Press, Corrected Proof.

[303] Wilson, D.G. and T. Korakianitis: *The design of high-efficiency turbomachinery and gas turbines.* Prentice Hall, Upper Saddle River, N.J., 2nd edition, 1998.

[304] Yang, V.: *Active Control of Engine Dynamics-Stability Characteristics and Control Approach.* In *Von Karman Institute Lecture Series: Active Control of Engine Dynamics*, Brussels, Belgium, 2001.

[305] Yu, K. H. and K. J. Wilson: *Scale-up experiments on liquid-fueled active combustion control.* Journal of Propulsion and Power, 18(1):53–60, 2002.

[306] Yu, K. H., K. J. Wilson and K. C. Schadow: *Active Instability Suppression by controlled injection of liquid fuel.* AIAA, (97-3324), 1997.

[307] Zähringer, K., D. Durox and F. Lacas: *Helmholtz behavior and transfer function of an industrial fuel swirl burner used in heating systems.* International Journal of Heat and Mass Transfer, 46(18):3539–3548, 2003.

[308] Zhu, M., A. P. Dowling and K. N. C. Bray: *Transfer function calculations for aeroengine combustion oscillations.* Journal Of Engineering For Gas Turbines And Power-Transactions Of The ASME, 127(1):18–26, 2005.

[309] Zinn, B. T. and M. E. Lores: *Application of Galerkin Method in Solution of Nonlinear Axial Combustion Instability Problems in Liquid Rockets.* Combustion Science and Technology, 4(6):269ff, 1972.

[310] Zinn, B. T., Y. Neumeier and T. Lieuwen: *Active Control of Combustion Instabilities in low NOx Gas Turbines.* Technical Report, Georgia Institute of Technology, 2002.

[311] Zoccola, P. J.: *Effect of opening obstructions on the flow-excited response of a Helmholtz resonator.* Journal Of Fluids And Structures, 19(7):1005–1025, 2004.

Publications

Five publications are associated with the work presented in this thesis:

Conferences

Niederberger, A. S. P., B. B. H. Schuermans, and L. Guzzella: *Modeling and Active Control of Thermoacoustic Instabilities.* In 16$^{\text{th}}$ IFAC World Congress, Prague, 2005.

Niederberger, A. S. P. and L. Guzzella: *Thermoacoustic Oscillations in Gas Turbine Combustors: Modeling, Identification and Control.* In Latsis Symposium 2006: Research Frontiers in Energy Science and Technology, Zürich, 2006. Submitted for Review.

Journals

Hansen, N., A. S. P. Niederberger, L. Guzzella, and P. Koumoutsakos: *Evolutionary Optimization of Feedback Controllers for Thermoacoustic Instabilities.* IEEE Transactions on Evolutionary Computing. Submitted for Review.

Niederberger, A. S. P., B. B. H. Schuermans, and L. Guzzella: *Thermoacoustic Instability Modeling and Identification at Various Operating Conditions.* ASME Journal of Engineering for Gas Turbines and Power. Submitted for Review.

Niederberger, A. S. P., D. Fritsche, K. Boulouchos, and L. Guzzella: *Thermoacoustic Instability Suppression by Robust $\mathcal{H}_\infty$ Controller Design for Secondary Fuel Injection.* IEEE Control Systems Technology. Submitted for Review.

Curriculum Vitæ

André Sven Paul Niederberger

born February 6th, 1978 in Stans, Switzerland
Son of Ernst Alois and Irène Niederberger-Murer, brother of Dominik
Direct descendant of Erni im Niderbärg, born 1366

June 2002– April 2006	**Swiss Federal Institute of Technology (ETHZ)**, Zürich, Switzerland. PhD student, research and teaching assistant at the Measurement and Control Laboratory IMRT. Advisor: Prof. Dr. Lino Guzzella.
Oct. 1997– March 2002	**Swiss Federal Institute of Technology (EPFL)**, Lausanne, Switzerland. Diploma in Mechanical Engineering.
Oct. 2001– March 2002	**University of Florida (UF)**, Gainesville, USA. Diploma thesis in Process Control Engineering. Advisor: Prof. Dr. Oscar Crisalle.
May 2000– Aug. 2000	**Ford Motor Company**, Kansas City and Dearborn, USA. Summer internship.
Aug. 1999– May 2000	**Carnegie Mellon University (CMU)**, Pittsburgh, USA. International student, Mechanical Engineering.
Feb. 1999– March 1999	**Pilatus Aircrafts Ltd.**, Stans, Switzerland. Internship.
Aug. 1990– June 1997	**Kollegium St. Fidelis**, Stans, Switzerland. Matura Typus C.